

https://dspace.org/

Analysis of injection spray patterns for common rail system

Alimia, Omid Iskander

2011-11-02
http://hdl.handle.net/10539/10687

Downloaded from a DSpace repository. https://dspace.org/

ANALYSIS OF INJECTION SPRAY PATTERNS FOR COMMON RAIL SYSTEMS

Omid Iskander Alimia

A research report submitted to the Faculty of Engineering and the Built Environment, University of the Witwatersrand, in fulfillment of the requirements for the degree of Master of Science in Engineering.

Johannesburg, 2011

“The ideal engineer is a composite ... He is not a scientist, he is not a mathematician, he is not a sociologist or a writer; but he may use the knowledge and techniques of any or all of these disciplines in solving engineering problems.” – N.W. Dougherty (1955)

ABSTRACT

The objective of this study was to investigate and compare the fuel spray characteristics of DME and diesel fuel being injected through a common-rail fuel injection system into a constant volume pressure vessel containing nitrogen gas. The fuel pressure and the chamber pressure were varied from 200-500bar and 1-10bar respectively, all at room temperature conditions. Images of the spray were captured at a rate of 7500fps utilizing a high speed camera, with a CMOS sensor, in conjunction with a schlieren optical system. The images were then analyzed to determine quantitative aspects of the spray such as spray penetration, cone angle and mean spray velocity and qualitative aspects like evaporation and flash boiling. The fuel line pressure was also recorded and analysed to determine the effect that injection had on the pressure in the line. For the same injection conditions it was found that the penetration of diesel was greater than that of DME and the cone angle of diesel was greater than that of DME except at atmospheric back pressure. The pressure oscillation in the DME fuel line was smaller in amplitude and longer in duration than that of diesel. The DME spray exhibited signs of flash boiling and evaporation when injected into an environment at atmospheric pressure and room temperature. As the chamber pressure was increased the DME spray shape became increasingly similar to that of the diesel spray shape. The spray boundaries, however, differed with DME exhibiting a more defined fuel-to-air barrier and diesel exhibiting a fine mist at its boundary. The predicted spray penetrations of DME, using existing correlations, were accurate for atmospheric back pressure conditions only.

ACKNOWLEDGEMENTS

I would like to thank Professor Daniele Cipolat for the help, support and guidance provided during the length of this study. Without it this particular study would not have been possible. I would like to thank Quinn Reynolds, from Mintek, for making it possible to use their high speed camera for this study and for the enthusiasm with which he helped me with my experimental work. Without the high speed camera, from Mintek, this study would have taken considerably longer to complete. I would like to thank Frank Testa, from DPA Diesel, for generously providing us with a lot of the diesel equipment needed for this study. I would finally like to thank Ralf, from TW Diesel, for the in-depth technical advice provided about the diesel equipment and for supplying us with some equipment.

CONTENTS

ABSTRACT iii

ACKNOWLEDGEMENTS iv

CONTENTS v

LIST OF FIGURES vii

LIST OF TABLES x

LIST OF SYMBOLS xi

NOMENCLATURE xii

1. INTRODUCTION 1

1.1 Background 1

1.2 Motivation 1

2. LITERATURE REVIEW 3

2.1 Common-rail injection systems [5][6] 3

2.2 Fuel injectors 4

2.3 Characteristics of DME 6

2.4 Sources and production methods of DME 7

2.5 Future emissions standards 8

2.6 Spray characteristics 9

2.6.1 Fuel atomization and jet divergence [13] 10

2.6.2 Fuel evaporation [13] 11

2.7 Models for spray penetration 12

2.8 Related studies conducted previously 14

2.8.1 Spray studies 14

3. OBJECTIVES 24

4. DESCRIPTION AND DEVELOPMENT OF APPARATUS 25

4.1 Description of existing setup 25

4.1.1 Pressure chamber 25
4.1.2 Common-rail system 26
4.1.3 AC motor and motor speed control system 28
4.1.4 Schlieren optical system 28
4.1.5 Pressure measurement system 29
4.2 Modifications and additions to existing setup 30
4.2.1 Pressure chamber/vessel 30
4.2.2 Common-rail system 30
4.2.3 Schlieren optical system 33
4.3 Final experimental setup 33
5. METHODOLOGY 37
5.1 Initial Start-up Procedures for Both Fuels 37
5.2 Test Procedure for Diesel 37
5.3 Test Procedure for DME 38
5.4 Post-processing of the Results 39
6. UNCERTAINTY ANALYSIS 41
6.1 Measurement Uncertainty 41
7. RESULTS AND DISCUSSION 43
8. CONCLUSION 66
REFERENCES 67
Appendix A: Image Post-processing 69
Appendix B: Sample calculations 71
Appendix C: Catalogue of diesel and DME spray images from experiments 75
Appendix D: Spray Penetration, Mean Spray Velocity and Cone Angle 92
Appendix E: Pressure Trace 108

LIST OF FIGURES

Figure 1: Common-rail system.[5] 3
Figure 2: Cross-section of a Bosch electronic injector.[6] 5
Figure 3: (a) Sac type nozzle and (b) VCO type nozzle.[7] 6
Figure 4: DME molecule.[8] 6
Figure 5: Various elements of a fuel spray.[13] 9
Figure 6: Effects of swirl on a fuel spray.[13] 10
Figure 7: Variation of various parameters with time during the evaporation process. [13] 11
Figure 8: Fuel line pressure versus time of diesel and DME. [Yu *et al.* [17; 18]] 14
Figure 9: Penetration versus time (a) diesel and DME at atmospheric pressure; (b) DME at various ambient pressures. [Suh *et al.* [19]] 16
Figure 10: Cone angle versus time of DME for various ambient pressures. [Suh *et al.* [19]] 16
Figure 11: Penetration versus time (a) diesel and DME at atmospheric pressure; (b) DME at various ambient pressures. [Suh *et al.* [4]] 17
Figure 12: (a) Spray penetration versus time; (b) cone angle versus time at 400bar injection pressure. [Kim *et al.* [20]] 18
Figure 13: (a) Spray penetration versus time; (b) cone angle versus time. [Hwang *et al.* [21]] 19
Figure 14: Comparison of theoretical and empirical penetration versus time. [Hwang *et al.* [21]] 19
Figure 15: (a) Spray penetration versus time; (b) cone angle versus time at P_b = 1.5MPa. [Wakai *et al.* [22]] 20
Figure 16: (a) Spray penetration versus time; (b) cone angle versus time at P_b = 0.1MPa. [Wakai *et al.*[22]] 20
Figure 17: (a) Spray penetration versus time for diesel and DME; (b) cone angle versus chamber pressure of diesel and DME. [Li *et al.* [23]] 21
Figure 18: (a) Spray penetration versus time for DME at various back pressures; (b) spray penetration versus time of DME for various orifice sizes. [Li *et al.* [23]] 21
Figure 19: (a) Spray penetration versus time for DME; (b) spray angle versus time for DME. [Lee *et al.* [24]] 23
Figure 20: Pressure vessel. 26
Figure 21: Common-rail system. 28
Figure 22: Double-mirror schlieren setup used for experiment. ("*Schlieren photography,* Eastman Kodak Company") 29

Figure 23: View through the adjacent windows in the pressure chamber; (a) before and (b) after the modification. 30
Figure 24: Top view of the pressure chamber showing the direction of the sprays. 31
Figure 25: Front and top views of the fuel spray from the injector tip. 32
Figure 26: Schematic diagram of the experimental layout. 35
Figure 27: Spray with circle of size $60D_o$. 40
Figure 28: Measurement of (a) penetration and (b) cone angle. 42
Figure 29: Theoretical penetration plot for various ΔP values (P_{inj} = 500b, P_b = atm) 44
Figure 30: Theoretical penetration plot for various ΔP values (P_{inj} = 500b, P_b = 10b). 44
Figure 31: Penetration versus time using Hiroyasu's and Dent's correlation (P_{inj} = 500b, P_b = 10b). 45
Figure 32: Penetration versus time for diesel and DME (P_{inj} = 500b, P_b = atmospheric) 47
Figure 33: Penetration versus time for diesel and DME (P_{inj} = 400b, P_b = atmospheric) 47
Figure 34: Penetration versus time for diesel and DME (P_{inj} = 500b, P_b = 10b) 48
Figure 35: Penetration versus time for diesel and DME (P_{inj} = 300b, P_b = 10b) 48
Figure 36: Penetration versus time for diesel and DME (P_{inj} = 400b, P_b = 6b) 48
Figure 37: Penetration versus time for diesel at various injection pressures at 10b back pressure. 49
Figure 38: Penetration versus time for DME at various injection pressures at 10b back pressure. 49
Figure 39: Penetration versus time for diesel at 400b injection pressure and various back pressures. 50
Figure 40: Penetration versus time for DME at 400b injection pressure and various back pressures. 50
Figure 41: Cone angle versus time for diesel at various injection pressures and 10b back pressure. 52
Figure 42: Cone angle versus time for DME at various injection pressures and 10b back pressure. 52
Figure 43: Cone angle versus time for diesel at various injection pressures and atmospheric back pressure. 52
Figure 44: Cone angle versus time for DME at various injection pressures and atmospheric back pressure. 53
Figure 45: Cone angle versus time for diesel and DME at 200b injection pressure and various back pressures 54
Figure 46: Cone angle versus time for diesel and DME at 300b injection pressure and various back pressures 54
Figure 47: Cone angle versus time for diesel and DME at 400b injection pressure and various back pressures 54
Figure 48: Cone angle versus time for diesel and DME at 500b injection pressure and various back pressures 55
Figure 49: Mean spray velocity versus time for diesel for various injection pressures. (P_b = atm) 56

Figure 50: Mean spray velocity versus time for DME for various injection pressures. (P_b = atm).....57
Figure 51: Mean spray velocity versus time for diesel for various injection pressures. (P_b = 10b) 57
Figure 52: Mean spray velocity versus time for DME for various injection pressures. (P_b = 10b).....57
Figure 53: Pressure versus time for diesel injected at 200b injection pressure. (P_b = atm) 59
Figure 54: Pressure versus time for diesel injected at 500b injection pressure. (P_b = 10b) 59
Figure 55: Pressure versus time for DME injected at 500b injection pressure. (P_b = 10b).....59
Figure 56: Pressure versus time for DME injected at 400b injection pressure. (P_b = 8b).....60
Figure 57: Pressure versus time for DME injected at 400b injection pressure. (P_b = 6b).....60
Figure 58: Magnified view of pressure versus time for diesel. (P_{inj} = 500b, P_b = atm) 60
Figure 59: Magnified view of pressure versus time for DME. (P_{inj} = 500b, P_b = atm).....61
Figure 60: DME spray images for 500b injection pressure and atmospheric back pressure.....63
Figure 61: Diesel spray images for 500b injection pressure and atmospheric back pressure. 63
Figure 62: DME spray images for 500b injection pressure and 10b back pressure. 64
Figure 63: Diesel spray images for 500b injection pressure and 10b back pressure. 64

LIST OF TABLES

Table 1: Properties of DME and diesel fuel.[9] 7
Table 2: Emissions standards for Europe and Japan.[10][11][12] 8
Table 3: Description of all the items in the schematic diagram. 36

LIST OF SYMBOLS

S	-	penetration	[m]
Δp	-	pressure difference across nozzle	[Pa]
ρ	-	density	[kg/m^3]
t	-	time	[s]
d	-	diameter	[m]
T	-	temperature	[K]
C_D	-	discharge coefficient	
α_d	-	volume fraction of droplets in spray	
μ	-	viscosity	[Pa.s]
r	-	radius	[m]

NOMENCLATURE

CI	-	compression ignition
DI	-	direct injection
IDI	-	indirect injection
DME	-	dimethyl ether
LPG	-	liquified petroleum gas
PTFE	-	polytetrafluoro ethylene
NG	-	natural gas
TDC	-	top dead centre
BDC	-	bottom dead centre
VCO	-	valve covered orifice
CCD	-	charge coupled device
ICCD	-	intensified charge coupled device
PDPA	-	phase doppler particle analyser

1. INTRODUCTION

1.1 Background

Compression ignition engines have become an integral part of the modern world. They can be found in light passenger vehicles, heavy commercial vehicles (buses and trucks), heavy industrial vehicles (earth movers, excavators), in locomotives, in marine applications (boats and ships) and in power generation (as generators and as starter motors for steam turbines). Numerous industries such as the transportation, logistics and power generation depend, either completely or partially, on CI engines. These industries further facilitate various other industries such as manufacturing, mining and retail and businesses which ultimately contribute to the national economy of a country. Thus it is apparent how significant a role the CI engines play in our day to day lives.

The majority of compression ignition engines throughout the world are currently run on diesel fuel. The potentially hazardous byproducts of diesel combustion are NO_x, CO, Hydrocarbons and particulate matter. These byproducts are thought to have a varying and widespread effect on the atmosphere and environment.

1.2 Motivation

Alternative fuels broadly refer to energy sources that do not originate from petroleum, have relatively high heating values and which exhibit lower emissions compared to those of petroleum when combusted.[1] With the advent of the depletion of global fossil fuel resources, especially petroleum, the need to identify and research alternative fuels is becoming increasingly important. The advent of global warming has resulted in stricter vehicle emissions regulations being implemented and this has resulted in the proliferation of studies into alternative fuels that are less harmful to the atmosphere. World petroleum production is estimated to have peaked and the consumption of petroleum has exceeded the rate at which new reserves are being found. The prospect of developing countries such as China, India, Brazil and Russia increasing their petroleum consumption could result in an increase of up to 75% from current levels.[2] This demand for fuel will have to be met and petroleum is not a viable long term solution due to the depletion of world reserves in the near future and the emissions that result from its combustion.

Diesel engines offer numerous advantages over their petrol counterparts such as higher thermal efficiency, lower fuel consumption and lower CO_2 emissions. However the particulate matter (soot) and NO_x emitted from diesel engines does pose serious environmental challenges. Research into fuels that can

be utilised in diesel engines and have better emissions characteristics are thus crucial. At present the most popular neat fuels for diesel engines are RME (which is used in Europe), bioethanol (which is used in the USA), and other vegetable oil esters (which are used in South Asia).[1] DME is a relatively new choice as an additive to diesel or for completely replacing diesel because of its high cetane number and low auto-ignition temperature. DME was initially used as an ignition improving agent for methanol in the 1980's however it was found that the engine performance was unsatisfactory. In addition it was relatively expensive to produce DME at the time. In 1995 a breakthrough was made regarding the low cost production of DME from natural gas which meant that DME could potentially become a commodity produced in large quantities at competitive prices.[3] Research has found that DME, being an oxygenated fuel, can provide lower NO_x emissions, almost no particulate matter emissions and significantly lower engine noise.[4]

2. LITERATURE REVIEW

2.1 Common-rail injection systems [5][6]

Common-rail diesel engines have been around since the early 1940s. They were initially used in marine and locomotive applications. Fiat and its subsidiaries were the first to develop a workable modern common-rail engine in the 1980s however due to the cost implications of Fiat producing the common-rail systems internally they decided to drop their own product. Bosch became the forerunner in the field of high speed light diesel engine technology. The first modern common-rail engines using Bosch technology was introduced in 1997 by Alfa Romeo and Mercedes Benz.

In the Bosch common rail system, fuel is drawn from a tank by a low pressure pump and subsequently fed through a fuel filter to a high pressure pump. The high pressure pump then pressurises the fuel and supplies it to a forged steel common-rail which acts as a fuel accumulator. The rail is usually as long as the cylinder head and supplies anywhere from 3 to 6 injectors. In order to minimize pressure fluctuations in the rail, due to injection, the rail has to be made as long as is practicable. A pressure regulator at one end of the common-rail governs the pressure that accumulates in the rail by controlling the amount of fuel that is dumped back into the fuel tank, at low pressure, from the rail. Fuel is taken from the rail to each injector via a separate high pressure steel line. The engine control unit (ECU) is responsible for controlling the pressure regulator, injection frequency, injection duration and quantity depending on the engine load. A common-rail system is illustrated below in Figure 1.

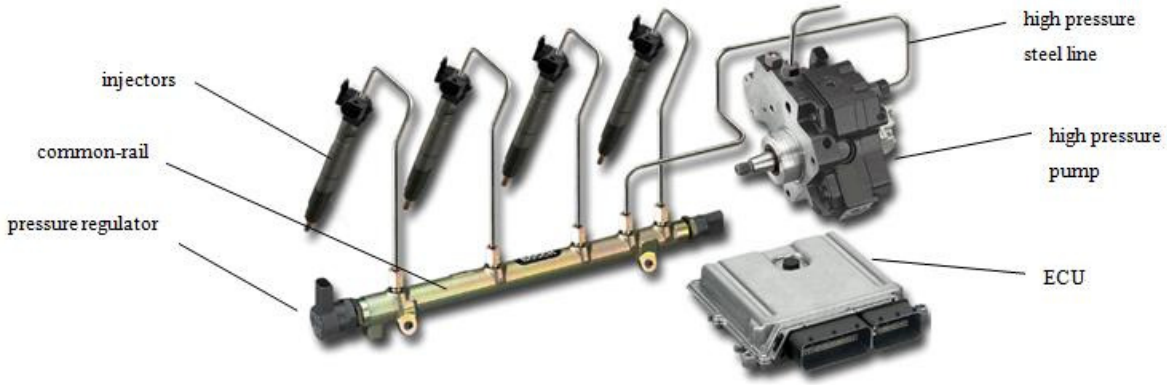

Figure 1: Common-rail system.[5]

The high pressure pump used to pressurise the fuel is usually driven by the camshaft at half the engine speed. The common-rail system maintains fuel pressure regardless of engine speed and injection quantity.

The first and second generation common-rail systems used injectors that utilised magnetic solenoids to control the injection processes whereas from the third generation onwards piezo injectors containing crystals that expand when current passes through them were utilised. The advantages of the common-rail system are that:

- it allows for fuel to be highly pressurised and stored, ready for injection
- very accurate injection timing can be achieved
- faster injection and accurate timing lead to better fuel consumption and performance

2.2 Fuel injectors

A cross-sectional view of an electronic, solenoid actuated, injector is illustrated below in Figure 2. Fuel from the common-rail initially passes into the injector's body through a thimble type filter. The fuel then travels in two directions: radially inwards through the input throttle to the valve control chamber and along the length of the injector through a feed hole to the nozzle chamber. Thus the force acting on the bottom of the injector needle and the top of the pushrod is equalized by having pressurised fuel in both the valve control chamber and the nozzle chamber, as shown in Figure 2. The needle therefore cannot lift and is held firmly in place on its seat by a spring. This design characteristic, of having equal pressures on both ends, allows for the needle to be very rapidly lifted by a relatively small force making injection a quiet operation.[6]

In order to inject fuel through the nozzle the solenoid has to be energized. This causes the valve to lift off its seat at the top of the valve control chamber and allow fuel to flow back into the fuel tank. This subsequently causes the pressure in the valve control chamber to drop below that of the nozzle chamber which causes the needle to lift and begin injection. Whilst the valve is open some fuel flows through the input throttle into the valve control chamber and out to the fuel tank. This circulation of fuel helps to cool the solenoid inside of the injector.[6]

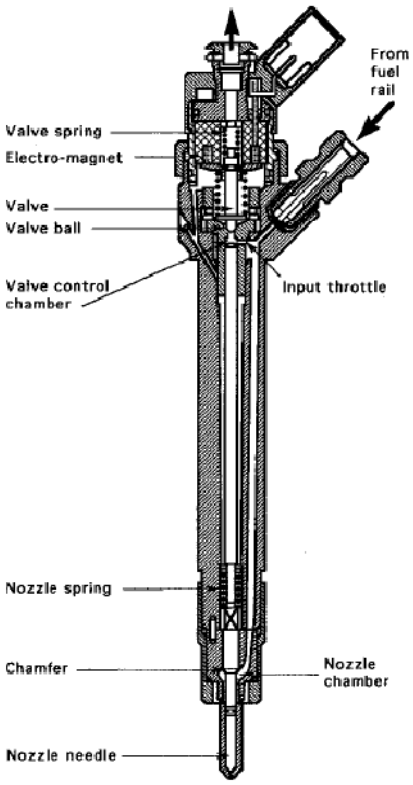

Figure 2: Cross-section of a Bosch electronic injector.[6]

Two types of nozzles are most commonly found in electronic injectors used in high speed light diesel engines: the sac type and the valve covered orifice (VCO) type. The differences between the nozzle types are illustrated below in Figure 3. With the sac type nozzle the fuel in the sac and the spray holes is heated by combustion and fuel sometimes enters the combustion chamber late within the combustion event. The late injection combusts partially and causes increased hydrocarbon emissions and deposits on and inside the nozzle. With the VCO type nozzle the amount of fuel that is injected into the chamber is reduced significantly and the flow of combusted fuel back into the nozzle sac is blocked. [7]

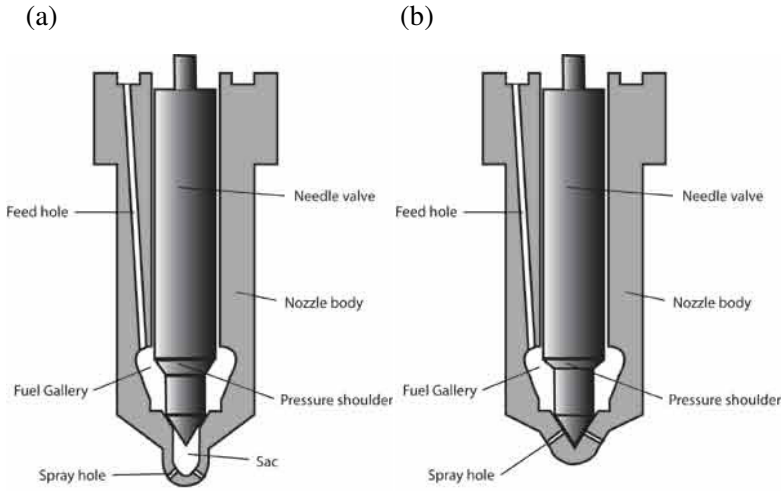

Figure 3: (a) Sac type nozzle and (b) VCO type nozzle.[7]

2.3 Characteristics of DME

Dimethyl ether is an ether with the chemical formula CH_3OCH_3. A DME molecule is represented below in Figure 4. DME has very similar properties to liquefied petroleum gas (LPG). DME is widely used in aerosol cans as a propellant because of its on-toxic nature and sweet ether-like odour. [2]

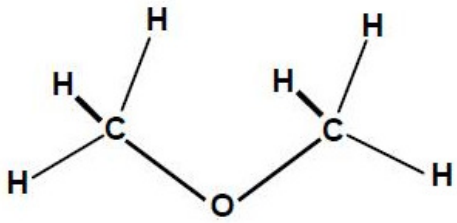

Figure 4: DME molecule.[8]

In addition to being non-toxic, DME is also non-carcinogenic and non-mutagenic. Studies conducted by Good *et al.* which modeled the lifetime and global warming potential of DME found that DME was environmentally benign.[2] The most challenging aspect of using DME has been found to be its physical properties. The boiling point of DME is -24.9°C and the vapour pressure is 5.1bar at room temperature (25°C). Thus DME is a gas at room temperature and as a result is much more difficult to handle than diesel because it requires specialized storage facilities.[3] In gas form DME's density is greater than air while in liquid form DME has about two thirds the density of water.[9] In comparison to diesel, DME has a lower liquid density, lower heating value, higher compressibility, lower viscosity and lower lubricity. The properties of both DME and diesel can be found below in Table 1. The higher compressibility of DME results in more work being required by a pump to pressurize DME. At very high engine loads, the

heat from the engine causes heating of the fuel which decreases the density and increases the compressibility of DME. This makes it a problem for the fuel pump to pressurize and supply enough fuel for the engine to maintain its full power. The viscosity of DME is significantly smaller than diesel and this leads to leakages through small clearances such as pump plungers and injector tip orifices. The lower lubricity of DME means that adjacent moving parts in the injection system wear much more rapidly than with diesel. In most experiments a lubricity additive is used to overcome this issue. [3]

DME is corrosive to most elastomers and causes seals made from such materials to deteriorate after lengthy exposure intervals. PTFE and Teflon compounds are however inert to DME but Teflon's creep and stiffness characteristics make it unsuitable for sealing applications. Thus any seals for DME should preferably be made from PTFE.[3][9]

Table 1: Properties of DME and diesel fuel.[9]

Property (unit/condition)	Unit	DME	Diesel fuel
Chemical structure		CH_3–O–CH_3	–
Molar mass	g/mol	46	170
Carbon content	mass%	52.2	86
Hydrogen content	mass%	13	14
Oxygen content	mass%	34.8	0
Carbon-to-hydrogen ratio		0.337	0.516
Critical temperature	K	400	708
Critical pressure	MPa	5.37	3.00[a]
Critical density	kg/m^3	259	–
Liquid density	kg/m^3	667	831
Relative gas density (air = 1)		1.59	–
Cetane number		>55	40–50
Auto ignition temperature	K	508	523
Stoichiometric air/fuel mass ratio		9.0	14.6
Boiling point at 1 atm	K	248.1	450–643
Enthalpy of vaporization	kJ/kg	467.13	300
Lower heating value	MJ/kg	27.6	42.5
Gaseous specific heat capacity	kJ/kg K	2.99	1.7
Ignition limits	vol% in air	3.4/18.6	0.6/6.5
Modulus of elasticity	N/m^2	6.37E+08	14.86E+08
Kinematic viscosity of liquid	cSt	<.1	3
Surface tension (at 298 K)	N/m	0.012	0.027
Vapour pressure (at 298 K)	kPa	530	≪10

2.4 Sources and production methods of DME

DME can be produced from an array of sources like natural gas (NG), crude oil, residual oil, coal, biomass and waste products.[9] Multiple sources are important when taking a long term view because it means that DME pricing will be competitive to petroleum as the demand for petroleum exceeds production and petroleum prices increase. A significant economic factor in favour of DME is to produce DME from NG that cannot be exploited for use as a gas. Such NG is located in several remote places

around the world. The excess NG from oil production that is usually flared or re-injected into the ground can also be used which saves significant cost and minimizes CO_2 emissions.[3]

DME can presently be produced in one of two ways:[9]

- Dehydrogenation of methanol
- Direct conversion from synthesis gas

The dehydrogenation process of making DME involves the following chemical processes:[2]

1) Methanol synthesis –

$CO + 2H_2 = CH_3OH$

2) Methanol dehydration –

$2CH_3OH = CH_3OCH_3 + H_2O$

3) Water-gas shift –

$H_2O + CO = H_2 + CO_2$

4) Net reaction –

$3H_2 + 3CO = CH_3OCH_3 + CO_2$

2.5 Future emissions standards

The emissions standards for the European Union and Japan, for diesel fuelled cars, can be found below in Table 2. A comprehensive list of all the emissions standards for every country can be obtained online.

Table 2: Emissions standards for Europe and Japan.[10][11][12]

Japan					
Passenger Cars	**Date**	**CO mean (g/km)**	**HC mean (g/km)**	**NO_x mean (g/km)**	**PM mean (g/km)**
<1250kg	by 2011	0.63	0.024	0.08	0.005
>1250kg	by 2011	0.63	0.024	0.08	0.005
Light Commercial Vehicles					
<1700kg	by 2011	0.63	0.024	0.08	0.005
>1700kg	by 2011	0.63	0.024	0.15	0.007
Heavy Commercial Vehicles					
>3500kg	by 2009	2.22	0.17	0.7	0.01

European Union					
Passenger Cars	**Date**	**CO (g/km)**	**HC+NO_x (g/km)**	**NO_x (g/km)**	**PM (g/km)**
Class M1	(Euro 6) by 2011	0.5	0.23	0.18	0.005
	(Euro 6) by 2014	0.5	0.17	0.08	0.005
Light Commercial Vehicles					
Class I (<1305kg)	(Euro 5) by 2011	0.5	0.23	0.18	0.005
	(Euro 6) by 2014	0.5	0.17	0.08	0.005
Class II (1305-1760kg)	(Euro 5) by 2012	0.63	0.295	0.235	0.005
	(Euro 6) by 2015	0.63	0.195	0.105	0.005
Class III (>1760kg)	(Euro 5) by 2012	0.74	0.35	0.28	0.005
	(Euro 6) by 2015	0.74	0.215	0.125	0.005
Heavy Commercial Vehicles	**Date**	**CO (g/kWh)**	**HC (g/kWh)**	**NOx (g/kWh)**	**PM (g/kWh)**
>3500kg	(Euro 6) by 2014	1.5	0.13	0.4	0.01

It is at once apparent from Table 2 above that each region or country has its own set of emissions targets for the next few years. The EU standards have to be adhered to by all the nations falling within its boundaries. Multiple nations within the EU especially Western Europe have further emissions targets of their own.

2.6 Spray characteristics

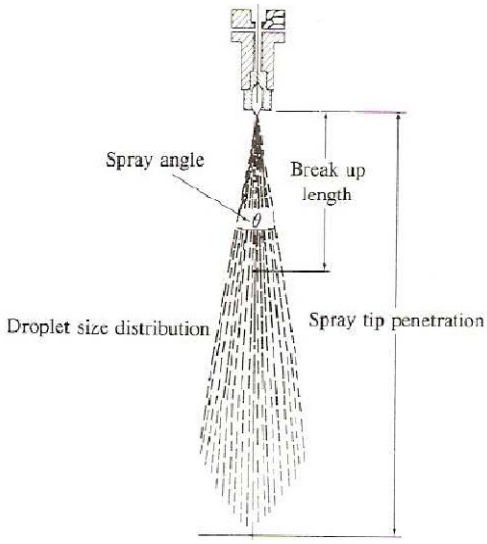

Figure 5: Various elements of a fuel spray.[13]

The typical fuel spray structure for a single jet of diesel fuel is illustrated in Figure 5 above. The various parameters of the fuel spray with reference to Figure 5 are:

- *Break up length* - the finite length over which the liquid jet leaving the nozzle disintegrates in the combustion chamber. [13]
- *Spray angle (Cone angle)* – the angle between the two peripheral sides of the fuel spray.
- *Spray tip penetration* – the extent to which the fuel jet manages to travel into the combustion chamber.

As the liquid jet exits the nozzle it quickly becomes turbulent and disperses as it mixes with the hot air in the combustion chamber. Upon moving away from the nozzle the spray slows down and disperses forming somewhat of a cone type pattern originating from the nozzle. The mass of air in the spray also increases during the dispersion. The fuel begins to evaporate as it begins to mix with more air due to the greater temperature of the air.

If the swirl of the air in the cylinder is taken into consideration then the spray structure that results is illustrated in Figure 6 below. As can be intuitively assumed the swirling air bends the spray and carries the spray along with it, more so the further the spray has traveled from the nozzle exit. In any combustion chamber a fuel jet will penetrate less with swirl than without it.[13]

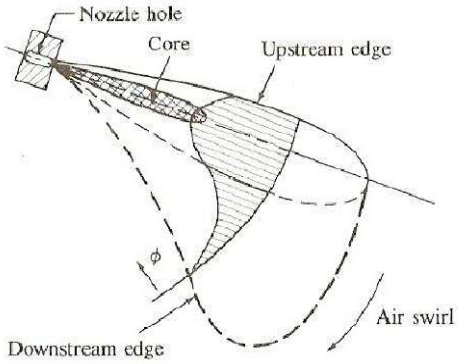

Figure 6: Effects of swirl on a fuel spray.[13]

2.6.1 Fuel atomization and jet divergence [13]

Atomization is the breakup regime of the fuel jet, where droplet sizes that are far smaller than the nozzle exit diameter are produced in the combustion chamber. Atomization occurs at large fuel jet velocities because the outer surface of the jet breaks up before actually leaving the nozzle exit, resulting in very small droplets forming.

There are multiple reasons for fuel jet divergence and the subsequent breakup. The jet divergence angle is dependent on gas density such that an increase in density results in greater divergence. Increasing the density also causes divergence to begin closer to the nozzle. Jet divergence angle is also dependant on

fuel viscosity such that decreasing the fuel viscosity will result in a greater divergence angle and as before cause divergence to occur closer to the nozzle. Jet divergence angles are also related to nozzle length. An increase in nozzle length will result in a decrease in the divergence angle.

2.6.2 Fuel evaporation [13]

Spray evaporation follows after spray atomization. The evaporation history of a fuel drop injected into air at conditions typically found at the end of compression in an engine, are dependant on the following phenomena:

- drop deceleration due to aerodynamic drag
- heat transfer from the air to the drop
- mass transfer away from the drop

As the drop velocity decreases there is a reduction in the convective heat-transfer coefficient between the drop and the air. As the temperature of the drop increases due to heat transfer, there is an increase in the fuel vapor pressure and hence the evaporation rate. As the mass transfer rate away from the drop increases, the heat transfer to the drop surface decreases. When the phenomena described above are combined, the resulting behaviour is shown in Figure 7.

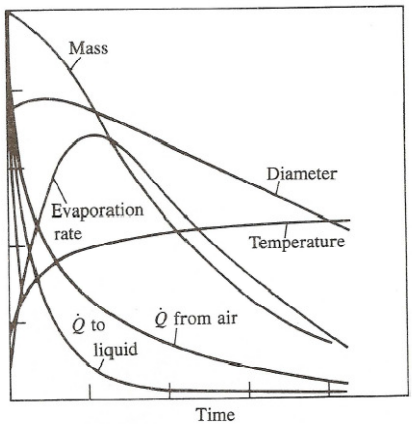

Figure 7: Variation of various parameters with time during the evaporation process. [13]

Studies have shown that combustion is limited far more by fuel-air mixing as opposed to evaporation because 70-95% of the injected fuel in diesel engines, under normal diesel operating conditions, is in the vapor phase at the beginning of combustion however only about 10-35% of the vaporized fuel has mixed appropriately with the fuel for combustion purposes.

2.7 Models for spray penetration

Spray penetration in the combustion chamber is a critical factor for the mixing of fuel and air. The equation determined by Dent [14] , in 1982, which describes spray penetration (*S*) is:

$$S = 3.07\left(\frac{\Delta p}{\rho_g}\right)^{\frac{1}{4}}(t d_n)^{\frac{1}{2}}\left(\frac{294}{T_g}\right)^{\frac{1}{4}} \quad \ldots (1)$$

where Δp is the pressure drop across the nozzle, ρ_g is the gas density, t is the time after the beginning of injection, d_n is the nozzle diameter and T_g is the gas temperature. Dent's equation is based on a gas jet mixing model for the spray. Other experiments have also been conducted to determine the location of the spray tip as a function of time. From the set of experiments conducted by Hiroyasu and Arai [15] it was found that the spray tip penetrates into the combustion chamber linearly with time until the advent of jet breakup and thereafter penetration varies as the square root of time. Hiroyasu and Arai developed the following equation for penetration:

$$S = 0.39\left(\frac{2\Delta p}{\rho_l}\right)^{\frac{1}{2}} t \qquad \ldots (2) \qquad \text{for } t < t_{breakup}$$

$$S = 2.95\left(\frac{\Delta p}{\rho_g}\right)^{\frac{1}{4}}(d_n t)^{\frac{1}{2}} \quad \ldots (3) \qquad \text{for } t > t_{breakup}$$

$$t_{breakup} = \frac{29\rho_l d_n}{(\rho_g \Delta p)^{\frac{1}{2}}} \qquad \ldots (4)$$

where Δp is the pressure drop across the nozzle, ρ_l and ρ_g are the liquid and gas densities respectively, d_n is the nozzle diameter, and t is the time. The experiments conducted by Reitz and Bracco revealed that jet breakup is also dependent on nozzle geometry as well as on diameter. Under large injection pressures and nozzle geometries where there are short length/diameter ratios, the breakup length becomes very short and breakup can occur on the exit plane of the nozzle.[13]

Work by Sazhin *et al.* [16] focused on determining equations for spray penetrations for two limiting cases: the initial stage and the two-phase flow regime. The initial stage is characterized by spray droplets, injected from the nozzle, which have velocities that are much greater than those of the gas that they are entering into. The two-phase flow regime is characterized by spray droplets which have the same velocity as the entrained air. For diesel sprays, breakup takes place almost immediately after the droplets leave the nozzle. This allows diesel spray penetration to be modeled using the two-phase flow approximation. The spray penetration model developed by Sazhin *et al.* is described as follows:

$$S = \frac{1.189(C_D d_n t)^{0.5}(\Delta p)^{0.25}}{\left((1-\alpha_d)\rho_a \rho_d\right)^{0.25}\sqrt{tan\theta}} \qquad \ldots (5)$$

where C_D is the discharge coefficient, d_n is the nozzle diameter, t is the time, θ is half of the spray cone angle, ρ_a is the air density and α_d is the volume fraction of droplets in the spray, defined as follows:

$$\alpha_d = \frac{9\mu_g}{2r_d^2 \rho_d} \qquad \ldots (6)$$

where μ_g is the viscosity of the droplets, r_d is the droplet radius and ρ_d is the droplet density. [16]

2.8 Related studies conducted previously

There have been numerous experimental and theoretical studies on fuel spray, combustion and emissions characteristics of DME fuel. Studies have also been conducted on the physical and chemical properties of DME. In most cases the fuel spray characteristics were investigated inside pressurised vessels to simulate engine conditions and the combustion and emissions characteristics were investigated inside diesel engines.

2.8.1 Spray studies

Studies by Yu *et al.* [17; 18] focused on the spray characteristics of DME and diesel fuel being injected into a constant volume pressure vessel using a common-rail fuel injection system. All the elements of the common-rail system were standard except for the pneumatic high pressure pump (Haskell) that was used to pressurise the fuel. Both fuels were pressurized to 250, 400 or 550bar and injected into either atmospheric or 30bar chamber pressure. A 5-hole sac type injector was used with an orifice diameter of 0.168mm. The macroscopic spray images were taken using Mie scattering which utilised a CCD camera and a strobe light system. Shadowgraphy was employed, using an Ar-ion laser and an ICCD camera, in one study[17] to investigate the evaporation characteristics of the fuels whereas in another study[18] a nano-light was used in place of the strobe light to visualize the spray at a microscopic level. Images of the spray were acquired at a maximum frame rate of 20 000fps. The start of injection was set to zero upon the first appearance of liquid phase fuel at the injector tip. The authors determined that the repeatability of injections were within 10% of each other. The fuel line pressure trace from Yu *et al.* [17; 18] for both fuels is illustrated below in Figure 8.

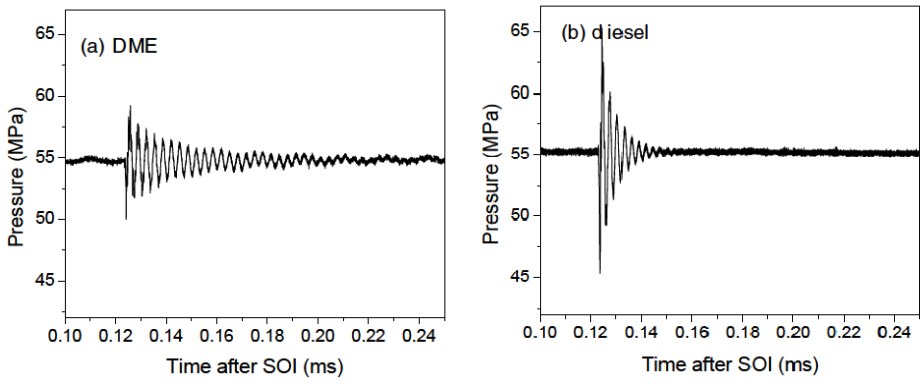

Figure 8: Fuel line pressure versus time of diesel and DME. [Yu *et al.* [17; 18]]

Yu *et al*. found that immediately after injection the fuel line pressure of DME had a smaller amplitude of oscillation but a longer period of oscillation when compared to diesel. This phenomenon is illustrated above in Figure 8. The relevant conclusions drawn by Yu *et al*. were:

1. DME spray is characterized by a mushroom-like tip and flash boiling at atmospheric conditions and that it becomes very similar to diesel at higher ambient pressures.
2. DME has a much shorter spray tip penetration than diesel at atmospheric conditions whereas at 30bar ambient pressure the penetrations are very similar.
3. DME has a much wider cone angle than diesel at atmospheric conditions whereas at 30bar ambient pressure the cone angle of DME is marginally wider.
4. The spray tip penetration of DME becomes longer at higher injection pressures, at constant ambient pressure, and becomes shorter at higher ambient pressures, at constant injection pressure.
5. At atmospheric conditions the cone angle decreased with an increase in injection pressure whilst at 30bar ambient pressure an increase in injection pressure had minimal effect on the cone angle.
6. The spray cone angle of DME was much wider at atmospheric conditions than at 30bar ambient pressure regardless of injection pressure.

Studies by Suh *et al*.[4; 19] focused on investigating the spray development and atomization characteristics of diesel and DME being injected through a common-rail injection system into a high pressure spray chamber. A pneumatic pump (Haskell, HSF – 300) was used to pressurise the fuel. The fuels were pressurised to 400, 500 or 600bar and injected into atmospheric, 10 or 20bar ambient pressures. The ambient gas temperature was also set to 293, 393 or 493K with all other parameters held constant. A mini-sac type injector with a 0.3mm orifice diameter and 0.8mm orifice length was used for the free sprays (in-cylinder sprays were also investigated but they will not be discussed here). The macroscopic spray development was visualized using a Nd:Yag laser in conjunction with a ICCD camera whereas for microscopic spray analysis a phase Doppler particle analyzer (PDPA) system was employed. Images of the spray were acquired at a maximum frame rate of 10 000fps. The start of injection was set to zero upon the first appearance of liquid phase fuel at the injector tip. All the data was obtained from averaging the values from 10 images for each condition. Some relevant results from Suh *et al*.[4; 19] are illustrated in Figure 9, Figure 10 and Figure 11 below. Hiroyasu's correlation is shown by the lines in the plots in Figure 9 and Figure 11 and Sazhin's correlation can also be found in Figure 11 for comparative purposes.

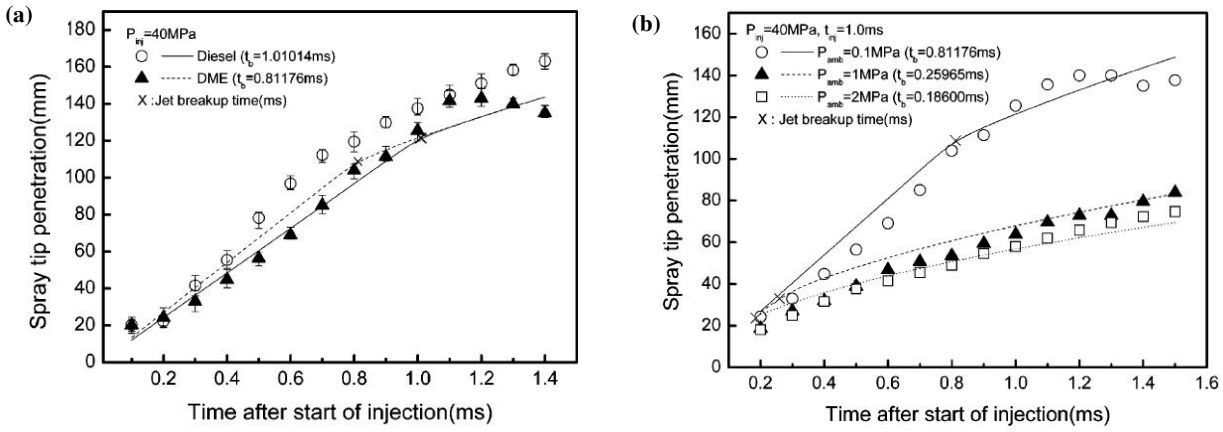

Figure 9: Penetration versus time (a) diesel and DME at atmospheric pressure; (b) DME at various ambient pressures. [Suh *et al.* [19]]

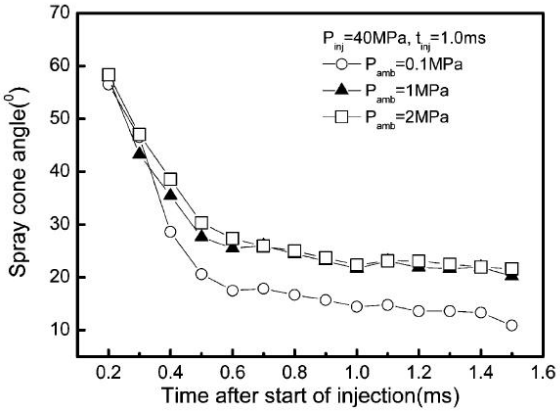

Figure 10: Cone angle versus time of DME for various ambient pressures. [Suh *et al.* [19]]

The two studies by Suh *et al.* drew slightly different conclusions therefore their results will be discussed separately. The relevant conclusions drawn by Suh *et al.* [19] from the first study were:

1. DME has a shorter penetration and a wider cone angle than diesel at atmospheric conditions due to DME evaporating quickly.
2. The spray penetration of DME decreased and cone angle increased with an increase in ambient pressure.
3. The spray tip penetration increased and the spray cone angle decreased with an increase in injection pressure.
4. DME exhibits far less evaporation than diesel along its outer spray region at high ambient pressures (10bar and 20bar) than at atmospheric ambient pressure.

5. Spray tip penetration increased and cone angle decreased with an increase in temperature and the penetration of diesel was always greater than that of DME regardless of the temperature.

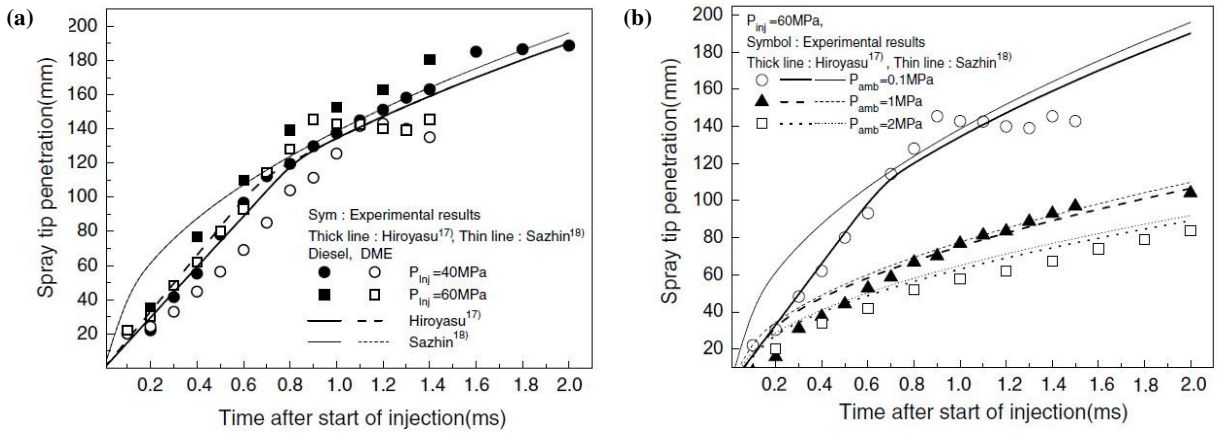

Figure 11: Penetration versus time (a) diesel and DME at atmospheric pressure; (b) DME at various ambient pressures. [Suh *et al.* [4]]

The relevant conclusions drawn by Suh *et al.* [4] from the second study were:

1. DME spray development was shorter and narrower than Diesel for the same injection conditions due to evaporation in the outer region of the DME spray. (note that in the previous study it was reported that DME had a wider cone angle)
2. DME spray development was slower (less penetration) and the cone angle was wider than that of diesel at higher ambient pressures.
3. Hiroyasu's correlation is in good agreement with the experimental results, at atmospheric ambient pressure, throughout the entire duration of the spray. For higher ambient pressures Hiroyasu's correlation overpredicts the penetration during the early stages of spray development.
4. Sazhin's correlation always overpredicts the penetration during the early stages of spray development, regardless of ambient pressure. During the latter stages of spray development the penetration predicted by Sazhin is much closer to the experimental values.

Kim *et al.*[20] studied the spray characteristics of DME being injected into a constant volume pressure vessel. Similar to the two authors above, a pneumatic pump and a common-rail injection system were used to pressurise and inject the fuel respectively. For the spray visualization component of the study the injection pressure was set to 400bar, injection duration to 3ms, temperature to either 300K or 600K and the back pressure to either 15bar or 30bar with nitrogen gas. A common-rail injector was used with an

orifice diameter of 0.22mm. Mie scattering technique was used to visualize the liquid phase of the spray whereas shadowgraphy was employed to visualize the vapour phase of the spray. The spray penetration and cone angle results are illustrated below in Figure 12.

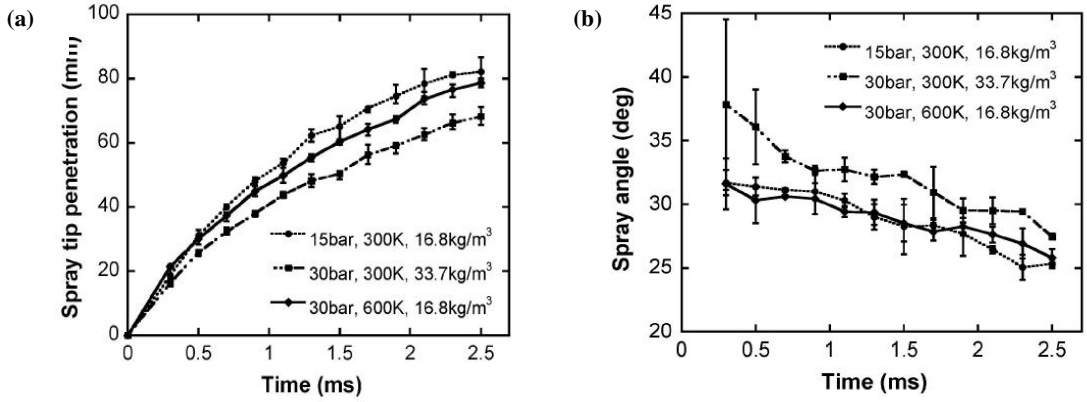

Figure 12: (a) Spray penetration versus time; (b) cone angle versus time at 400bar injection pressure. [Kim *et al.* [20]]

The relevant findings made by Kim *et al.*[20] from the spray visualization component of the study were:

1. The spray tip penetration of DME became shorter and the cone angle became wider with increasing ambient pressure.
2. The liquid phase spray of DME did not penetrate past a specific length (24mm) when the ambient temperatures and pressures were high.

Hwang *et al.*[21] also studied the spray characteristics of DME in a common-rail injection system that utilised a pneumatic pump (Haskell, MS-71) to pressurise the fuel. The injection pressure was fixed at 350bar throughout all the experiments and the ambient pressure was set to 6, 10 and 15bar with nitrogen gas. The effect of injector orifice size was also investigated with three different sized orifices: 0.2, 0.3 and 0.4mm. The cone angle was measured at three distances from the orifice: $30D_o$, $45D_o$ and $60D_o$. The macroscopic spray properties were measured using shadowgraphy and PMAS (Particle Motion Analysis System). All the data gathered from the images were obtained by averaging the values from 30 images for each condition. Some results from Hwang *et al.* are illustrated below in Figure 13 and Figure 14.

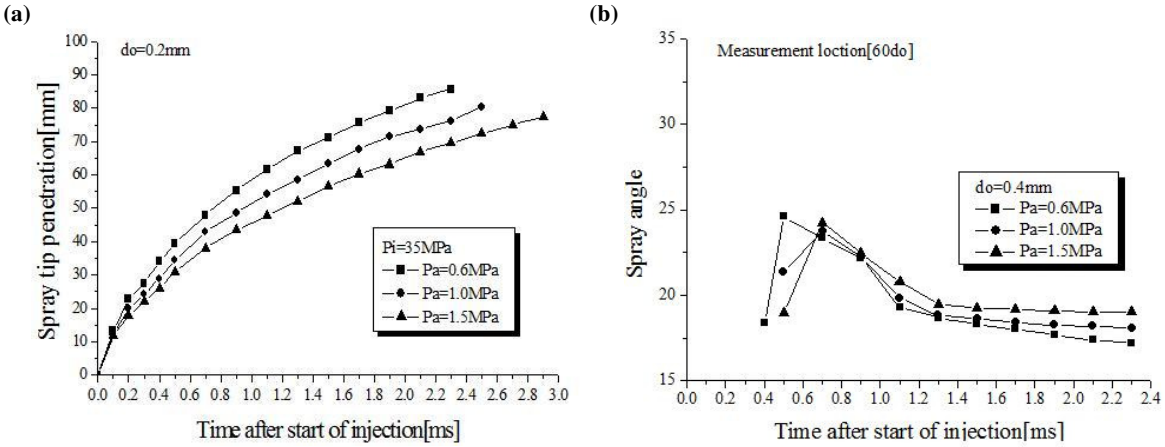

Figure 13: (a) Spray penetration versus time; (b) cone angle versus time. [Hwang *et al.* [21]]

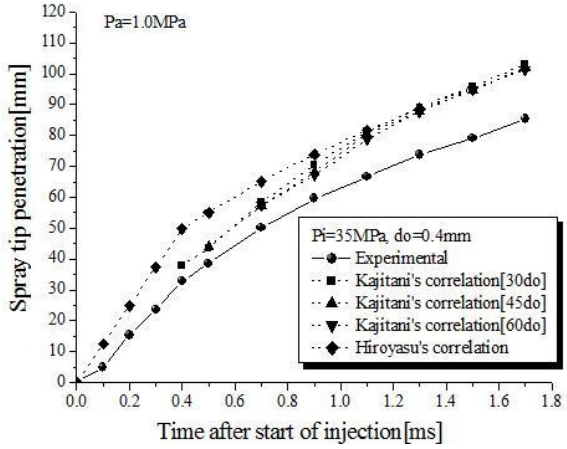

Figure 14: Comparison of theoretical and empirical penetration versus time. [Hwang *et al.* [21]]

The relevant findings made by Hwang *et al.*[21] were:

1. Spray tip penetration decreases with an increase in ambient pressure and increases with an increase in orifice diameter.
2. An increase in ambient pressure causes an increase in cone angle regardless of the location of measurement. (the authors recommended the DME be measured anywhere between $30D_o$ and $45D_o$ downstream of the nozzle)
3. Kajitani's correlation is in closer agreement with the empirical results than Hiroyasu's however neither correlation predicts the empirical results accurately.

Wakai *et al.*[22] studied the spray characteristics of DME and diesel being injected into a pressure vessel as part of their study. An in-line fuel pump was used to supply the fuel to a single-hole injector with an orifice size of 0.2mm and orifice length of 0.8mm. The study employed a schlieren optical system along

with a digital still camera to visualize the fuel sprays (this implies that successive photos of the same spray were not captured, rather photos were taken of different sprays at fixed time increments to obtain a complete set of spray development images). The fuel pressure was set to 98bar for the spray study and the ambient pressure was set to either atmospheric or 15bar with nitrogen gas. Some results from Wakai *et al.* are illustrated below in Figure 15 and Figure 16.

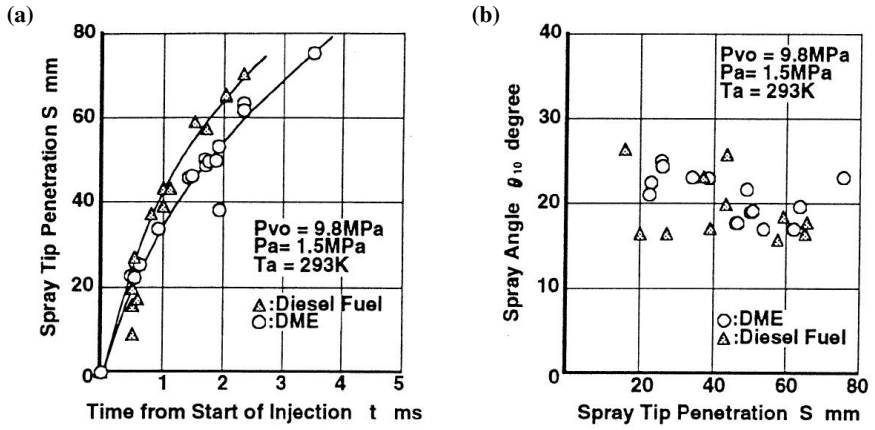

Figure 15: (a) Spray penetration versus time; (b) cone angle versus time at P_b = 1.5MPa. [Wakai *et al.* [22]]

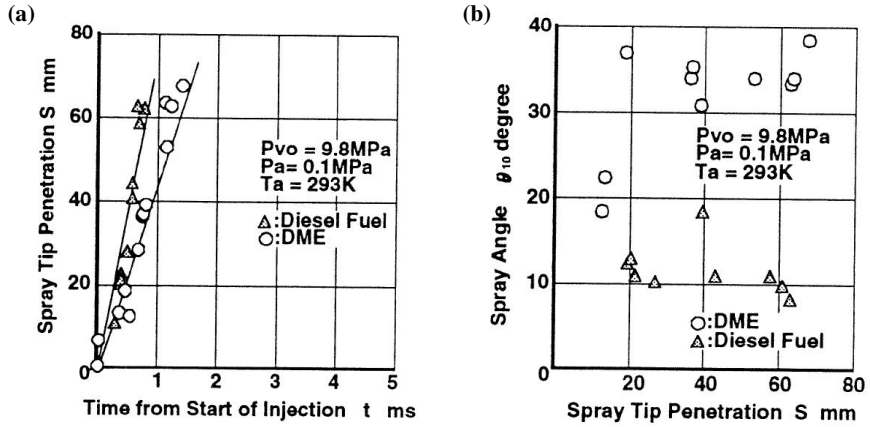

Figure 16: (a) Spray penetration versus time; (b) cone angle versus time at P_b = 0.1MPa. [Wakai *et al.*[22]]

The relevant findings made by Wakai *et al.*[22] from the spray analysis portion of the study were:

1. At atmospheric conditions the DME spray exhibited clusters of vapour clouds at its periphery.
2. Spray penetration of DME is marginally less than that of diesel for identical injection conditions.
3. Spray penetration of DME and diesel both decrease with an increase in ambient pressure.
4. The cone angle of DME is far greater than that of diesel at atmospheric conditions but become very similar at high ambient pressures.

5. The cone angle of DME increases as the ambient pressure decreases whereas diesel behaves to the contrary.

Li *et al.*[23] studied the spray characteristics of DME being injected through a common-rail system into a pressure vessel. Diesel fuel was supplied by a high pressure diesel pump. Solenoid type DME injectors were employed with 3 different orifice sizes: 0.5, 0.7 and 1.2mm. The injection pressure was set to 100, 130 or 160bar and the ambient pressure was set to 20, 30 or 40bar with nitrogen gas. The injection quantity was also varied from 10mm^3/str to 72mm^3/str to see the effect it had on the spray. A schlieren optical system in conjunction with a high speed camera was used to record the spray images. The camera was set to capture images at a rate of 9000fps. Some results from Li *et al.*[23] are illustrated below in Figure 17 and Figure 18.

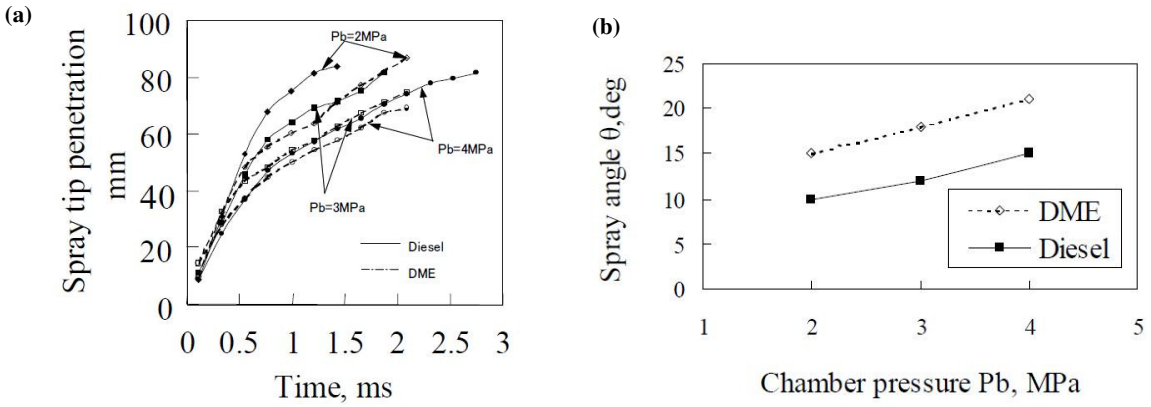

Figure 17: (a) Spray penetration versus time for diesel and DME; (b) cone angle versus chamber pressure of diesel and DME. [Li *et al.* [23]]

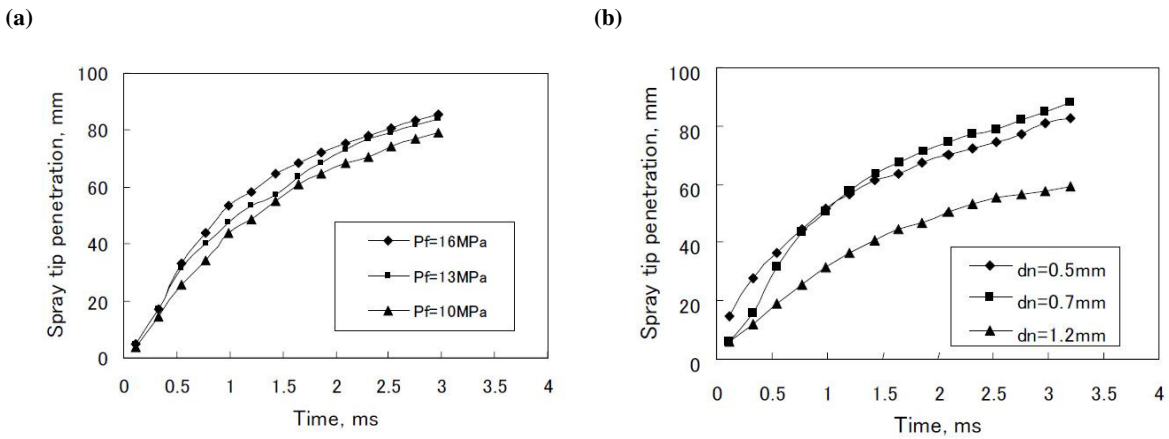

Figure 18: (a) Spray penetration versus time for DME at various back pressures; (b) spray penetration versus time of DME for various orifice sizes. [Li *et al.* [23]]

The relevant findings made by Li *et al.*[23] from this study were:

1. DME spray behaves similarly to diesel spray with the variation of chamber pressure, however the penetration of DME is shorter and the cone angle wider than that of diesel for identical conditions. The differences between the two fuels decrease at higher chamber pressures.
2. The spray tip penetration of DME increases with an increase in injection pressure and orifice diameter and the cone angle increases with an increase in orifice diameter.
3. During the latter stages of spray development the spray front became wider at higher injection pressures.
4. The spray penetration of DME remains largely unaffected with injection quantities greater than 20mm^3/str. However for lower injection quantities (10mm^3/str) the penetration was much smaller than at larger injection quantities. The spray front was wider at larger injection quantities.

Lee *et al.*[24] investigated the spray characteristics of DME being injected into a constant volume chamber through a common-rail system as part of his study. The system used a hand pump to manually pressurise the fuel. A single-hole electronic injector with orifice diameter of 0.25mm was used. The fuel was pressurised to either 350bar or 500bar injection pressure. The gas in the chamber had an ambient density of either 16kg/m^3 or 28kg/m^3 at an ambient temperature of 300K. The cone angle was measured at a distance of 10mm downstream of the injector tip ($40D_o$). Spray images were taken using a backlight scattering technique that used a parallel strobe light and a high speed camera which took images at a maximum frame rate of 9000fps. The measurement of the spray started from the time of appearance of the first fuel droplet. The results for the spray tip penetration and cone angle are illustrated below in Figure 19.

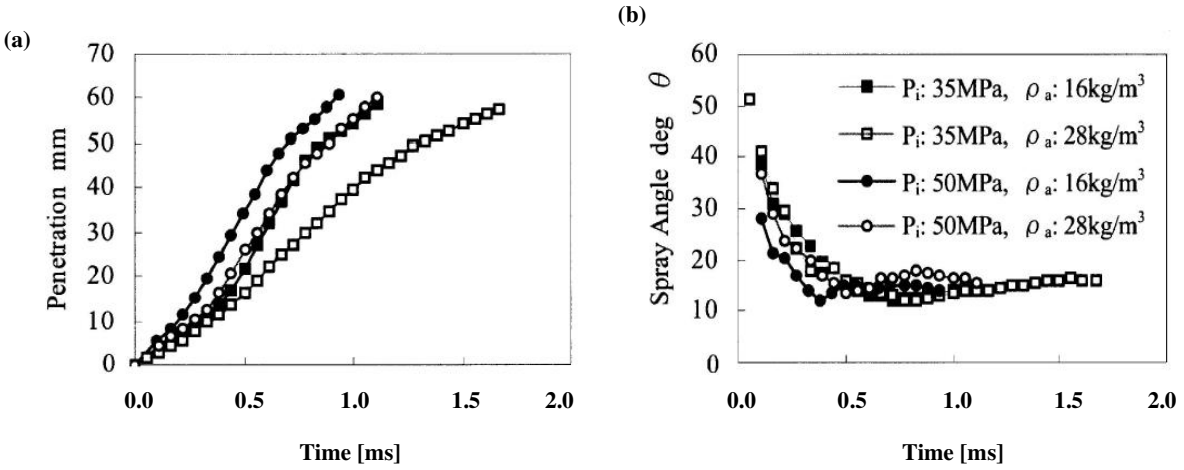

Figure 19: (a) Spray penetration versus time for DME; (b) spray angle versus time for DME. [Lee *et al.* [24]]

The relevant findings from this study were:

1. As the ambient gas density increased the spray penetration decreased and the spray dispersed widely.
2. At higher injection pressures the spray penetration was greater.
3. The DME spray dispersed rapidly, near the nozzle exit, in the early stages of injection due to the flash boiling effect.
4. The injected DME fuel atomized effectively due to its physical properties.

3. OBJECTIVES

The three primary objectives of this particular study on diesel and DME fuel sprays were to:

1. Investigate the behaviour of the fuel spray penetration, cone angle and mean spray velocity for various injection pressures and ambient conditions.
2. Investigate the differences in spray characteristics between diesel and DME both qualitatively and quantitatively.
3. Investigate the behaviour of the fuel pressure in the common-rail system during injection and assess the suitability of the common-rail system for DME injection.

4. DESCRIPTION AND DEVELOPMENT OF APPARATUS

4.1 Description of existing setup

The original setup consisted of the following sub-systems:

- Pressure chamber
- Common-rail system
- AC motor and motor speed control system
- Schlieren optical system
- Pressure measurement system

A description of each of the components contained in each of the sub-systems, their function and their method of operation follows in the sub-sections below. The modifications and additions made to each of the sub-systems are discussed in the next section.

4.1.1 Pressure chamber

The pressure chamber is essentially a cylindrical pressure vessel of 220mm outer diameter, 10mm wall thickness and 370mm length. The vessel has 3 circular windows, 95mm in diameter, to allow for visual access. Two of the windows are opposite each other while the third window is perpendicular to both. An illustration of the vessel can be found in Figure 20 below. The chamber has two lids bolted onto it on either end. To ensure proper sealing an O-ring is fitted into a groove on the inner surface of both lids before bolting them in place.

The top lid is where injectors are mounted onto the chamber. The top lid contains a 10mm hole through which the tip of the injector can be inserted. It also contains 2 studs which in conjunction with some bolts and washers and a mounting plate are used to fasten the injector tightly onto the pressure chamber. The bottom lid contains a sloping inner surface so that any diesel that has been injected into the chamber drains through a centrally located valve on the plate and into a collection beaker outside of the chamber.

Circular quartz (N-BK7) windows were fitted to the opposite facing windows. The chamber has an inlet on its one side whereby nitrogen gas can be fed into the chamber to pressurise it. In addition a pressure gauge is fitted so that the chamber's ambient pressure can be monitored.

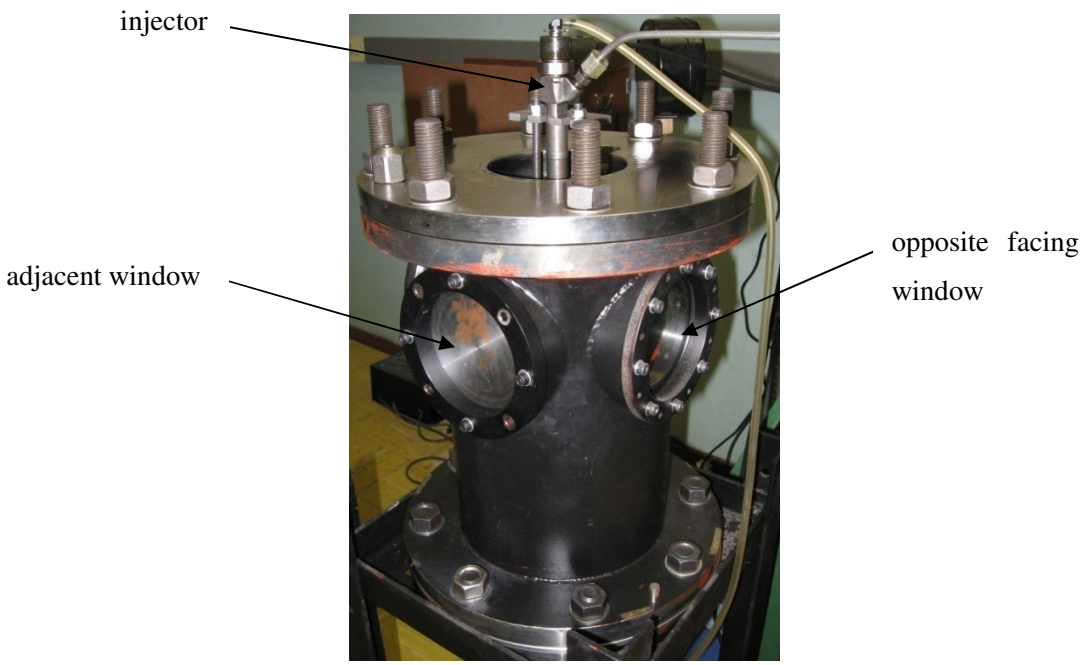

Figure 20: Pressure vessel.

4.1.2 Common-rail system

The common rail system initially comprised of the following components:

- Bosch common-rail (A612 070 00 95)
- Bosch high pressure fuel pump (A611 070 05 01)
- Mechanical fuel injector
- High pressure steel tubing
- Bosch common-rail pressure regulator
- Bosch diaphragm-type pressure transducer
- 12V DC power supply
- Variable resistor
- Diesel reservoir and tubing to supply fuel to the high pressure pump

Diesel was supplied to the high pressure fuel pump from a diesel reservoir, mounted 0.5m above the pump. The pump used was a three piston positive displacement type pump rated to 1500bar. It pressurized the fuel and fed it to the common-rail via high pressure steel tubing. Any excess or overflow fuel from the pump was fed back into the reservoir at low pressure via a feed line from the pump. The common-rail pressure regulator was responsible for building up pressure in the rail itself. The pressure regulator was controlled by adjusting the amount of current supplied to it by a 12V DC power source connected in

series to a variable resistor. When the resistance was high, minimal current would go to the pressure regulator and hence most of the fuel in the common-rail would be sent back to the reservoir at low pressure via a feed from the regulator and hence the pressure would be low in the common-rail. When the resistance was low, more current would be supplied to the regulator and very little fuel would be sent back to the reservoir and hence the pressure would build up in the common-rail. An analogy to explain this would be that the pressure regulator, by accumulating diesel in the common-rail and not releasing it back into the reservoir, provided a resistance against which the pump could pressurize the fuel. The common-rail then fed a mechanical injector which had been set to inject fuel at a specified pressure, by adjusting the spring contained within it. Any excess fuel would flow from the injector at low pressure to a fuel collection beaker. The fuel pressure was effectively built up by adjusting the common-rail pressure regulator or by changing the speed of the fuel pump. Only when the fuel pressure exceeded that set in the mechanical injector did injection begin.

The actual fuel pressure in the fuel line was monitored by a Kistler pressure transducer fitted in the line between the common-rail and the injector. The Bosch pressure transducer was initially not utilized to take any pressure measurements due to the fact that its accuracy was unknown and its resolution was not fine enough. Depending on the reading from the Kistler transducer the amount of current going to the pressure regulator was adjusted to obtain the target system pressure. If at a given pump speed the system pressure could not be increased any further by only adjusting the pressure regulator then the pump speed was further increased. An illustration of the existing common-rail system can be found below in Figure 21.



Figure 21: Common-rail system.

4.1.3 AC motor and motor speed control system

A 2kW AC electric motor (G.E.C PD 5756/67) was used to provide rotational power to the high pressure pump discussed previously. The speed of the motor was governed by a speed regulator (FRENIC 5000G11) which essentially used pulse width modulation (PWM) to control the voltage supplied to the motor.

4.1.4 Schlieren optical system

The images of the spray were captured using a schlieren optical system. A schlieren setup essentially allows the user to see various density gradients which is useful if the object being photographed is transparent. Schlieren photography relies on the principle of refraction to create an image of varying brightness. The darker the portion of the image taken using the schlieren setup the greater the density in that part of the image. The basic components of the schlieren system used were:

- Light source
- Condenser lenses (2 in total)
- Knife edges (2 in total)
- Parabolic mirrors (2 in total)

- Stands for light source, condenser lenses and knife edges (2 in total)
- High speed camera and camera triggering box
- Image storing card

A schematic diagram for the schlieren setup used during the experiment can be found below in Figure 22. In the schlieren system an artificial light source is focused by a condenser lens. At the focal point of the light, a knife edge is placed to cut-off any stray light and create a beam of light with a well defined edge. The beam then strikes the first parabolic mirror which collimates the light and passes it through the test section. The collimated light then strikes another parabolic mirror which un-collimates the light and focuses it. At the focal point a second knife edge is placed orientated perpendicular to the first knife edge. The light then passes through a second condenser lens which focuses the light onto a camera's sensor.

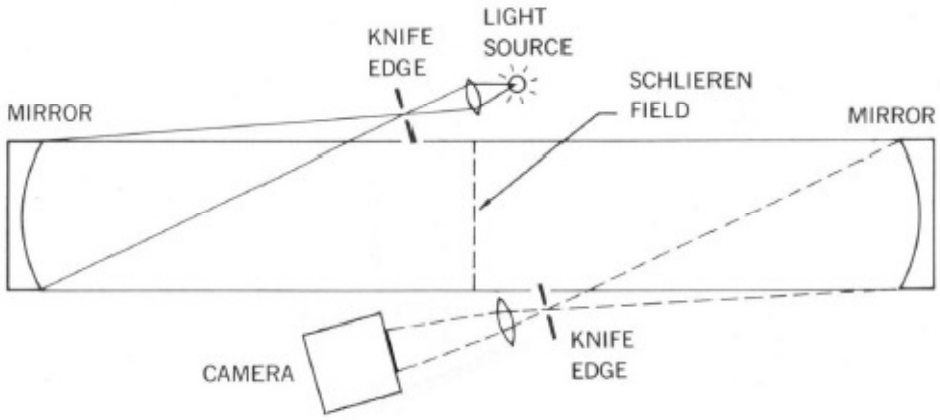

Figure 22: Double-mirror schlieren setup used for experiment. ("*Schlieren photography,* Eastman Kodak Company")

4.1.5 Pressure measurement system

A Kistler piezo-type pressure transducer (Kistler 6229A) that was rated to 1500bar was used in conjunction with a Kistler charge amplifier (Type 5015) to track the pressure of the fuel in the high pressure line between the common-rail and the injector. A signal was first sent from the pressure transducer to the charge amplifier upon a change in pressure. The amplified and calibrated signal from the charge amplifier was then supplied to a Graphtec (GL 1000 Hard Disk Logger) data logging device which subsequently recorded the pressure trace onto a PC. The pressure trace data was recorded at a sampling rate of 50µs.

4.2 Modifications and additions to existing setup

4.2.1 Pressure chamber/vessel

The existing view of the injector tip through the windows can be seen in part (a) of Figure 23 below. The problem with the existing setup was that the hole for the injector tip was centrally located on the top lid of the pressure chamber. As such the full extent of the spray could not be seen due to it being cut off by the edge of the window as a result of the large angle θ between the spray axes of opposite sprays. The value of θ generally varies between 140° to 160° for most multi-hole diesel injectors.

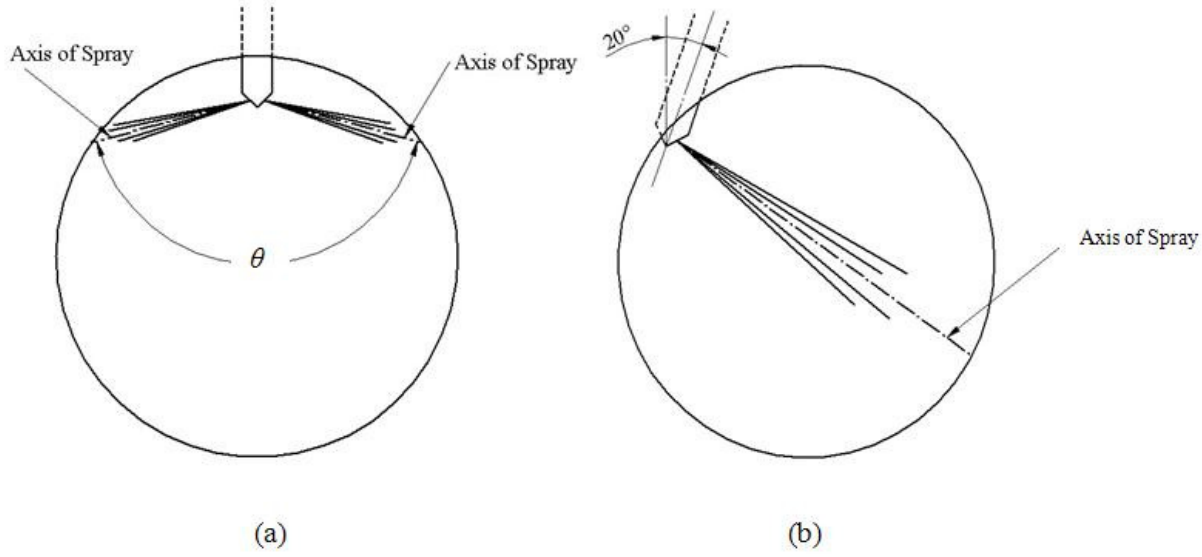

Figure 23: View through the adjacent windows in the pressure chamber; (a) before and (b) after the modification.

A method was then devised to capture as much of the spray penetration as possible by shifting the injector away from the centre and inclining it at 20° to the vertical as seen in part (b) of Figure 23 above. This modification was done to have the injector spray across the diameter of the window and thereby allow for as much of the spray to be photographed as possible. This modification required new holes to be drilled into the top lid of the pressure chamber. The injector tip also had to be modified. A description of the modifications can be found in the section that follows on the common-rail system.

4.2.2 Common-rail system

The injector tip had to be modified for two main reasons. The first was that the sprays from the injector that were out of plane impinged on the windows and dispersed thereby smearing them in diesel as is illustrated in Figure 24. This diesel had to be wiped off the inner side of the windows after every test

which was very time consuming and any nitrogen that was in the chamber had to be dumped before the windows could be cleaned. This was wasteful because the chamber would have to be re-pressurised with nitrogen before every test.

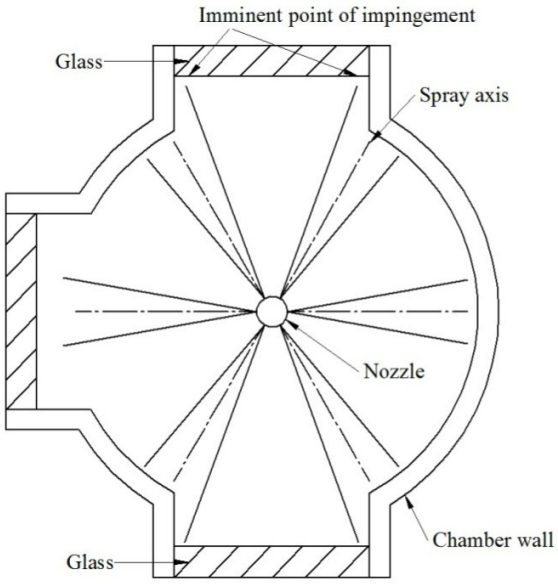

Figure 24: Top view of the pressure chamber showing the direction of the sprays.

The second reason was that the sprays overlapped or rather that they appeared to overlap when an image of the spray was taken. This effect is better illustrated in Figure 25. The spray that is out-of-plane is in front of the spray that is in plane and as a result only the out-of-plane spray is seen when the two sprays overlap. Spray overlap is undesirable because the out-of-plane spray is not of interest, only the spray that is in-plane is of interest because it gives the real penetration and spray angle as well as various other data. The multi-hole injectors that were used had all but one of their injection orifices soldered shut in order to overcome the problems mentioned above. The injector was then mounted such that the spray's axis was parallel to the two parallel windows. Care was taken to not compromise the ability of the plunger inside the nozzle tip from sealing properly on its seat because this would have caused undesirable leaking from the injector tip.

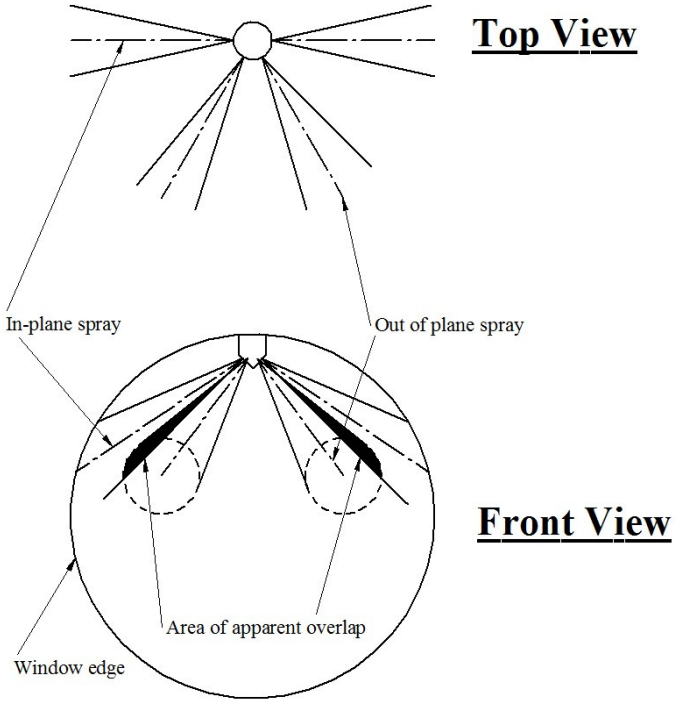

Figure 25: Front and top views of the fuel spray from the injector tip.

The following additions were also made to the common-rail system:

- Electronic injectors (A611 070 13 87)
- Mounting plates for holding the electronic injectors in place
- Injector driver (designed and assembled by Mr. B Mclean)
- Car battery (12V)
- Square wave modulator (SWM) circuit for controlling the Bosch pressure regulator
- Voltage display for the Bosch pressure transducer on the one end of the common-rail
- Low pressure pump for feeding the high pressure pump with diesel fuel

Electronic injectors were a logical addition because they can inject fuel at far higher pressures than mechanical injectors. Thus electronic injectors, rated to 1500bar, were used with an orifice diameter of 0.17mm and their tips were modified such that only one orifice was open. New mounting plates had to be designed and made for fitting and clamping the electronic injectors tightly in place atop of the pressure chamber. The injector driver was used to set the injection frequency to 3.5ms as well as the injection duration to 3ms and was powered by the car battery. The SWM circuit was designed and built specifically for controlling the pressure regulator as opposed to the previous method of using a 12V DC power supply connected to a variable resistor. The screen from the voltage display showed the signal being sent from

the diaphragm-type pressure transducer. The output on the screen corresponded to the fuel pressure in the rail. A calibration sheet showing voltage readings and the corresponding pressure was used to check that the readings from the Kistler transducer were similar to those of the Bosch transducer. The readings from the Bosch transducer were never recorded, but were used as a means of double checking the line pressure before taking any spray images. A low pressure pump was added to the line feeding the fuel to the high pressure pump. This low pressure pump was only used for diesel and not for DME.

The new injector driver mentioned earlier was designed my Mr. Brendon Mclean as part of his final year Research Project. The driver is only capable of triggering Bosch injectors and allows the user to adjust the frequency of injection as well as the duration of injection. When it is switched on it essentially activates a MOSFET switch that closes the circuit between the injector and the 12V car battery. There are two onboard electronic timers, one for controlling the injection frequency and one for the injection duration. The values for these timers are manually adjusted via dials (potentiometers) on the top face of the injector driver's enclosure.

4.2.3 Schlieren optical system

The only change made to the existing setup was that new condenser lenses were fitted because the old lenses were somewhat scratched and a new high-speed camera system was used. The new camera was an Olympus *i-Speed* 3 unit with a full colour CMOS sensor. Images were taken at a resolution of 636×476 pixels at a frame rate of 7500fps.

4.3 Final experimental setup

A schematic diagram of the apparatus used to conduct the experiments in this study is illustrated below in Figure 26. The flow of diesel, DME, nitrogen and information are all represented by different colour lines. The passage of light through the schlieren optical system is represented by the dashed lines travelling from the light source to the camera.

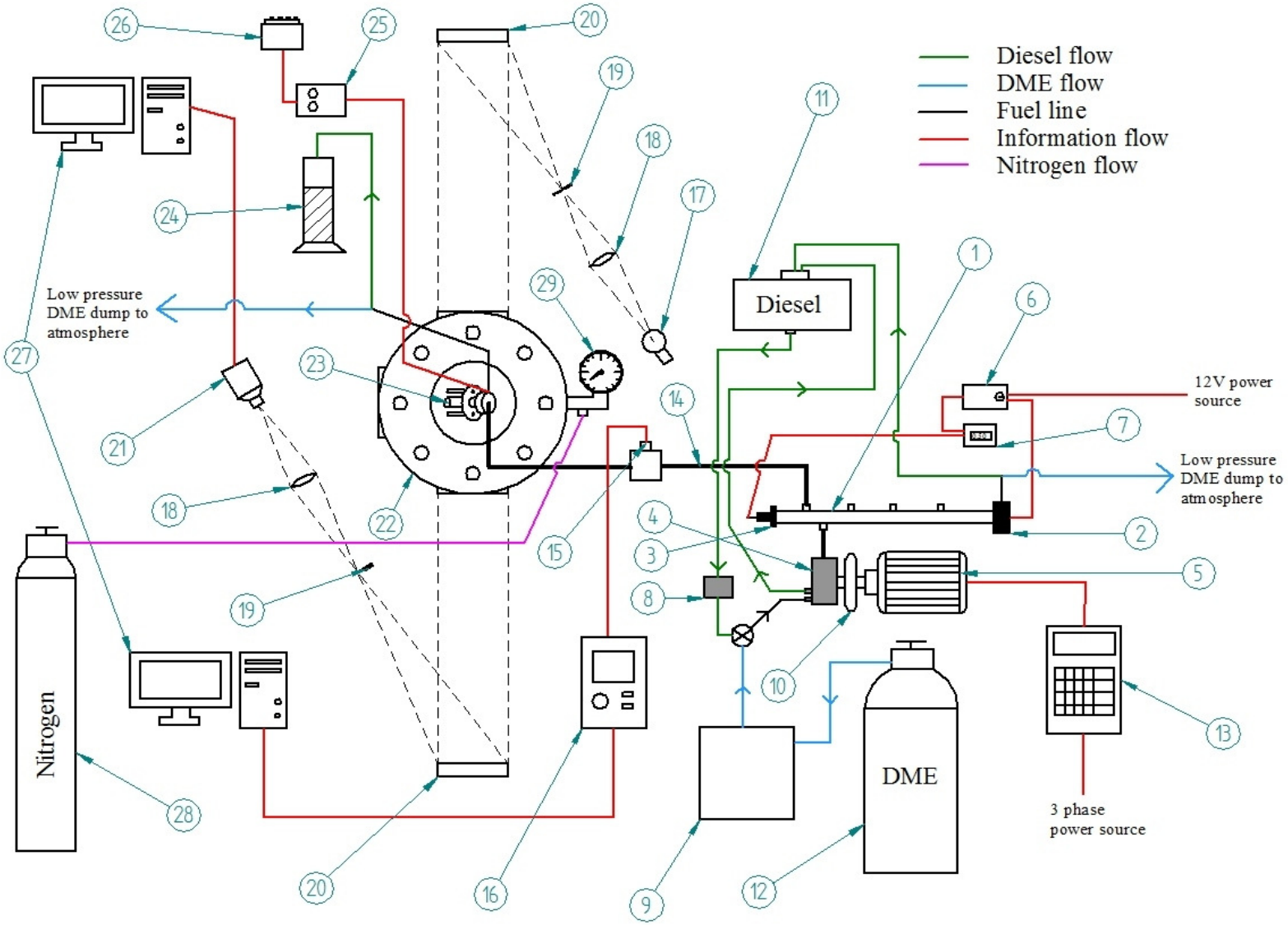

Figure 26: Schematic diagram of the experimental layout.

Table 3: Description of all the items in the schematic diagram.

No.	Description
1)	Bosch common-rail
2)	Bosch pressure regulating valve
3)	Bosch pressure transducer
4)	Bosch common-rail high pressure pump
5)	DC motor
6)	Pressure regulator controller
7)	Voltage readout from pressure transducer
8)	Low pressure diesel pump
9)	DME compressor
10)	Coupling device for pump
11)	Overhead diesel supply
12)	DME cylinder
13)	Controlling unit for DC motor
14)	High pressure fuel line
15)	Kistler piezo pressure transducer
16)	Kistler charge amplifier
17)	Light source
18)	Condenser lense
19)	Knife edge
20)	Parabolic mirror
21)	High speed camera
22)	Pressure vessel
23)	Bosch electronic fuel injector
24)	Diesel collecting beaker
25)	Injector driving unit
26)	12V car battery
27)	Data collecting PC's
28)	Nitrogen cylinder
29)	Pressure gauge for chamber

5. METHODOLOGY

The processes followed when conducting the experiments with diesel and DME fuels are detailed in the sections that follow. The diesel utilised in the experiment had a sulphur content of 50ppm (parts per million) as this represents the highest grade of diesel readily available at fuel stations. The DME used in this experiment was pure DME and did not have any additives mixed to it to enhance its viscosity.

5.1 Initial Start-up Procedures for Both Fuels

The initial step was to activate the 10.8V power supply for the Bosch pressure regulator, voltage display and the Bosch diaphragm-type pressure transducer as well as the 12V power supply for the schlieren light source and the low pressure fuel pump (for diesel fuel only). Thereafter the Kistler charge amplifier was activated and subsequently both the pressure transducers were checked to see that they did in fact give zero readings at atmospheric pressure. The Kistler charge amplifier was then set to transmit a calibrated output signal to the data logger which was viewed through a PC monitor to see if it did indeed correspond to the system pressure.

The next step was to ensure that the image of the test section was focused adequately on the camera sensor. The camera was focused by initially adjusting the condenser lens immediately before it such that the test section's window had a sharply defined edge. A screw with a relatively fine thread was then placed in the test section and if the thread could be clearly distinguished then it was assumed that the image was focused. No adjustments were made to compensate for spherical aberration or chromatic aberration. There was a small degree of chromatic aberration present due to the one condenser lens used immediately before the camera sensor however this had very little impact on the results.

The camera was set to record images at 7500fps until it would fill up its onboard memory used for rapid image storage. This meant the camera could effectively record for approximately 1.2 seconds thus the injection frequency was set on the injector driver such that 3-4 consecutive sprays would be captured for each injection condition.

5.2 Test Procedure for Diesel

The diesel experiments required that the diesel be gravity-fed from the reservoir to a low pressure pump which then supplied the fuel to the inlet of the high pressure pump. If the fuel was to be injected into ambient pressures greater than atmospheric pressure then the pressure chamber was pressurised with nitrogen to the required pressure. Time was given for the nitrogen in the chamber to settle after it had

reached the required pressure. The live-view function of the high speed camera was used to check whether the gas in the chamber had indeed settled (note that this is only possible because the schlieren system highlights density gradients). The low pressure pump was started before the high pressure pump to effectively remove any air bubbles from within the high pressure pump. The high pressure pump was then started by starting the AC motor. The pressure regulator and hence the fuel pressure was adjusted using the dial on the face of the square wave modulator box. When the required fuel pressure was reached the common-rail system was allowed to run for a few seconds at that pressure to ensure that the fuel pressure was indeed stable. Before starting injection the fuel pressure readings from both the pressure transducers were checked to see if they were in agreement with each other. If there were no discrepancies greater than 10bar between their readings then the data logging unit and the camera were first triggered followed very shortly afterward by the injector. At times a significant amount of fouling occurred on the windows when injecting diesel into the pressure chamber. This fouling had to be cleaned off the window before the experimentation could continue.

After having captured a set of results at a specific injection condition, the sprays images were viewed on the monitor attached to the camera. They were then saved to a portable memory source, without using any image compression, before being transferred to a PC for post-processing. The fuel pressure recordings were similarly saved for post-processing. A number of experiments were carried out in this manner with diesel fuel for various injection conditions.

5.3 Test Procedure for DME

The DME experiments required that DME be fed directly to the high pressure pump at a pressure greater than its vapour pressure at room temperature (P_{vapour} = 5.1b at room temperature). The low pressure return from the high pressure pump was blocked because it was not possible to feed the DME back into the cylinder that it was stored in. As with diesel the chamber was pressurised when required and the nitrogen gas was allowed to settle after having reached the correct pressure. DME was then allowed to flow from the tank into the pump and the rest of the common-rail system. The connection between the injector and high pressure steel tubing was then loosened in order to allow for the residual diesel to be purged from the system by the pressurised DME. In addition to this precaution the first few injections after switching from diesel to DME were ignored because it was found that there was still residual diesel remaining in the injector.

The high pressure pump was then started by starting the AC motor and the fuel pressure was set by adjusting the dial on the square wave modulator box. In the DME experiments the common-rail system was not allowed to run for a few seconds after it had reached the target fuel pressure, especially for fuel

pressures of 400bar and 500bar, because it was observed that the system could not hold these pressures reliably for a few seconds. Thus immediately when the target pressure was reached the pressure reading from the two separate transducers were compared and if there were no discrepancies, greater than 10bar between them, then the camera and data logger were first triggered followed very shortly by the injector. The fouling on the windows, due to DME, was negligible when compared to diesel thus very little cleaning had to be done. The same process was followed for saving the images and the pressure readings as with the diesel tests. A number of DME experiment were carried out in this manner for various injection conditions.

5.4 Post-processing of the Results

After the initial images were taken they were post-processed before any meaningful data could be extracted from them. In Appendix A, Figure A1 and Figure A2 show two flow-charts that illustrate the steps taken to process the images. As mentioned previously, the high speed camera was triggered just before the injector. This resulted in a set of background images being taken followed by a set of spray images. The image immediately before a spray appeared was set as the "Background Image". With reference to Figure A1, in step 1 the "Spray Image" was subtracted from the "Background Image" to get a "Subtracted Image". The colour scheme of the "Subtracted Image" was not ideal so in step 2 the colours were inverted and the image was converted to a grayscale colourmap. There was still some noise in and around the spray because the glass windows through which the images were taken could not be kept perfectly clean and free of fuel particles. Thus in step 3 any pixel in the grayscale image that had a white intensity greater than 90% of the whitest white in the image was set to complete white. This eradicated the background noise and created a better defined spray edge which is desirable for measuring penetration and cone angle. In step 4 the "Edge Enhanced Grayscale Image" was cropped and rotated such that the spray was vertical. This was done to make the measurement of cone angle and penetration in particular simpler.

All of the images presented in Appendix B are grayscale images of the spray. With reference to Figure A2, in Appendix A, the grayscale images were obtained by first converting the colourmap of the original image to grayscale and then cropping and finally rotating the image. In a similar way the black and white images were obtained by specifying a threshold limit (between 0 and 1) which converted the original images to a black and white colourmap. The images were subsequently cropped and rotated. The black and white images are not presented here because it was found that different threshold limits had to be employed to various sets of images when converting from the original images. This resulted in an

inconsistent sensitivity scale across all the sets of images, when converting, thus they were not used for qualitative or quantitative analysis.

The spray penetration was determined by initially measuring the vertical pixel distance from the injector orifice to the spray tip. The diameter of the window on either side of the pressure chamber was measured and this was used in conjunction with the size of the window in the images, measured in pixels, to determine a calibration factor. The measured pixel distance between the orifice and the spray tip multiplied by the calibration factor yielded the actual penetration. The cone angle was defined as the angle formed by the lines connecting the injector orifice to two peripheral points on the spray edge at a distance of 10.2mm from the orifice (which is sixty times the orifice diameter of D_o = 0.17mm). The injector orifice was located by examining the images immediately before and after injection. After the orifice was located MATLAB® was used to draw a circle, of diameter $60D_o$ with its origin at the orifice, over the images. Such a spray is illustrated below in Figure 27. The cone angle was determined by first measuring the pixel distance between the two points where the circle intersects the spray and then by trigonometric manipulation the angle was determined.



Figure 27: Spray with circle of size $60D_o$.

The mean spray velocity was determined by finding the difference in spray tip penetration between successive images and dividing it by the time interval between successive images (0.1333ms). This yielded the average velocity of the spray tip from one image to the next image.

6. UNCERTAINTY ANALYSIS

6.1 Measurement Uncertainty

The penetration and the cone angle were measured directly off the image of the spray using the image processing toolbox in MATLAB®. Examples of how penetration and cone angle were measured are illustrated below in Figure 28. The mean spray velocity was then derived from the penetration values.

The degree of measurement uncertainty of the spray penetration was greater for the earlier part of the spray development. In any image the measurement of the penetration may be inaccurate by up to 1 pixel, at most. This translates into a larger percentage of the total spray length when the spray length is shorter, which would be during the early part of the spray. For the majority of the penetration measurements, which exclude the first image where a spray was seen emanating from the spray tip, the degree of uncertainty ranged from 0.25-3.5%. The maximum uncertainty in the measurement of the penetration was determined as being 11.4%. This was for the first spray image at a particular injection condition.

Unlike the penetration, the degree of measurement uncertainty of the cone angle was greater during the latter part of the spray development. The measurement of the line across the spray, at a distance of 10.2 mm from the injector tip, which is used to determine the cone angle, may be inaccurate by up to 2 pixels. Thus when the cone angle is smaller, during the latter parts of the spray development, the uncertainty is greater. The actual measurement uncertainty of the cone angle is greater than that of penetration because the spray boundary along the sides of the spray did not form a regular straight line. Rather the spray appeared to peel off the sides at times, thus forming an irreguar spray boundary. For the majority of the cone angle measurements the uncertainty ranged from 5.5-11.5%. The maximum measurement uncertainty for the cone angle was determined as being 14.15%. A sample calculation which illustrates how the measurement uncertainty was determined can found in Appendix B.

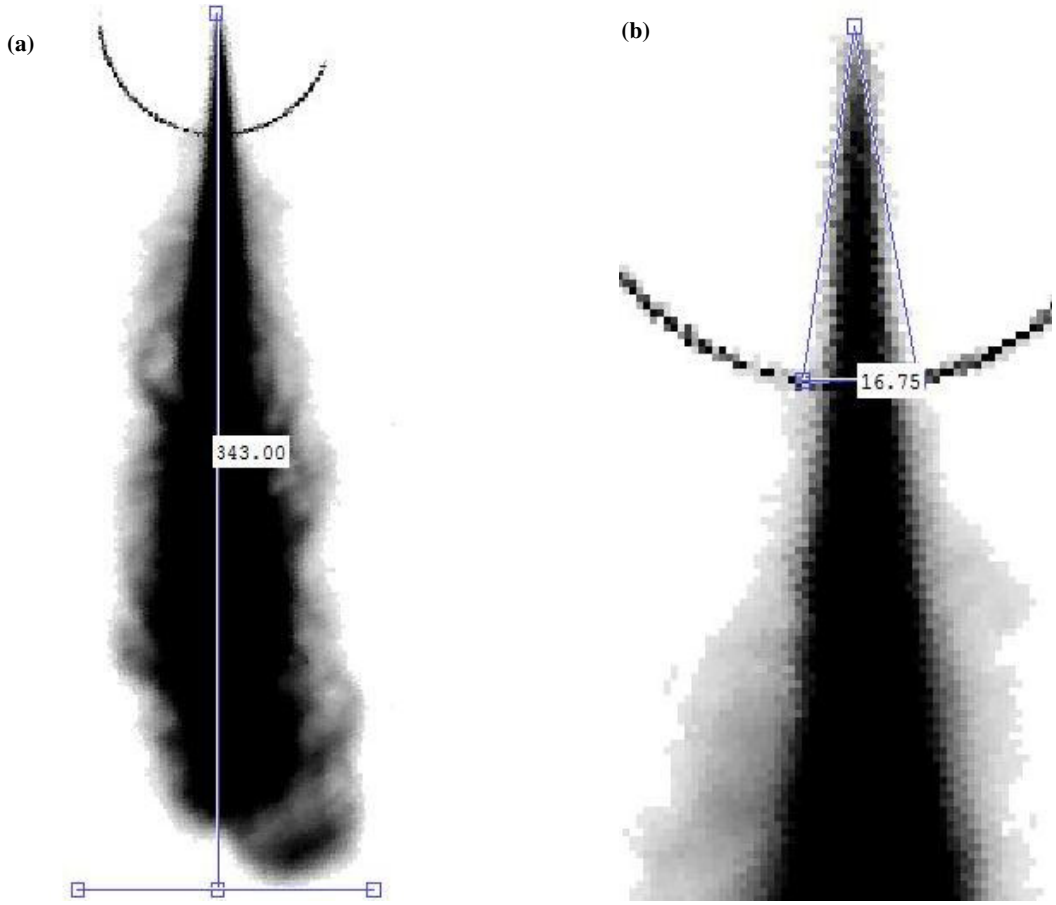

Figure 28: Measurement of (a) penetration and (b) cone angle.

7. RESULTS AND DISCUSSION

An investigation of the spray characteristics of DME versus diesel in a common-rail injection system was conducted in this study. A high speed camera, recording images at 7500fps, in conjunction with a schlieren optical system was used to capture both diesel and DME injection sprays. The injection pressures were varied from 200 to 500bar in 100bar increments and the back pressure was set to: atmospheric, 6bar, 8bar or 10bar. In addition, the fuel line pressure between the injector and the common-rail was also recorded at a sampling rate of 0.05ms.

It should be mentioned at the outset that the high speed camera and the data logging system used to record the pressure trace were not triggered synchronously with the injector as in studies conducted by some researchers. As a result the graphical data presented here is not as a function of time after start of energizing (triggering the injector). Subsequently the first image where a fuel spray was seen emanating from the injector tip was assumed to be half a time frame (0.0667ms) after the start of injection whereas previous studies by Yu *et al*. and Suh *et al*. both set the start of injection to zero upon first appearance of liquid phase fuel at the injector tip. The reason for the difference in the start of injection from these two authors is due to the fact that both the above authors had better time resolution of 20 000fps and 10 000fps respectively. Thus their assumed start of injection was nearer to the actual start of injection than would have possible with a time resolution of 7500fps. The time between successive images of 0.1333ms and the data sampling rate of 0.05ms of the data logger offers enough time resolution to negate any effects of being unable to trigger the high speed camera and the data acquisition system synchronously with the injector.

A comprehensive set of results can be found in Appendices C-E. Appendix C contains a set of spray images, for both diesel and DME, for every injection pressure and chamber back pressure. Appendix D contains the graphs, for both fuels, for spray tip penetration, mean spray velocity and cone angle for every injection pressure and chamber back pressure. Appendix E contains graphs, for both fuels, which depict the pressure history in the fuel line for every injection pressure and chamber back pressure. A selection from the entire set of results is presented here in order to facilitate a better understanding of the discussion that is to follow.

Penetration

Figure 29 and Figure 30 show the theoretical penetration, using Hiroyasu's correlation, for a range of ΔP values. The ΔP, the pressure drop across the nozzle, is the difference in pressure between the common-rail

and that inside the chamber [13]. The fuel pressure in the nozzle tip was set to 100, 90, 80 or 70% of the fuel pressure in the common-rail and the corresponding ΔP was calculated. In both Figure 29 and Figure 30 the injection pressure is 500bar but the former is for atmospheric back pressure whereas the latter is for 10bar atmospheric pressure. In Figure 31 the difference in penetration between Hiroyasu's and Dent's model is illustrated for 500bar injection pressure and 10bar back pressure.

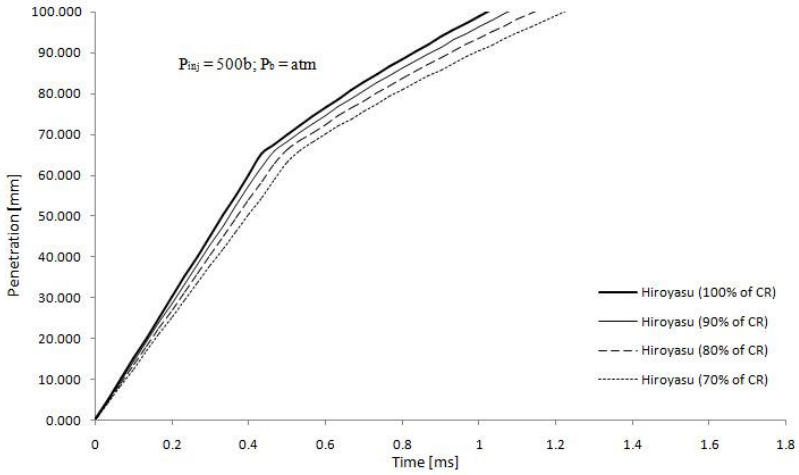

Figure 29: Theoretical penetration plot for various ΔP values (P_{inj} = 500b, P_b = atm)

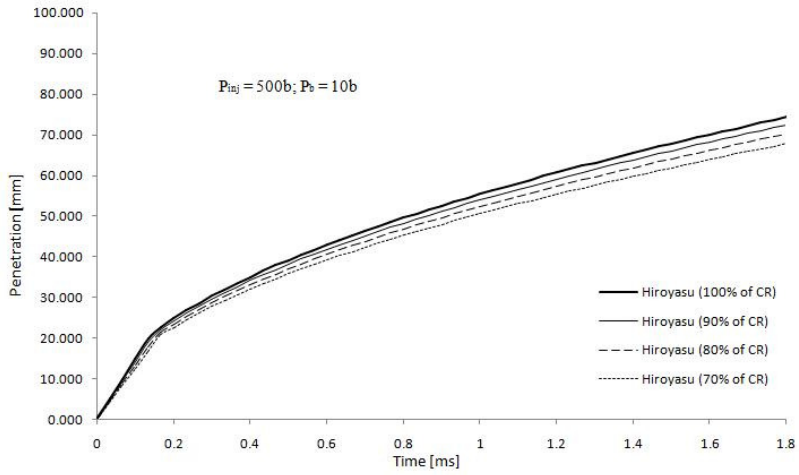

Figure 30: Theoretical penetration plot for various ΔP values (P_{inj} = 500b, P_b = 10b).

A set of sample calculations for the values obtained in Figure 31 can be found in Appendix B.

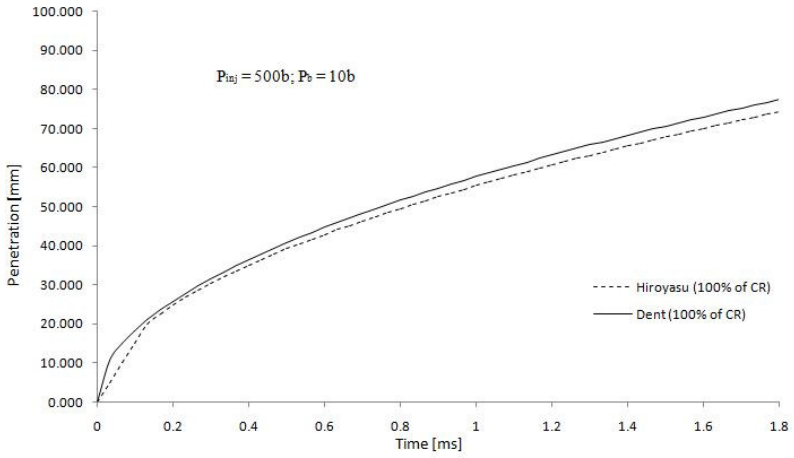

Figure 31: Penetration versus time using Hiroyasu's and Dent's correlation (P_{inj} = 500b, P_b = 10b).

When comparing empirical penetration values to theoretical models, Hiroyasu's correlation was chosen above that of Dent. It was found that although both models overestimated the penetration values during the early stages of injection in most cases, Dent's equation did so by a much larger margin. In Figure 31 the difference between the two models is illustrated for the same conditions. Dent's model differs greatly to Hiroyasu's during the early stages of injection. Thus Hiroyasu's twin regime model with a separate equation for penetration before and after breakup was chosen as the primary theoretical model for comparative purposes because it was a better fit for the data. When using Hiroyasu's equation the pressure gradient across the tip of the nozzle ΔP was taken as being 90% of the common-rail pressure less the back pressure. A sensitivity analysis was conducted to see the effect on penetration if the pressure in the nozzle was reduced from 100% to 70% of the common-rail pressure, in 10% decrements. The results are illustrated in Figure 29 and Figure 30. The penetration decreased anywhere between 2.6% to 5.3% for every 10% reduction in pressure from the common-rail to the nozzle tip. The sensitivity analysis shows that if the actual pressure in the injector tip is ±10% of the assumed amount (90% of rail pressure) then there is a small difference in the penetration value as shown in Figure 29 and Figure 30. It should also be noted that all the spray penetration and cone angle data for diesel is an average of three spray sets whereas the same data for DME is from one spray set. This is due to the fact that during experiments the common-rail injection system was unable to hold the system pressure, in most cases, to within a reasonable range after the first injection had occurred when using DME. This may be symptomatic of the fact that the common-rail system used is specifically intended for operation with diesel. It is speculated that the temperature of the liquid DME fuel (-25˚C) may have caused the pressure regulator on the common-rail and the common-rail pump to malfunction because neither were designed to operate at such low temperatures. In addition the physical characteristics of DME itself may have caused some vapour lock

scenarios inside the pump during operation. During experimentation the seals inside the pump had to be replaced on three separate occasions because of leakage, however, this is a well known occurrence when using diesel seals with DME.

In Figure 32 to Figure 36, the empirical spray tip penetration of diesel is compared to that of DME for the same conditions and Hiroyasu's and in some cases Dent's theoretical penetration model is provided for comparative purposes. The reason for the penetration axes being capped at 100mm from Figure 32 to Figure 40 is due to the fact that the window size only allowed for a spray of approximately 96mm length to be photographed. Anything longer would have exceeded the size of the viewing area and hence would have been cut off. The penetration range of greatest significance, however, is the part during the early stages of the injection because by the time the spray has penetrated 100mm it should ideally have already combusted.

In Figure 32 it can be seen that at 500bar injection pressure and atmospheric back pressure, the penetration of diesel and DME both appear to agree with Hiroyasu's correlation with DME falling just short of Hiroyasu's predicted values before jet-breakup. After the advent of jet-breakup, Hiroyasu's correlation marginally under-predicts the penetration of diesel whereas it over-predicts the penetration of DME. In Figure 33, where the injection pressure is decreased to 400bar, the empirical diesel penetration behaves very similarly to the 500bar case, both before and after jet-breakup when compared to Hiroyasu. The empirical DME penetration, however, is consistently less than that predicted by Hiroyasu with there being discrepancies just greater than 10mm in some cases. Dent's model is also provided in Figure 32 and Figure 33. It is apparent that the model significantly over predicts the penetration during the early stages of the spray when compared to empirical results. In Figure 34, where the injection pressure is 500bar and the back pressure is increased to 10bar, it can be seen that the empirical values for penetration, especially during the early stages of injection, fall short of Hiroyasu's correlation. In some cases the empirical DME penetration is approximately half of those predicted by Hiroyasu. About 0.7ms after the start of injection, the penetration of both fuels seems to reach Hiroyasu's predicted values. The difference between the empirical penetration values and the theoretically expected values decreases with time after jet-breakup. In Figure 35, where the injection pressure is decreased to 300bar, the empirical results are again smaller than those predicted by Hiroyasu during the early stages of injection. In addition, it also takes longer for the empirical diesel penetration values to reach those predicted by Hiroyasu's correlation, taking approximately 1.1ms.

In Figure 36, where the injection pressure is 400bar and the back pressure is 6b, the empirical diesel penetration is seen to exceed that predicted by Hiroyasu at about 0.6ms after injection. This was found to

be the exception rather than the rule during this study with only two other incidences exhibiting this behavior (see Appendix D). It is also evident from Figure 32 to Figure 36 that for the same injection pressure and back pressure the spray penetration of diesel is greater than that of DME. Figure 35 may suggest something to the contrary but it must be borne in mind that the injection pressure for DME was 7% greater than that of diesel for this particular spray set. Furthermore the DME spray data was taken from only one set of sprays and not averaged from three sets as in the case of diesel. The trends from Figure 32 to Figure 36 also suggest that Hiroyasu's correlations over-predict the penetration values at higher back pressures but are more accurate at atmospheric back pressures.

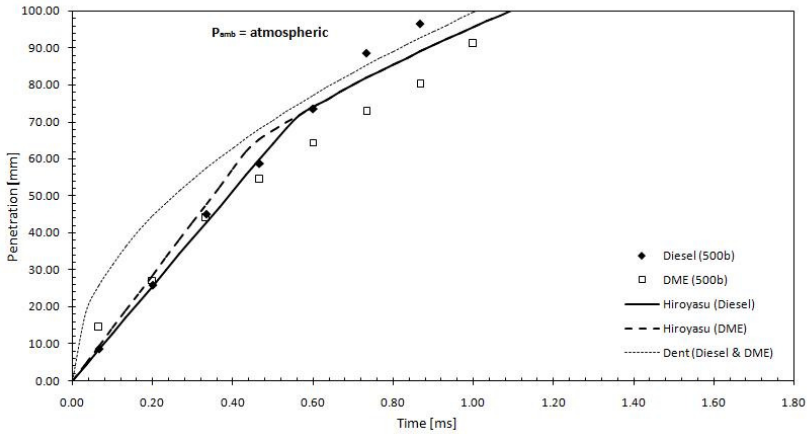

Figure 32: Penetration versus time for diesel and DME (P_{inj} = 500b, P_b = atmospheric)

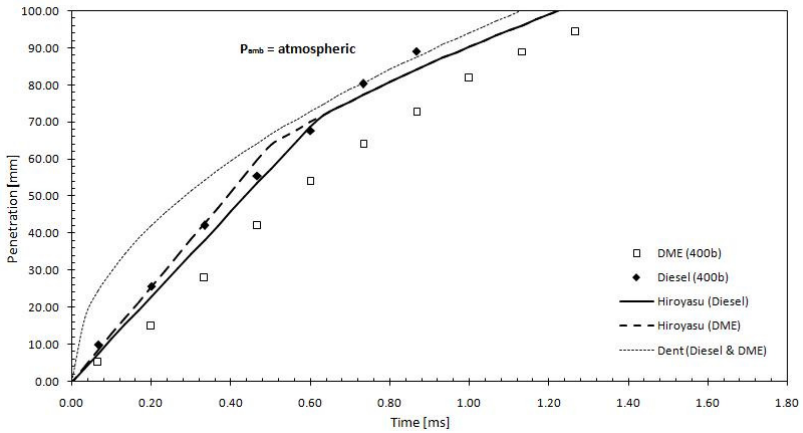

Figure 33: Penetration versus time for diesel and DME (P_{inj} = 400b, P_b = atmospheric)

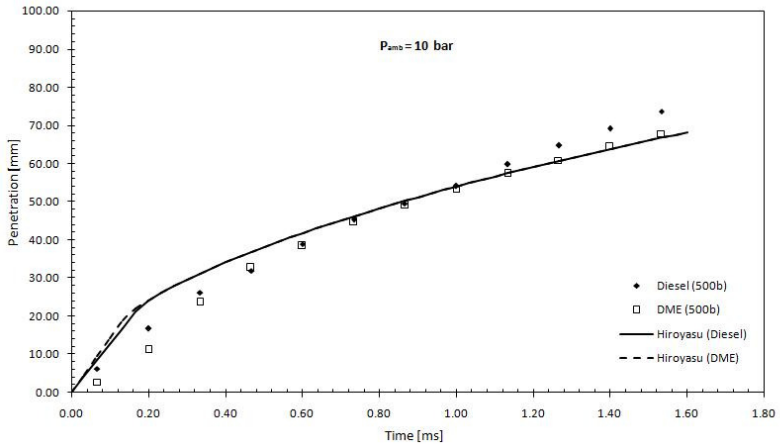

Figure 34: Penetration versus time for diesel and DME (P_{inj} = 500b, P_b = 10b)

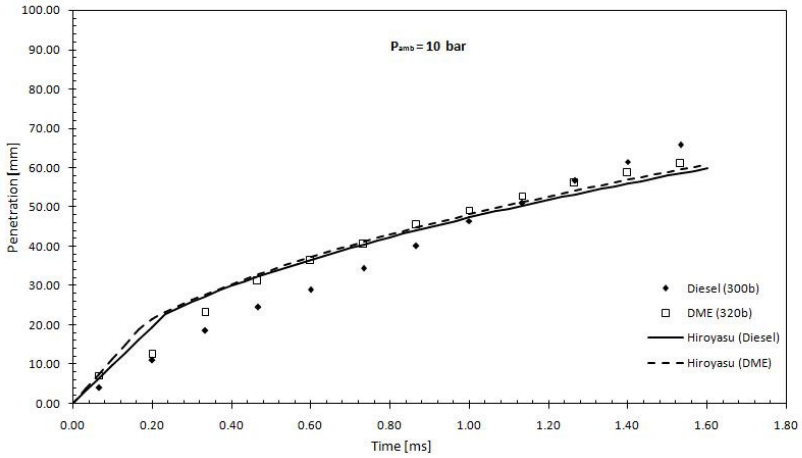

Figure 35: Penetration versus time for diesel and DME (P_{inj} = 300b, P_b = 10b)

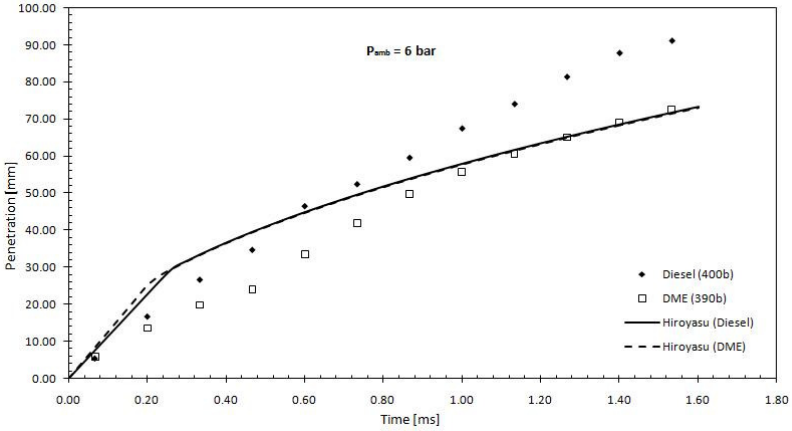

Figure 36: Penetration versus time for diesel and DME (P_{inj} = 400b, P_b = 6b)

In Figure 37 and Figure 38, the empirical spray tip penetration of diesel and DME respectively are plotted for various injection pressures at a fixed back pressure. In Figure 39 and Figure 40, the empirical spray tip penetration of diesel and DME respectively are plotted for a fixed injection pressure at various back pressures.

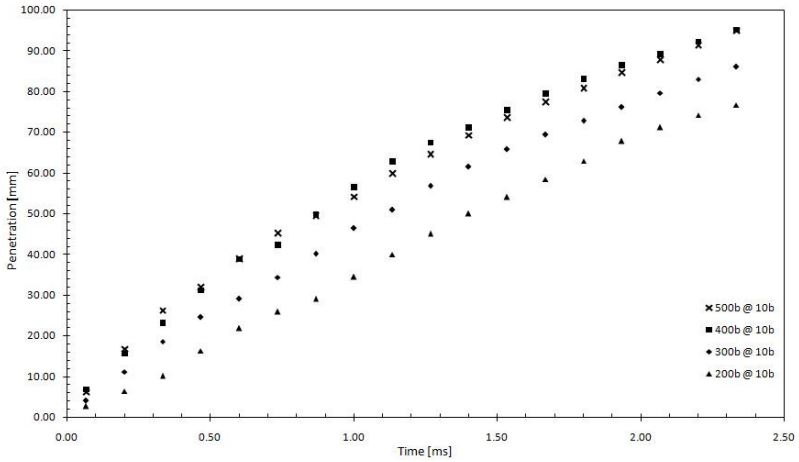

Figure 37: Penetration versus time for diesel at various injection pressures at 10b back pressure.

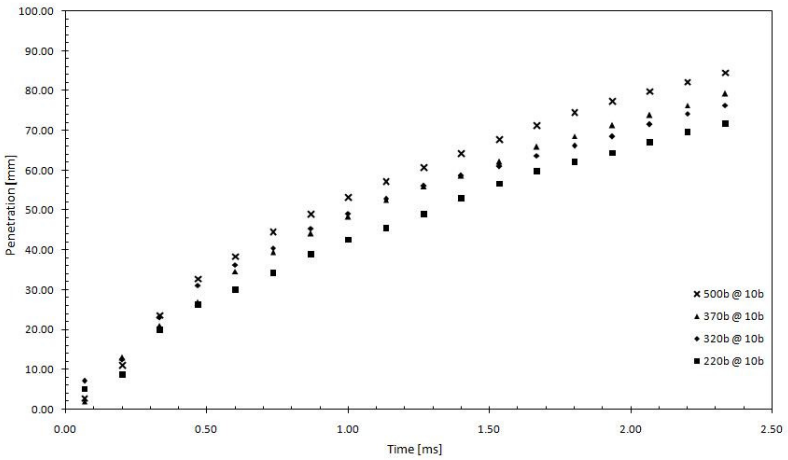

Figure 38: Penetration versus time for DME at various injection pressures at 10b back pressure.

From Figure 37 and Figure 38 it can be seen that as the injection pressure is increased, so too does the penetration increase for both diesel and DME. In both cases it can be said that as the penetration increases with time its rate of change decreases and hence the penetration curve begins to flatten out during the latter stages of injection. As was previously noted, the penetration of diesel is slightly greater than that of

DME for the same conditions. From Figure 39 and Figure 40 it can be seen that the penetration of diesel and DME, at any given time, decreases with an increase in back pressure. The penetration of diesel and DME seems to be almost linear for atmospheric back pressures but as the back pressure is increased the rate at which penetration increases gradually drops with time.

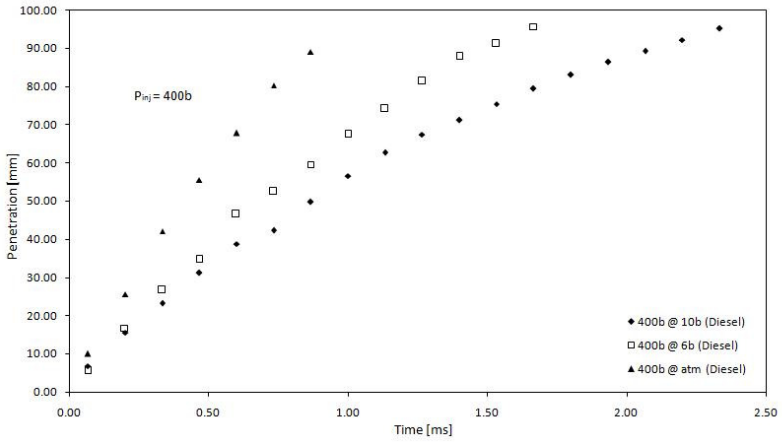

Figure 39: Penetration versus time for diesel at 400b injection pressure and various back pressures.

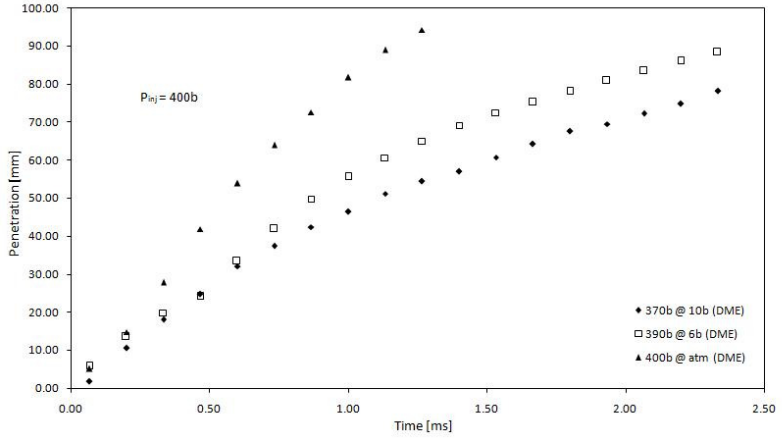

Figure 40: Penetration versus time for DME at 400b injection pressure and various back pressures.

The penetration results from this study are in good agreement with those of Suh *et al* [4; 19], for atmospheric back pressures, because in both cases the empirical penetration is very close to that predicted by Hiroyasu's correlation. It should be mentioned that Suh *et al* [4; 19] used an injector with a larger orifice size of 0.3mm. Yu *et al* [17; 18] conducted the only studies where a similar sized orifice was used to that in the present study. For the same injections conditions it was found that the penetrations from the present study were slightly greater than those found by Yu *et al* [17; 18]. Hwang *et al* [21] found that Hiroyasu's

correlation consistently over-predicted the experimental data whereas Sorenson *et al* [25] found the opposite. Suh *et al* [4; 19], Yu *et al* [17; 18], Wakai *et al* [22] and Li *et al* [23] all found that the penetration of diesel was greater than that of DME, if only marginally greater in some cases, for the same injection conditions.

Cone Angle

The cone angle results are now considered. In Figure 41 and Figure 43, the empirical cone angles of diesel are plotted at fixed back pressures for various injection pressures. The same is done for DME in Figure 42 and Figure 44. The reason for the values of all of the cone angles not beginning at the same time in the plots below is due to the fact that the cone angle was measured at a constant radial distance from the origin of the spray as mentioned earlier (it was measured at $60D_o$). The spray took more time to travel this distance when the injection pressure was lower or when the back pressure was higher. Thus a spray injected at 500bar would reach $60D_o$ sooner than a spray injected at 400bar if the ambient pressure was constant. As a result it would be possible to measure the cone angle of the 500bar spray at an earlier point in time than it would be for the 400bar spray.

In Figure 41 and Figure 42 the variation of cone angle at constant back pressure, 10bar, and changing injection pressures are illustrated. Both diesel and DME behave similarly in that their cone angles decrease with time and converge to a certain range nearing the end of the spray. The cone angle range of diesel varies between 20˚and 50˚ whereas that of DME varies between 20˚ and 35˚. In Figure 43 and Figure 44 the variation of cone angle at a lower constant back pressure, atmospheric, and changing injection pressures is illustrated. Again the cone angle decreases with time, however, in the case of diesel the cone angle, at any point in time, after 0.45ms diverges whereas the cone angle of DME tends to converge. As before, the range of the diesel cone angles is generally larger than that of DME. It was also observed, from Figure 41 and Figure 43, that with diesel the cone angle at lower injection pressures was smaller than that at higher injection pressures during the very early stages of the spray. During the latter spray stages, however, this behavior was reversed with the lower injection pressures having larger cone angles. No such pattern could be seen with DME, however, it can be said that the cone angle of DME does not change much with an increase in injection pressure or with time relative to diesel.

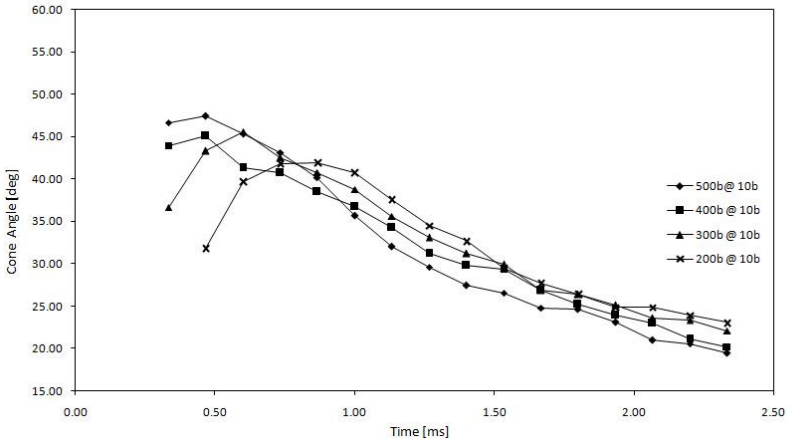

Figure 41: Cone angle versus time for diesel at various injection pressures and 10b back pressure.

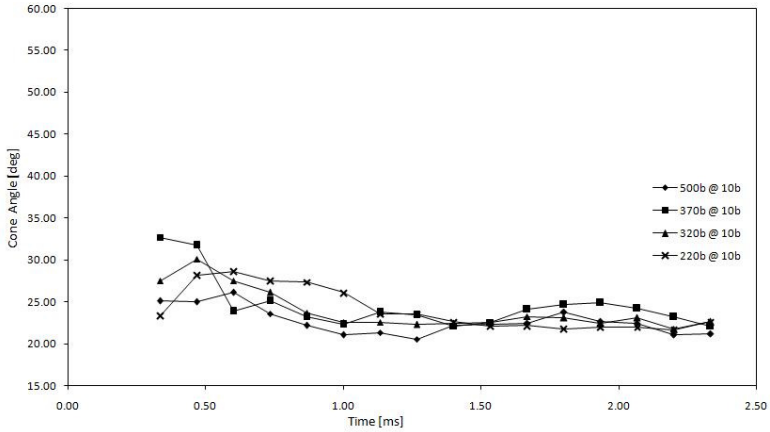

Figure 42: Cone angle versus time for DME at various injection pressures and 10b back pressure.

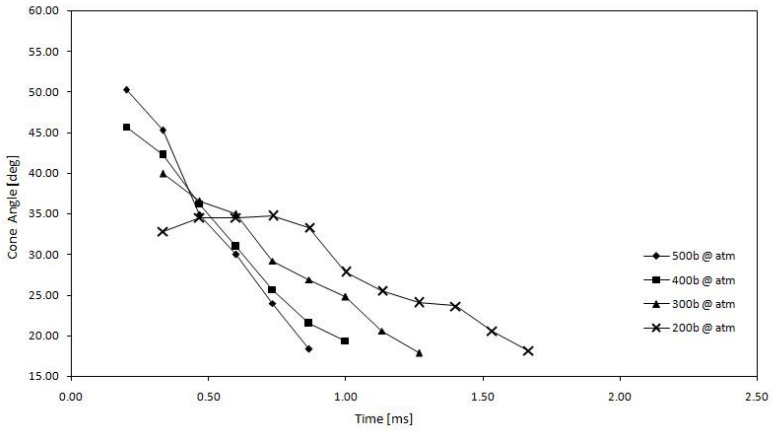

Figure 43: Cone angle versus time for diesel at various injection pressures and atmospheric back pressure.

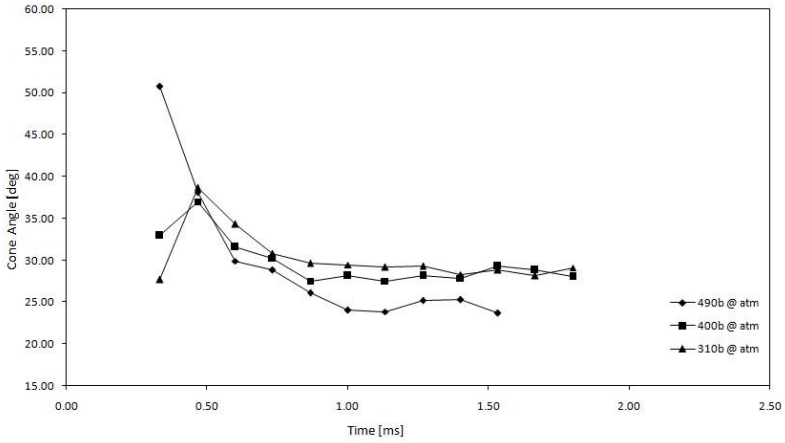

Figure 44: Cone angle versus time for DME at various injection pressures and atmospheric back pressure.

In Figure 45 to Figure 48, the empirical cone angles of both fuels are plotted on the same set of axes for the same injection pressures at different back pressures for comparative purposes. The injection pressures were held constant and the back pressures were varied to see the effect this would have on the cone angle. It was found that the cone angle for diesel sprays were consistently larger than those of DME sprays for the same conditions, with the exception of one case. This occurred during the latter part of the spray development at atmospheric back pressure conditions (see Appendix D). The cone angles of the diesel sprays consistently increased with an increase in back pressure however the same cannot be said about the DME sprays which did not show any particular trends in this regard. Interestingly though, it was observed that for the DME sprays the cone angle was consistently the smallest at the highest back pressure of 10bar regardless of the injection pressure. The reason being that DME experiences rapid expansion due to flash boiling when it is injected into atmospheric pressure at room temperature. This phenomenon is further elaborated later on where the actual spray images are discussed.

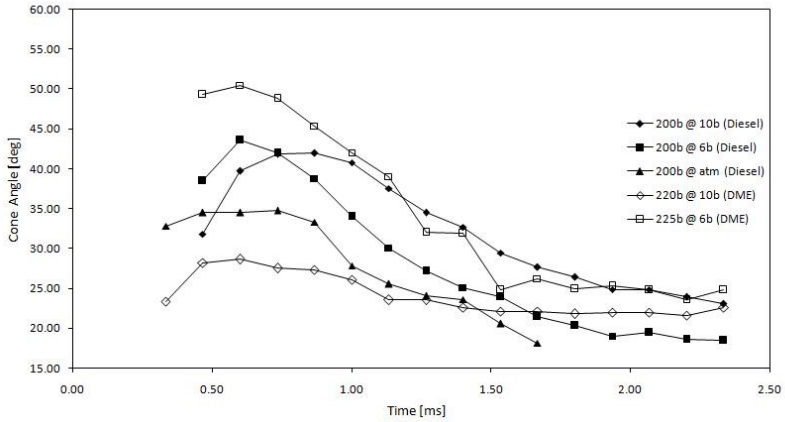

Figure 45: Cone angle versus time for diesel and DME at 200b injection pressure and various back pressures.

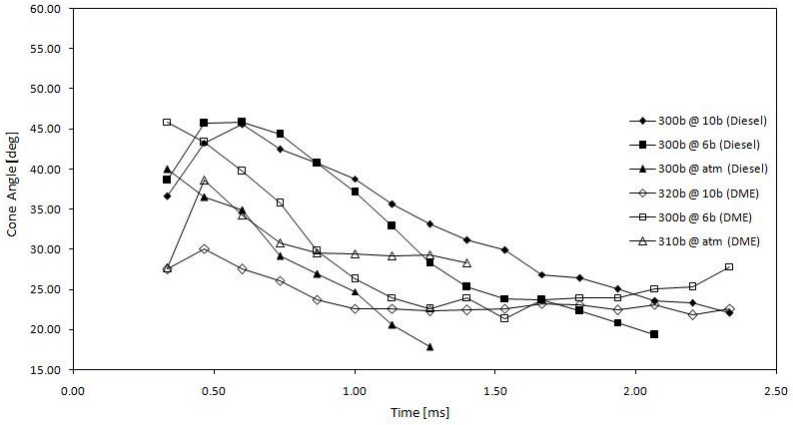

Figure 46: Cone angle versus time for diesel and DME at 300b injection pressure and various back pressures.

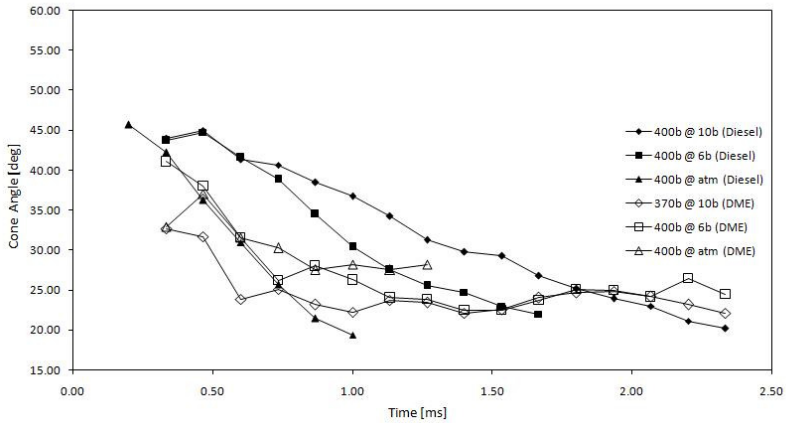

Figure 47: Cone angle versus time for diesel and DME at 400b injection pressure and various back pressures.

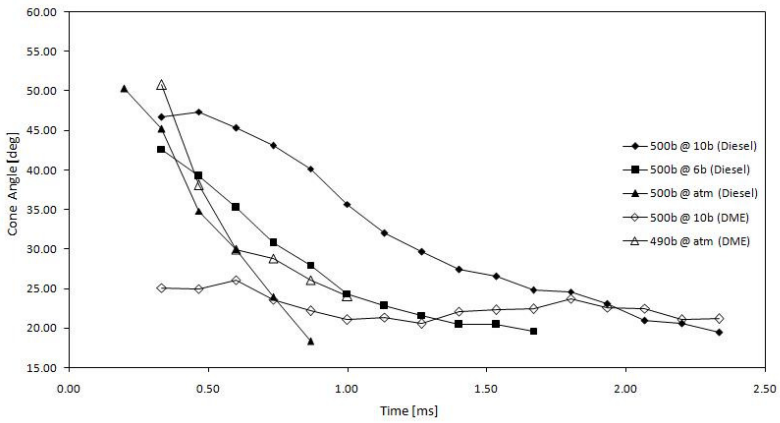

Figure 48: Cone angle versus time for diesel and DME at 500b injection pressure and various back pressures.

When comparing the cone angles from this study to similar studies one must be cognisant of the fact that no singular method was used to measure cone angles across all the studies. The most common method is to measure cone angle at $60D_o$ and that method was used in this particular study. However it was observed that two straight lines drawn from the orifice along the spray boundary to a distance of 10.2mm from the orifice did not accurately follow the spray boundary which often curved in or out from the orifice. As a result this method would sometimes cut-off some spray or include too much spray. When comparing with DME results of Kim *et al* [20] and Hwang *et al* [21] (who both employed the same method) for similar conditions the cone angle results from this study are somewhat comparable especially if the behavior of cone angle with time is considered. Yu *et al* [17; 18] simply defined the cone angle as the angle between the two lines from the orifice that are tangential to both the spray edges near the nozzle tip. In comparison to Yu *et al* [17; 18] the cone angle results from this study are much smaller at atmospheric back pressure for DME and there is very little correlation with the diesel results. The cone angle results of DME from this present study behave very similarly to those of Yu *et al* [17; 18] and Wakai *et al* [22] in that the cone angle of DME was greater at atmospheric back pressure than at higher back pressures. At higher back pressures (10bar) the cone angle results for DME are in agreement with Yu *et al* [17; 18] regarding the fact that there is minimal change in the cone angle from the start of injection regardless of injection pressure.

Mean Spray Velocity

The mean spray velocity results are now considered. In Figure 49 and Figure 51 the mean spray velocity for diesel fuel is illustrated for various injection pressures at atmospheric and 10bar back pressures respectively. In Figure 50 and Figure 52 the mean spray velocity for DME is illustrated for various injection pressures at atmospheric and 10bar back pressures respectively. From Figure 49 to Figure 52 it can be seen that the mean spray velocity initially increases with time, peaks and then decreases. In the case of high back pressures the mean spray velocity for both fuels during the latter half of the spray development stays relatively constant. The spray velocities of the two fuels are also very comparable, regardless of injection pressure, during the latter half of the spray development. The mean spray velocity of both fuels also tends to peak earlier when the injection pressure is greater. At atmospheric back pressure the diesel fuel attained a greater maximum velocity whereas at 10bar back pressure the DME fuel attained a greater maximum velocity.

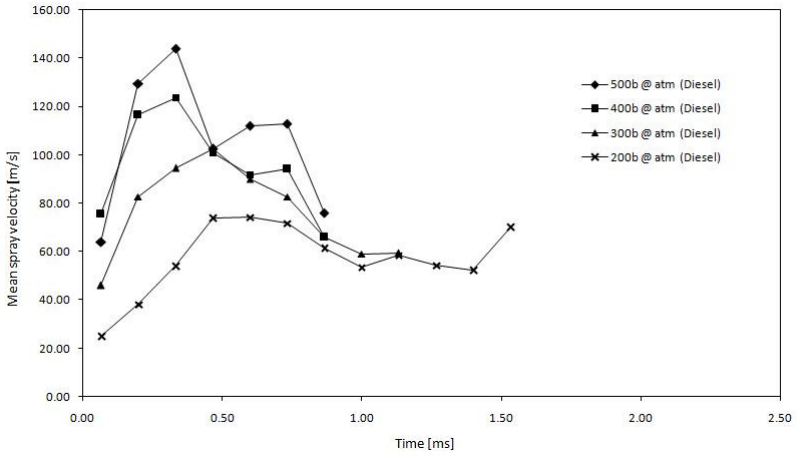

Figure 49: Mean spray velocity versus time for diesel for various injection pressures. (P_b = atm)

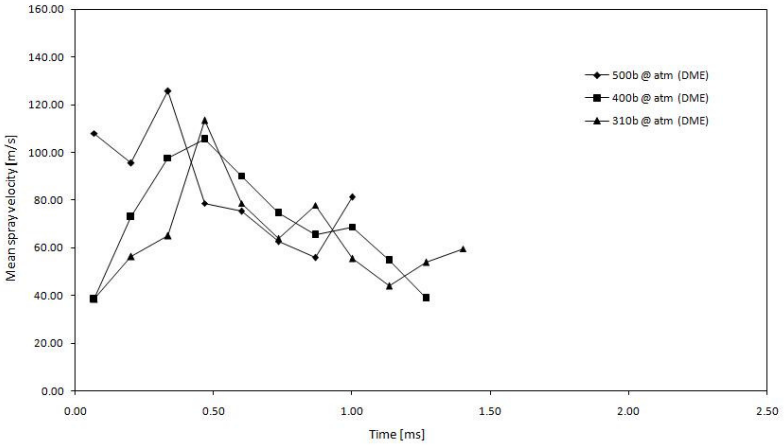

Figure 50: Mean spray velocity versus time for DME for various injection pressures. (P_b = atm)

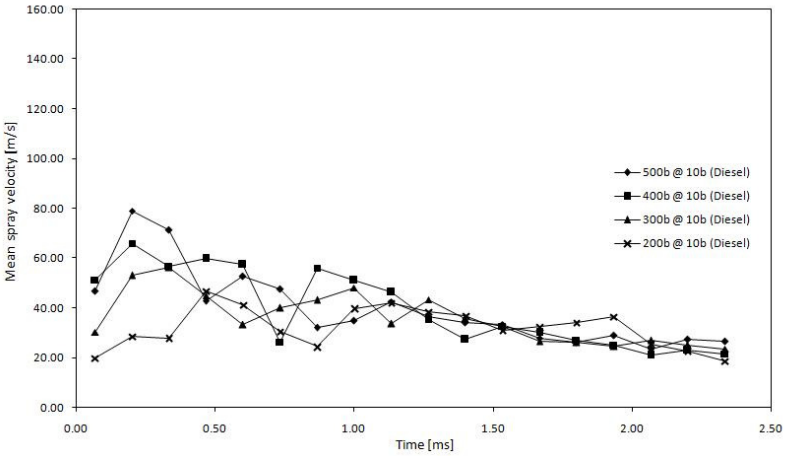

Figure 51: Mean spray velocity versus time for diesel for various injection pressures. (P_b = 10b)

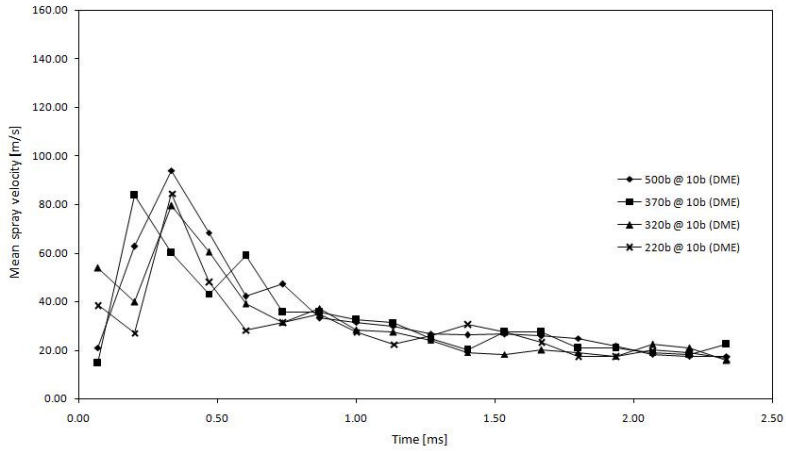

Figure 52: Mean spray velocity versus time for DME for various injection pressures. (P_b = 10b)

Fuel Line Pressure

Fuel line pressure results are now considered. In Figure 53 and Figure 54, the empirical pressure trace for diesel is plotted for 200bar and 500bar injection pressures respectively. In Figure 55 to Figure 57, the empirical pressure trace for DME is plotted for 500bar and 400bar injection pressures. In Figure 58 and Figure 59 a magnified view of the 500bar empirical pressure trace for diesel and DME is provided.

From the two diesel pressure traces in Figure 53 and Figure 54 it was observed that immediately after injection there is a period of pressure oscillation within the system which is accompanied by a drop in fuel pressure of approximately 10-15%. The fuel pressure then increases to the levels it was at prior to injection and the injection cycle is then repeated. It was noted that the fuel pressure, when using diesel, always recovers regardless of the pressure in the common-rail (see Appendix E). Upon closer inspection it is also possible to notice the humps on the pressure trace. This is a characteristic of the positive displacement common-rail pump used which employs three pistons to pressurise the fuel. The three pistons are exactly 120˚ out of phase so each piston provides peak pressure every 120˚ of shaft rotation. In Figure 55 to Figure 57 the pressure traces are shown for DME for 500bar and 400bar injection pressures. The system failed to consistently hold the fuel pressure after the first injection when using DME as is clearly illustrated in Figure 55 and Figure 57. In fact the system did not maintain the fuel pressure after the first injection most of the time. At times the fuel pressure would drop significantly by the time of the third or fourth injection. From Figure 55 it is apparent that in this particular instance the fuel pressure dropped from 500bar just before the first injection to below 400bar just before the fourth injection and from Figure 57 it can be seen that the fuel pressure again drops although not as significantly as before. The humps in the pressure trace, however, are greater and behave somewhat erratically when compared to those of diesel. For this reason when any data was extracted from the DME images, only the first spray was used. Figure 56 illustrates one of the very few instances in this study where the system was able to hold the fuel pressure for more than four consecutive injections. As mentioned earlier it is speculated that the problem with pressurising DME arises due to the operating temperature of liquid DME (-25˚C) as well as the physical characteristics of DME.

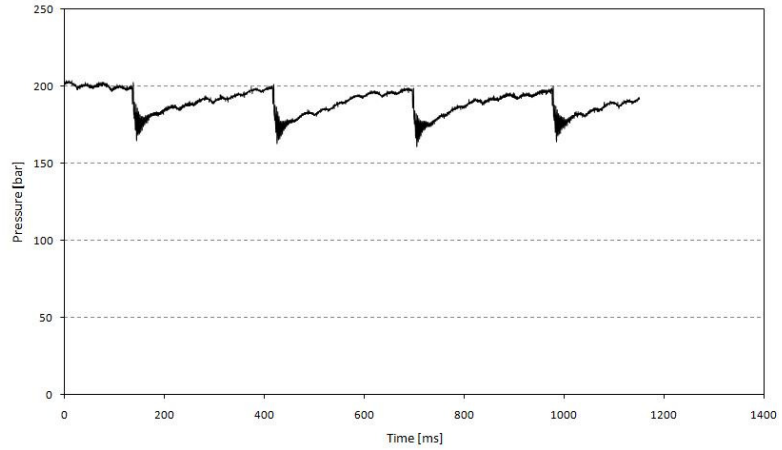

Figure 53: Pressure versus time for diesel injected at 200b injection pressure. (P_b = atm)

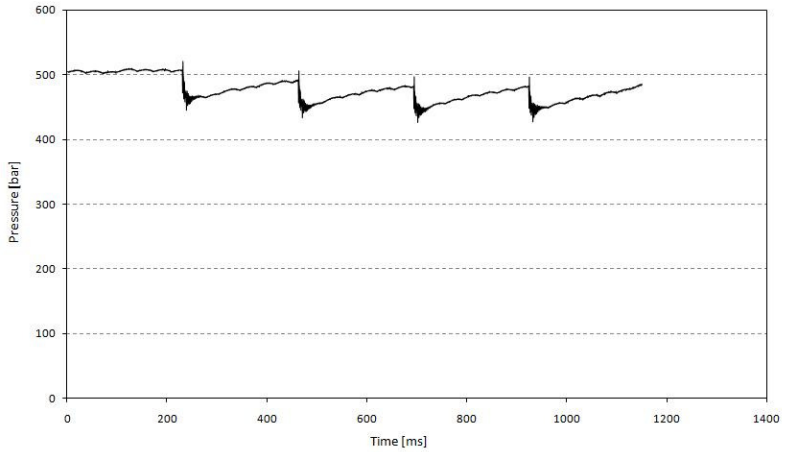

Figure 54: Pressure versus time for diesel injected at 500b injection pressure. (P_b = 10b)

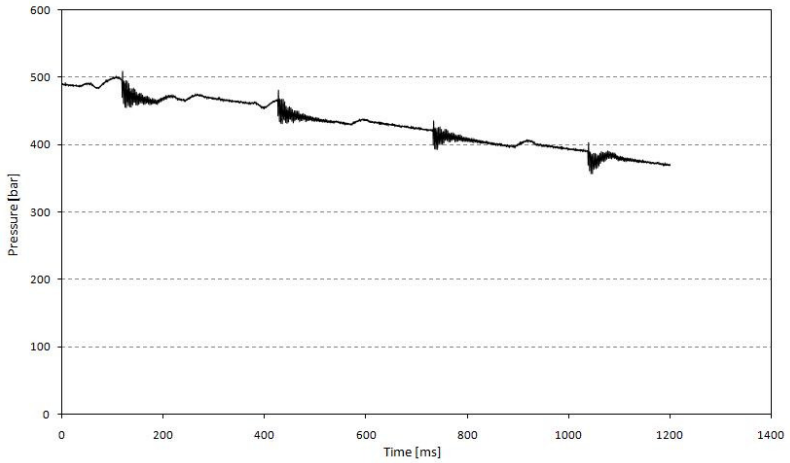

Figure 55: Pressure versus time for DME injected at 500b injection pressure. (P_b = 10b)

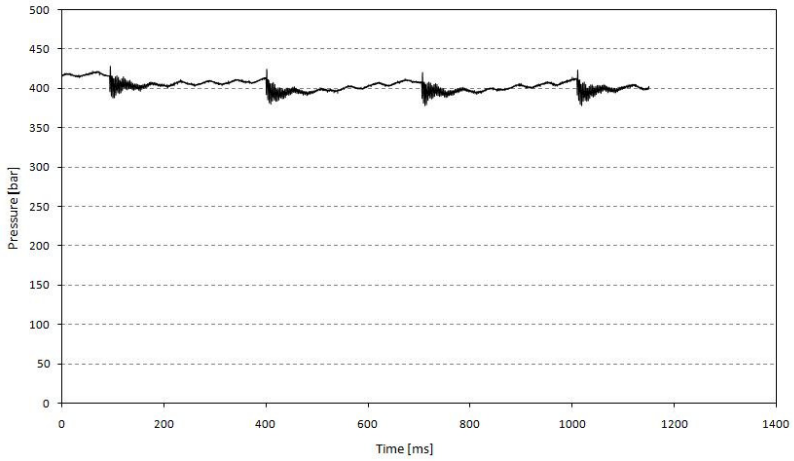

Figure 56: Pressure versus time for DME injected at 400b injection pressure. (P_b = 8b)

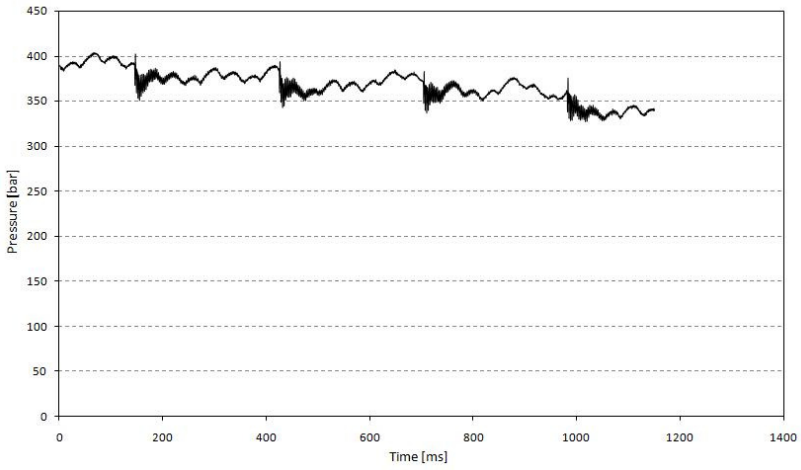

Figure 57: Pressure versus time for DME injected at 400b injection pressure. (P_b = 6b)

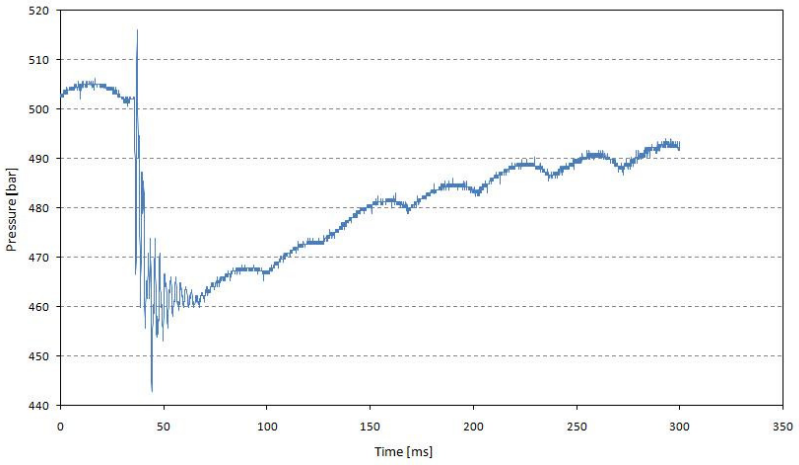

Figure 58: Magnified view of pressure versus time for diesel. (P_{inj} = 500b, P_b = atm)

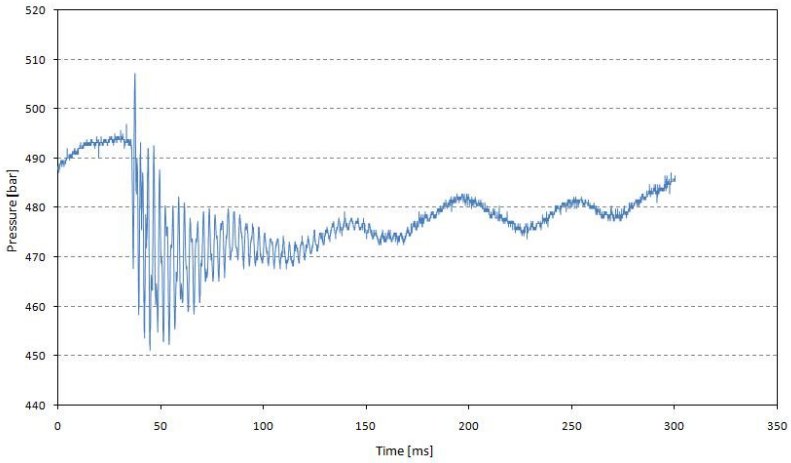

Figure 59: Magnified view of pressure versus time for DME. (P_{inj} = 500b, P_b = atm)

Figure 58 and Figure 59 above illustrates a magnified view of the pressure trace for diesel and DME respectively for 500bar injection pressure. The diesel pressure trace has a larger amplitude of oscillation of approximately 75bar as opposed to 60bar for DME. The DME pressure trace however exhibits a much longer period of oscillation than that of diesel. These two trends were noticed across all of the pressure traces. The smaller amplitude of oscillation and longer oscillation time are both consistent with the fact that DME has a lower modulus of compressibility than diesel. This result is consistent with those of Yu *et al* [17; 18] and Sorenson *et al* [25].

Spray Images

In Figure 60 and Figure 62 the empirical spray images for DME, of the first spray, are provided. In both cases the injection pressure is set to 500bar, however, in Figure 60 the back pressure is atmospheric whereas in Figure 62 the back pressure is 10bar. In Figure 61 and Figure 63 the empirical spray images for diesel, of the first spray, at the same conditions as above are provided.

When comparing the DME sprays in Figure 60 to the diesel sprays in Figure 61 the following differences become apparent:

- the spray tip of the diesel spray is much sharper than that of the DME spray
- the spray tip of the DME forms something similar to a mushroom-like shape during the latter stages of the spray
- the tail of the DME spray, near the orifice, is much thicker than that of the diesel spray

The thicker tail of the DME spray and the mushroom-like tip can both be attributed to the flash boiling effect as well as evaporation. The flash boiling effect refers to the rapid expansion of DME when it is

suddenly exposed to an environment with an ambient pressure well below its vapour pressure (P_{vapour} = 530kPa at 298K). Evaporation of DME takes place at the tip of the spray because the ambient temperature is well above its boiling temperature (T_{boil} = 248K at 1atm) and the ambient pressure is also well below DME's vapour pressure. When looking at the DME spray images at the same injection pressure but at 10bar back pressure, in Figure 62, it can be seen that there appears to be no flash boiling taking place and there seems to be very little incidence of evaporation as well. DME spray exhibits a much more clearly defined spray edge when compared to that of diesel at the same conditions, as seen in Figure 63. The fine mist around the main diesel spray, in Figure 63, suggests that the periphery of the diesel spray experienced more atomization and evaporation. It could also be that the DME did not mix with the air as well as the diesel at 10bar back pressure thus there was a clear liquid to air barrier between the DME and the air. The diesel spray was well entrained in the air and thus had a fine mist around its main body. The DME spray seemed to peel its outermost layers off while travelling into the pressure chamber. This phenomenon is not so clearly evident with the images but much more so with the videos (see the CD provided for videos). At 10bar back pressure the spray tip of the diesel is no longer sharp and is comparable to that of DME at this condition. In general the spray shapes of diesel and DME are somewhat similar at 6bar back pressure and very similar at 10bar back pressure (see Appendix C).

When injecting DME into atmospheric conditions Yu *et al* [17; 18] found that the spray tip formed something similar to a mushroom-like shape and Wakai *et al* [22] described the spray as having clusters of vapour clouds at its periphery. Both of these phenomena were somewhat present in the DME sprays from the present study as can be seen in Figure 60. Lee *et al* [24] also found that the DME spray dispersed rapidly during the early stages of injection when injected into atmospheric pressure and attributed this to the flash boiling effect.

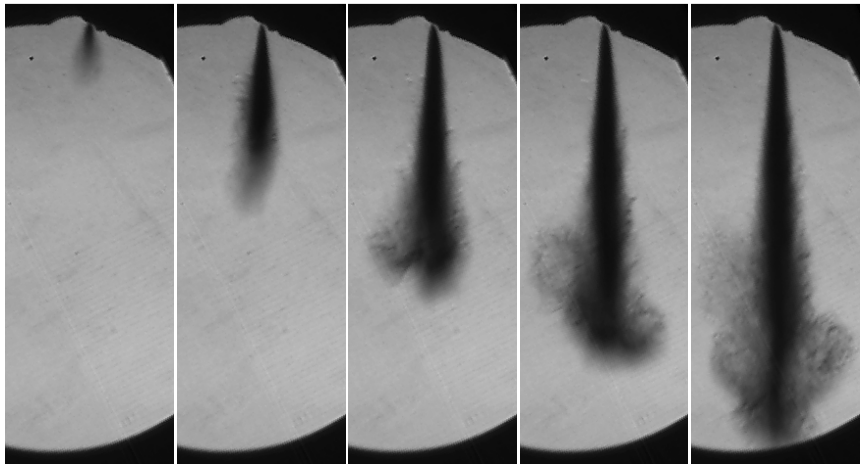

Figure 60: DME spray images for 500b injection pressure and atmospheric back pressure.

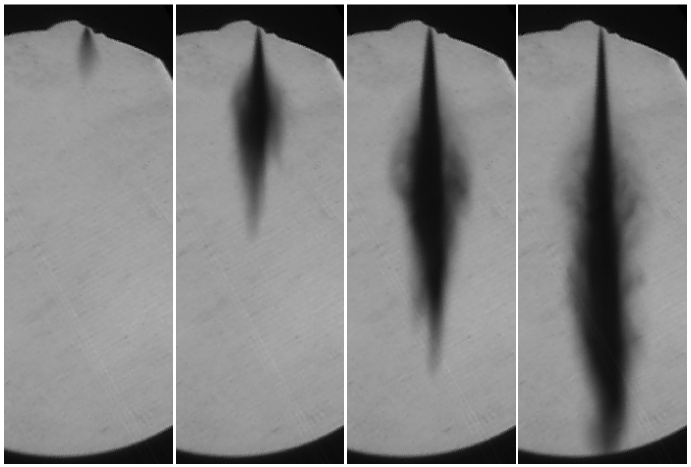

Figure 61: Diesel spray images for 500b injection pressure and atmospheric back pressure.

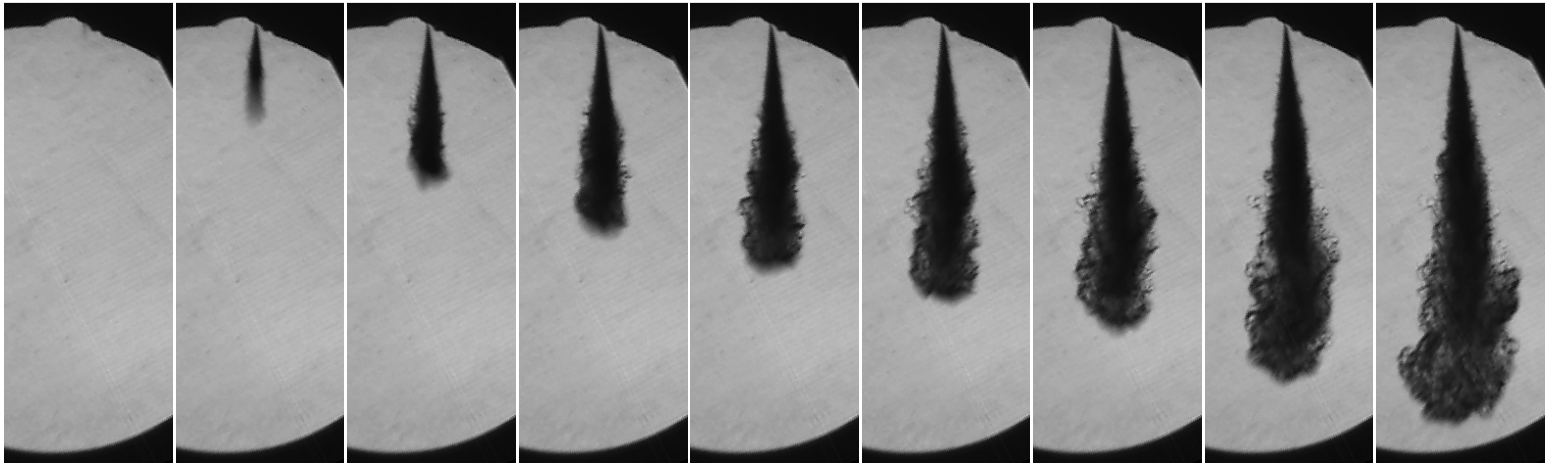

0.067ms 0.333ms 0.6ms 0.867ms 1.133ms 1.4ms 1.667ms 2.2ms 2.733ms

Figure 62: DME spray images for 500b injection pressure and 10b back pressure.

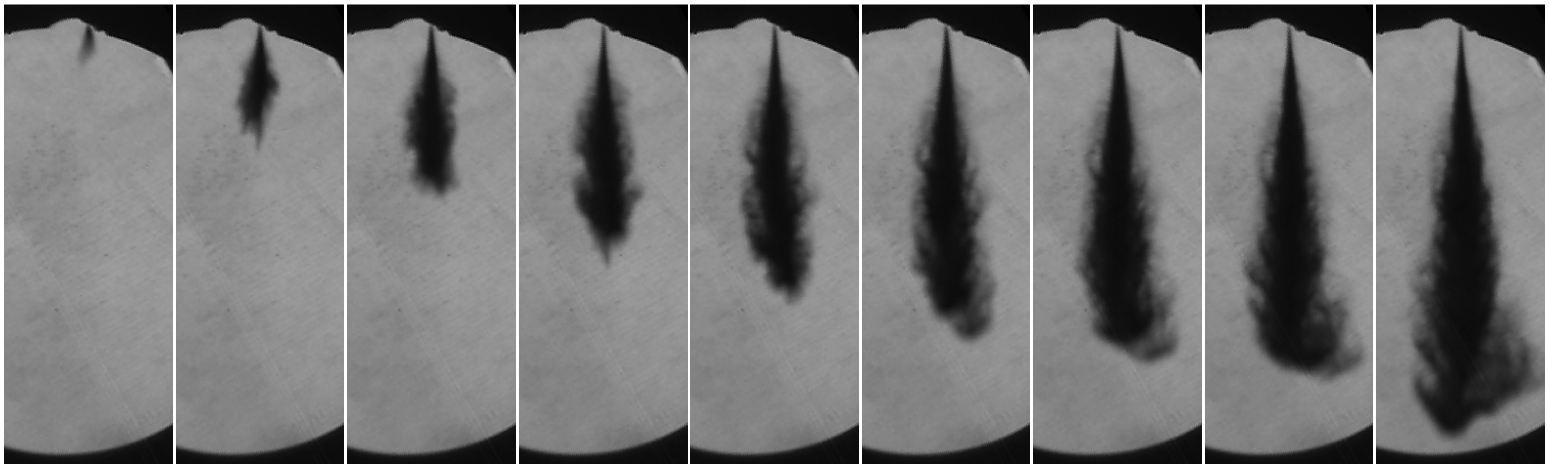

0.067ms 0.333ms 0.6ms 0.867ms 1.133ms 1.4ms 1.667ms 1.933ms 2.467ms

Figure 63: Diesel spray images for 500b injection pressure and 10b back pressure.

8. CONCLUSION

The following conclusions can be drawn from this particular study:

- The penetration predicted by Hiroyasu's correlation for diesel and DME is accurate for atmospheric back pressures, however, at higher back pressures of 6bar and 10bar the penetration is over predicted during the early stages of injection.
- For the same injection conditions the penetration of diesel is greater than that of DME.
- For the same injection conditions the cone angle of diesel is larger than that of DME except at atmospheric back pressure.
- The penetration of diesel and DME both increase with an increase in injection pressure and decrease with an increase in back pressure.
- The cone angle of diesel increases with an increase in back pressure and decreases with an increase in injection pressure
- The cone angle of DME changed very little with an increase in injection pressure and it was greater at atmospheric back pressure than at higher back pressures.
- The pressure oscillation of DME in the fuel line is smaller in amplitude and longer in duration than that of diesel.
- A standard common-rail rail system is unable to reliably pressurise DME fuel and maintain the fuel pressure after the start of injection.
- DME shows signs of flash-boiling and evaporation as well as a distinct mushroom-like spray tip when injected into an environment at atmospheric back pressure and room temperature.
- At higher back pressures the fuel spray shapes of diesel and DME appear to be very similar in their structure however their spray boundaries differ with diesel exhibiting a fine mist at its boundary and DME having a more defined fuel-to-air barrier.

REFERENCES

1. *Alternative fuels and their appliccation to combustion engines.* **A Kowalewicz, M Wojtyniak.** 2005, Journal of Automobile Engineering, Vol. 219 Part D. D02404 © IMechE 2005.

2. *Dimethyl ether (DME) as an alternative fuel.* **T A Semelsberger, R L Borup, H L Greene.** s.l. : Elsevier, 2006, Journal of Power Sciences, Vol. 156, pp. 497-511.

3. *Dimethyl Ether in Diesel Engines: Progress and Perspectives.* **Sorenson, S C.** July 2001, ASME, Vol. 123, pp. 652-658. [DOI: 10.1115/1.1370373].

4. *Experimental and analytical study on the spray characterisitics of dimethyl ether and diesel fuels within a common-rail injection system in a diesel engine.* **HK Suh, CS Lee.** s.l. : ScienceDirect, 2008, Vol. Fuel 87, pp. 925-932.

5. Common Rail Diesel. [Online] [Cited: April 19, 2010.] http://www.commonrail.info/.

6. **T K Garrett, K Newton and W Steeds.** *The Motor Vehicle.* s.l. : Butterworth Heinemann, 2001. ISBN 07506 4449 4.

7. *Vegburner.* [Online] [Cited: April 23, 2010.] http://vegburner.co.uk/suitability.htm.

8. *Thermochemical Characteristics of Dimethyl Ether - An Alternative Fuel for Compression-Ignition Engines.* **Ho Teng, James C McCandless and Jeffrey B Schneyer.** January 2001, SAE. 2001-01-0154. ISSN 0148-7191.

9. *The potential of di-methyl ether as ana alternative fuel for compression-ignition engines: A review.* **C Arcoumanis, C Bae, R Crookes, E Kinoshita.** s.l. : ScienceDirect, 2007, Fuel, Vol. 87, pp. 1014-1030.

10. "On-road Vehicles and Engines". *DieselNet.* [Online] [Cited: March 2010, 2010.] http://www.dieselnet.com/standards/jp/onroad.php.

11. "Cars and Light Trucks". *DieselNet.* [Online] [Cited: March 06, 2010.] http://www.dieselnet.com/standards/eu/ld.php.

12. "Heavy-duty Diesel Truck and Bus Engines". *DieselNet.* [Online] [Cited: March 06, 2010.] http://www.dieselnet.com/standards/eu/hd.php.

13. **Heywood, John B.** *Internal Combustion Engine Fundamentals.* Intl. Ed. s.l. : McGraw-Hill, 1988. ISBN 0-07-100499-8.

14. *Basis for the comparison of various experimental methods for studying spray penetration.* **JC, Dent.** s.l. : SAE Trans., 1971, Vol. 80. SAE paper 710571.

15. *Fuel spray penetration and spray angle in diesel spray.* **Hiroyasu H, Arai M.** s.l. : Trans JSAE, 1980. 21:5 - 11.

16. *A model for spray penetration.* **SS Sazhin, G Feng and MR Heikal.** s.l. : Elsevier, 2001, Vol. Fuel 80 (2001), pp. 2171 - 2180.

17. *Dimethyl ether (DME) spray characteristics in a common-rail fuel injection system.* **J Yu, C Bae.** Part D, 2003, Journal of Automobile Engineering, Vol. 217. D14502 © IMechE 2003.

18. *Dimethyl ether spray characteristics compared to diesel in a common-rail fuel injection system.* **Jun Yu, Jookwang Lee and Choongsik Bae.** October 21, 2002, SAE Paper. No. 2002-01-2898. ISSN 0148-7191.

19. *Atomization characteristics of Dimethyl Ether fuel as an alternative fuel injected through a common-rail injection system.* **Hyun Kyu Suh, Sung Wook Park, Chang Sik Lee.** May 24, 2006, Energy and Fuels, Vol. 20, pp. 1471-1481.

20. *A study of the dimethyl ether spray characteristics and ignition delay.* **Y Kim, J Lim, and K Min.** 2007, International Journal of Engine Research, Vol. 8. JER02105 © IMechE 2007.

21. *Spray characteristics of DME in conditions of common-rail injection system.* **Jin Sik Hwang, Jong Suk Ha and Soo Young No.** June 2003, International Journal of Automotive Technology. KSAE.

22. *Spray and ignition characteristics of dimethyl ether injected by a D.I. diesel injector.* **K Wakai, K Nishida, T Yoshizaki, H Hiroyasu.** 1998. The fourth international symposium COMODIA 98. pp. 537-542.

23. *An Experimental Study on DME Spray Characteristics us Using a Schlieren Optical System.* **Jun Li, Yoshio Sato, Akira Noda.** Jilin University, Environment and Energy Research Division.

24. *Spray and combustion characteristics of dimethyl ether fuel.* **Seang-Wock Lee, Yukata Murata, Yasuhiro Daisho.** Part D, August 4, 2004, Journal of Automotive Engineering, Vol. 219. D13003 © IMechE 2005.

25. *Dimethyl Ether in Diesel Fuel Injection Systems.* **SC Sorenson, M Glensvig and DL Abata.** s.l. : SAE, 1998. SAE paper 981159.

Appendix A: Image Post-processing

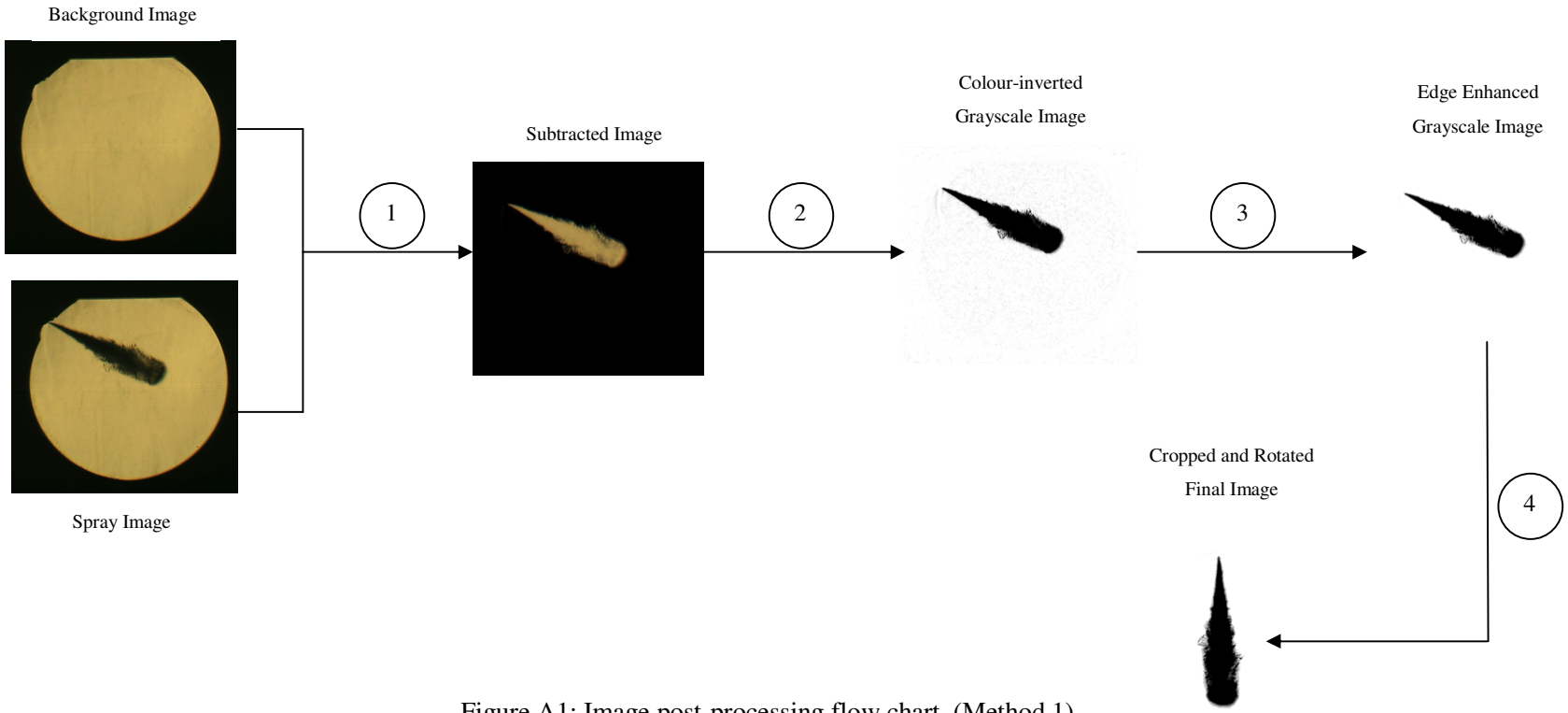

Figure A1: Image post-processing flow chart. (Method 1)

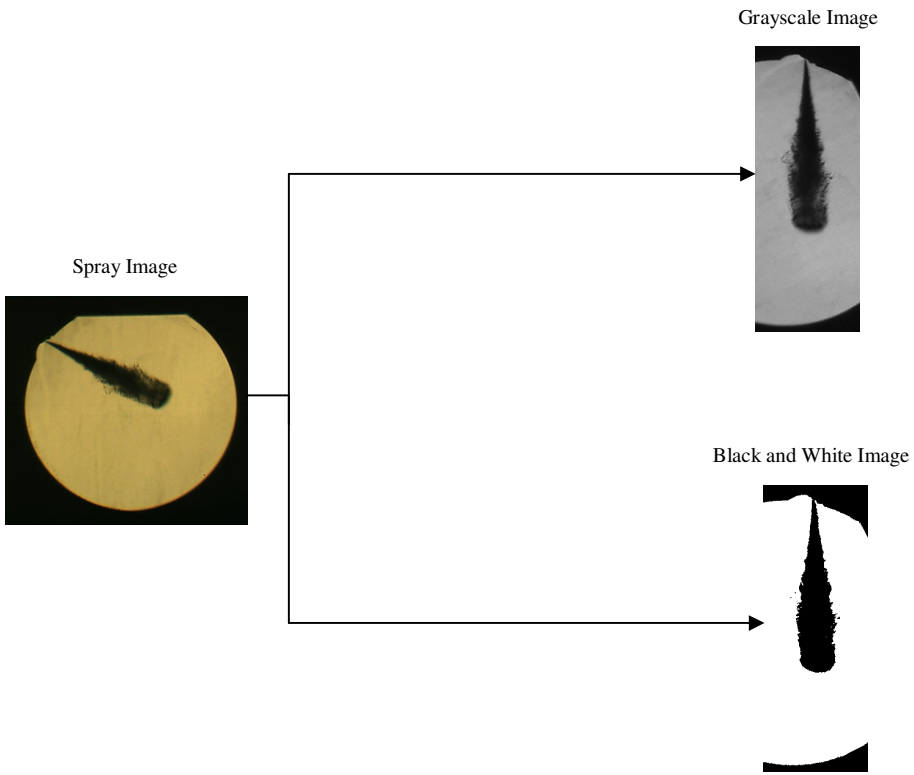

Figure A2: Image post-processing flow chart. (Method 2)

Appendix B: Sample calculations

Penetration

Dent's equation for penetration is illustrated below:

$$S = 3.07\left(\frac{\Delta p}{\rho_g}\right)^{\frac{1}{4}}(t d_n)^{\frac{1}{2}}\left(\frac{294}{T_g}\right)^{\frac{1}{4}} \quad \ldots (1)$$

Hiroyasu's equations for penetration are illustrated below:

$$S = 0.39\left(\frac{2\Delta p}{\rho_l}\right)^{\frac{1}{2}} t \quad \ldots (2) \quad \text{for } t < t_{breakup}$$

$$S = 2.95\left(\frac{\Delta p}{\rho_g}\right)^{\frac{1}{4}}(d_n t)^{\frac{1}{2}} \quad \ldots (3) \quad \text{for } t > t_{breakup}$$

$$t_{breakup} = \frac{29\rho_l d_n}{(\rho_g \Delta p)^{\frac{1}{2}}} \quad \ldots (4)$$

The physical conditions for the plots in Figure 31 are as follows:

P_{inj} = 500bar	(injection pressure)	D_n = 0.17mm	(orifice diameter)
P_b = 10bar	(back pressure)	ρ_{DME} = 667kg/m^3	(DME liquid density)
T_g = 293K	(gas temperature)	ρ_g = 11.38kg/m^3	(gas density)

Assuming no pressure loss from the common-rail to the injector nozzle, the pressure drop across the nozzle (Δp) is thus:

$\Delta p = P_{inj} - P_b =$ 490bar

and the break-up time for Hiroyasu's correlation from equation (4) is $t_{breakup}$ = 0.139ms

Time [ms]	Penetration (Dent) [mm]	Penetration (Hiroyasu) [mm]
0.1	18.25	14.95
0.2	25.8	24.78
0.4	36.5	35.04
0.6	44.7	42.92
0.8	51.62	49.56
1.0	57.71	55.4
1.2	63.22	60.69
1.4	68.28	65.56
1.6	73	70.08
1.8	77.43	74.34

For t = 0.4, first the penetration due to Dent's model then due to Hiroyasu's model is calculated.

Dent

$$(1)\ \ldots \qquad S = 3.07\left(\frac{490\times10^{5}}{11.38}\right)^{0.25}\left((0.17\times10^{-3})(0.4\times10^{-3})\right)^{0.5}\left(\frac{294}{293}\right)^{0.25} = 0.0365\text{m} = 36.5\text{mm}$$

Hiroyasu

Because t = 0.4 is greater than $t_{breakup}$ equation (3) must be used as opposed to equation (2):

$$(3)\ \ldots \qquad S = 2.95\left(\frac{490\times10^{5}}{11.38}\right)^{0.25}\left((0.17\times10^{-3})(0.4\times10^{-3})\right)^{0.5} = 0.03504\text{m} = 35.04\text{mm}$$

Uncertainty analysis

A sample calculation illustrating how the measurement uncertainty of spray penetration was determined can be found in this section. The measured spray penetration of diesel for 300bar injection pressure (P_{inj}) and atmospheric back pressure (P_b) is illustrated in the table below. Note that the values are an average of three images for the same injection condition.

Time [ms]	Penetration [mm]	% Uncertainty
0.067	6.12	3.60
0.200	17.16	1.29
0.333	29.76	0.74
0.467	43.40	0.51
0.600	55.39	0.40
0.733	66.43	0.33
0.867	75.26	0.29
1.000	83.13	0.27
1.133	91.03	0.24

The measurement of spray penetration spray penetration was inaccurate by up to 1 pixel at most. One pixel was found to be equal to 0.22069mm, using calibration. The degree of uncertainty was then determined as follows:

$$\%\ Uncertainty = \frac{uncertainty}{measured\ length} \times 100 \quad \text{..... (7)}$$

For the penetration at t = 0.067ms and t = 0.6ms respectively:

$$\%\ Uncertainty = \frac{uncertainty}{measured\ length} \times 100 = \frac{0.22069}{6.12} \times 100 = 3.60\ \%$$

$$\%\ Uncertainty = \frac{uncertainty}{measured\ length} \times 100 = \frac{0.22069}{55.39} \times 100 = \ 0.4\ \%$$

The uncertainty of the cone angle was determined in similar manner.

Appendix C: Catalogue of diesel and DME spray images from experiments

P_{inj} = 200b, P_{back} = atmospheric, DME

P_{inj} = 300b, P_{back} = atmospheric, DME

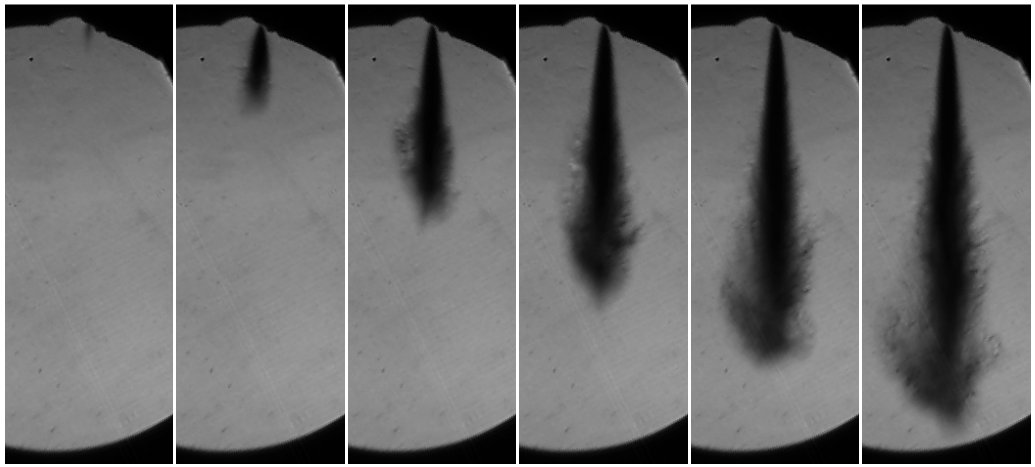

0.133ms 0.4ms 0.667ms 0.933ms 1.2ms 1.467ms

P_{inj} = 400b, P_{back} = atmospheric, DME

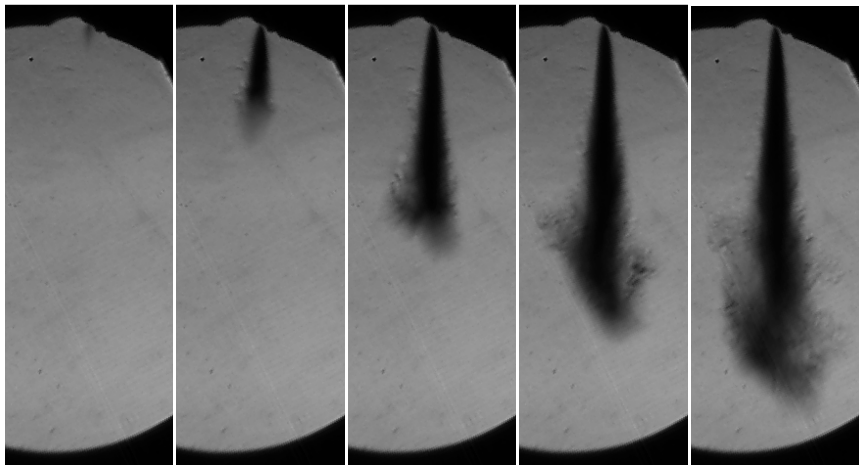

0.133ms 0.4ms 0.667ms 0.933ms 1.2ms

P_{inj} = 500b, P_{back} = atmospheric, DME

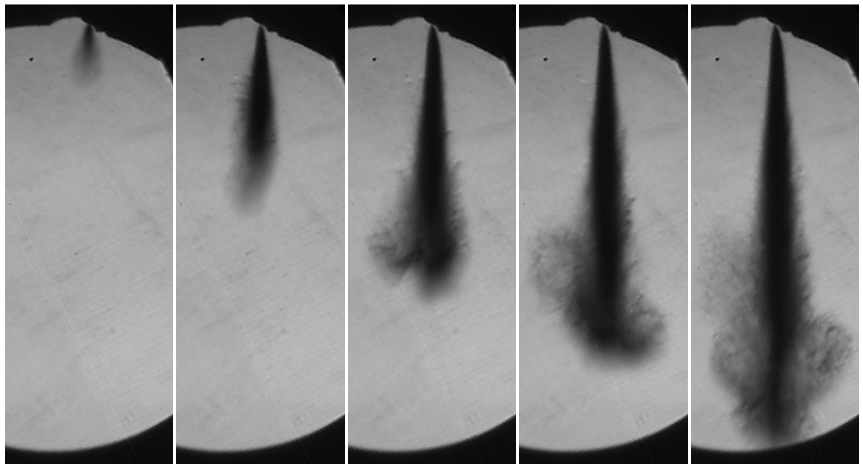

0.133ms 0.4ms 0.667ms 0.933ms 1.2ms

P_{inj} = 200b, P_{back} = 6b, DME

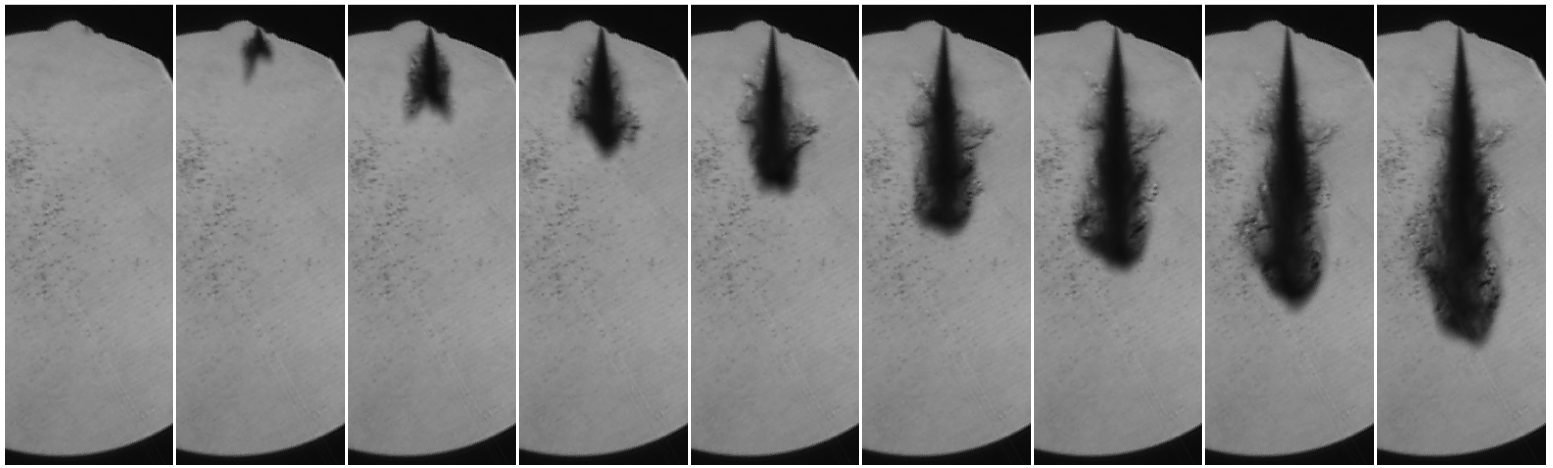

0.133ms 0.4ms 0.667ms 0.933ms 1.2ms 1.467ms 1.733ms 2.0ms 2.267ms

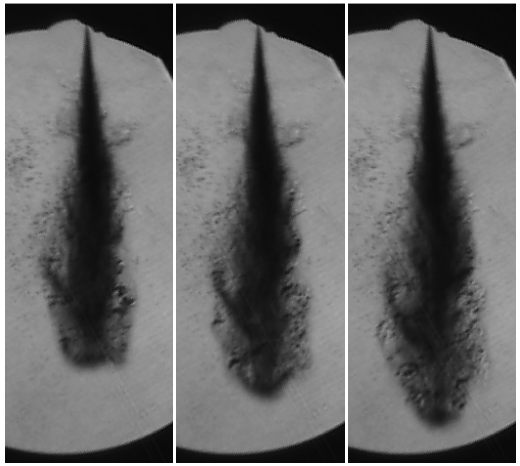

2.533ms 2.8ms 3.067ms

P_{inj} = 300b, P_{back} = 6b, DME

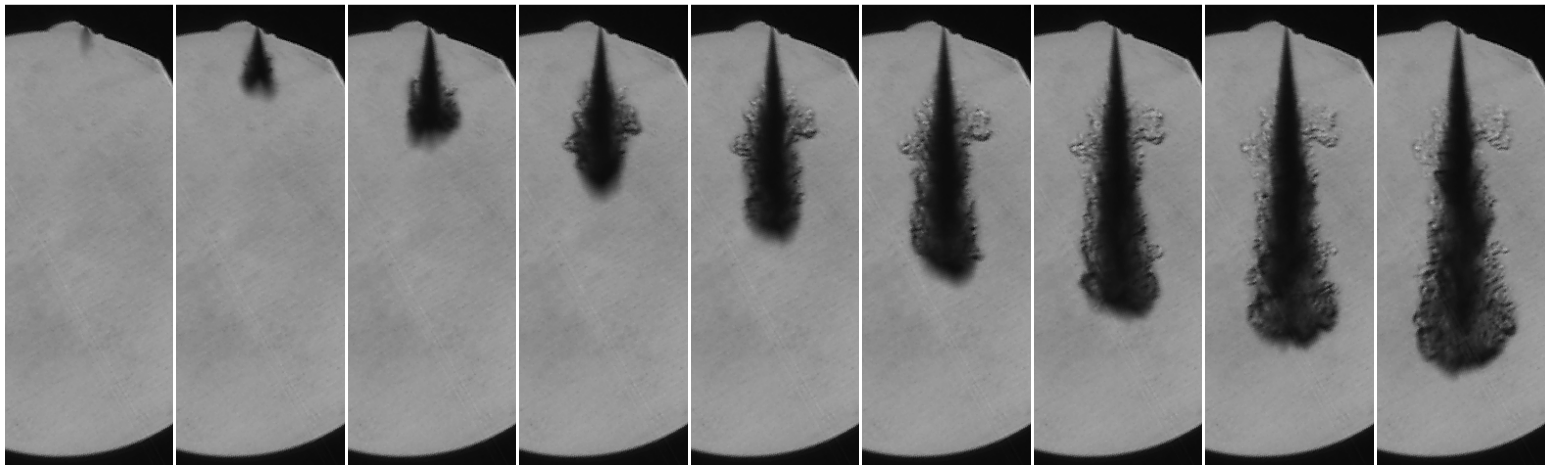

0.133ms 0.4ms 0.667ms 0.933ms 1.2ms 1.467ms 1.733ms 2.0ms 2.267ms

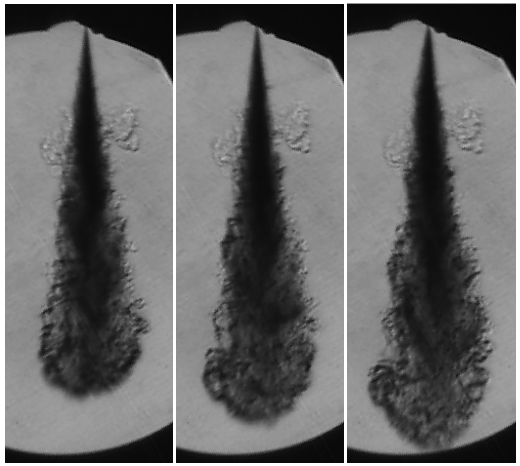

2.533ms 2.8ms 3.067ms

P_{inj} = 400b, P_{back} = 6b, DME

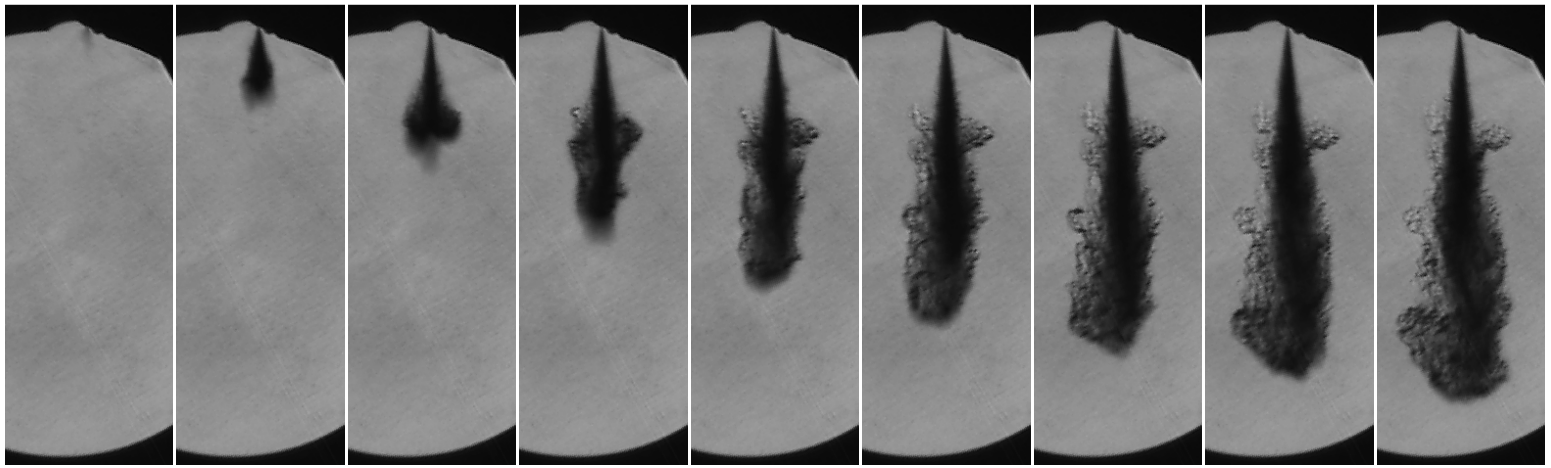

0.133ms 0.4ms 0.667ms 0.933ms 1.2ms 1.467ms 1.733ms 2.0ms 2.267ms

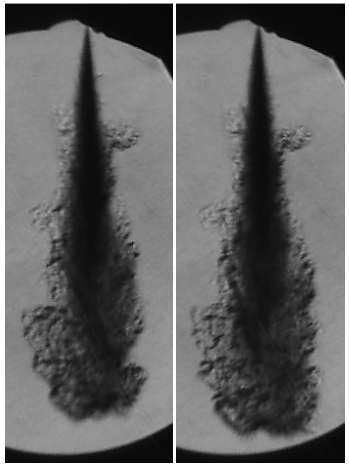

2.533ms 2.8ms

P_{inj} = 200b, P_{back} = 10b, DME

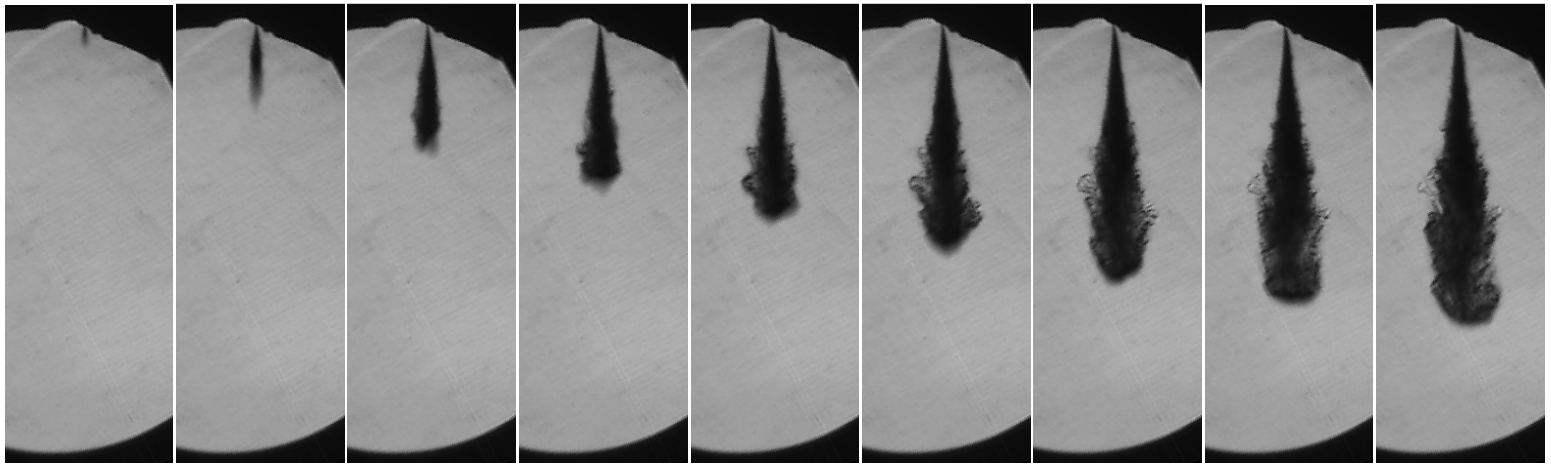

0.133ms 0.4ms 0.667ms 0.933ms 1.2ms 1.467ms 1.733ms 2.0ms 2.267ms

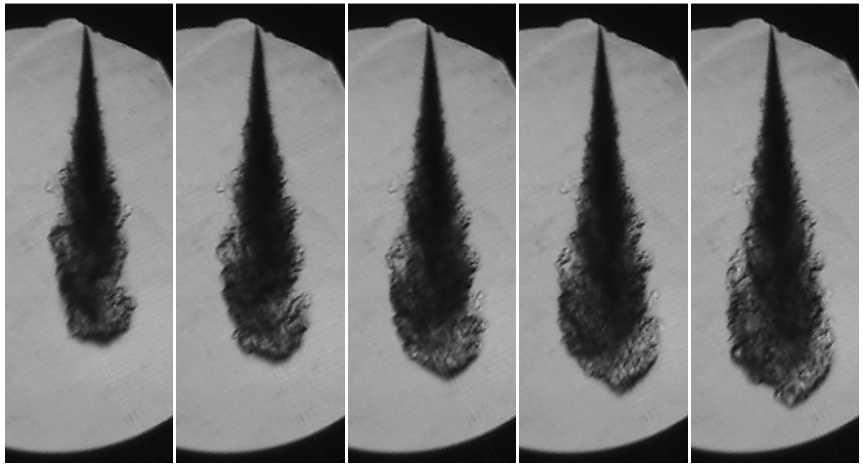

2.533ms 2.8ms 3.067ms 3.333ms 3.6ms

P_{inj} = 300b, P_{back} = 10b, DME

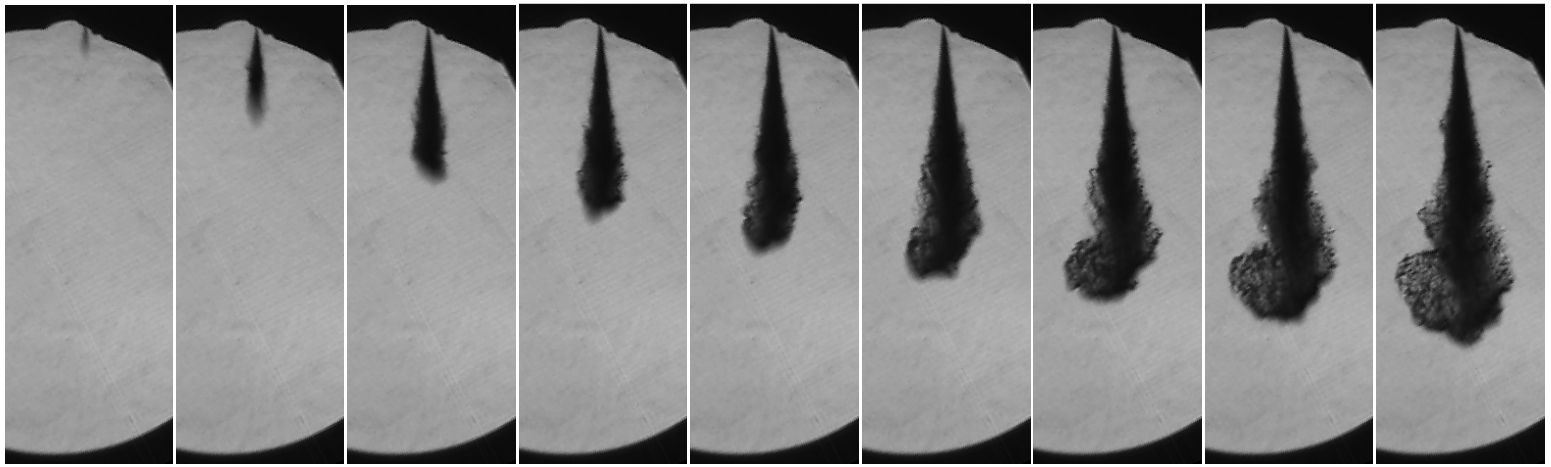

0.133ms 0.4ms 0.667ms 0.933ms 1.2ms 1.467ms 1.733ms 2.0ms 2.267ms

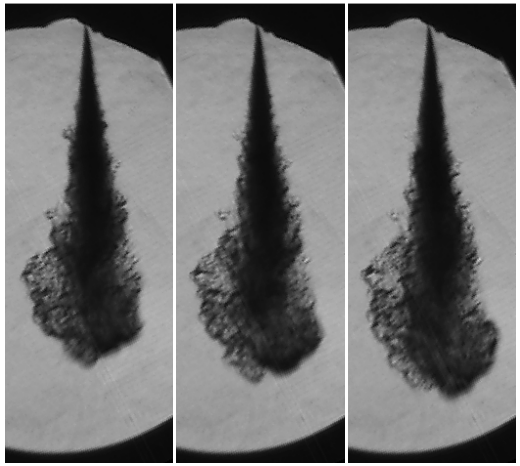

2.533ms 2.8ms 3.067ms

P_{inj} = 400b, P_{back} = 10b, DME

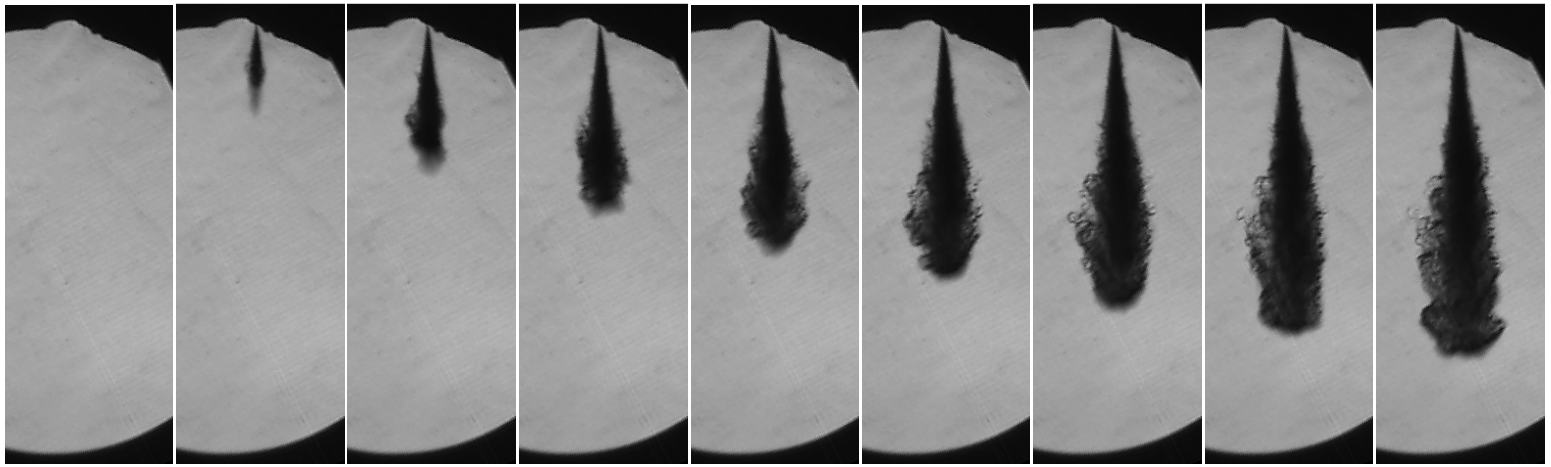

0.133ms 0.4ms 0.667ms 0.933ms 1.2ms 1.467ms 1.733ms 2.0ms 2.267ms

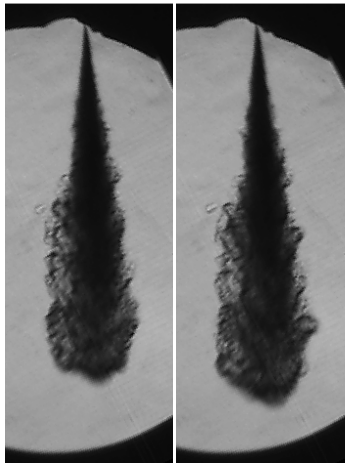

2.533ms 2.8ms

P_{inj} = 500b, P_{back} = 10b, DME

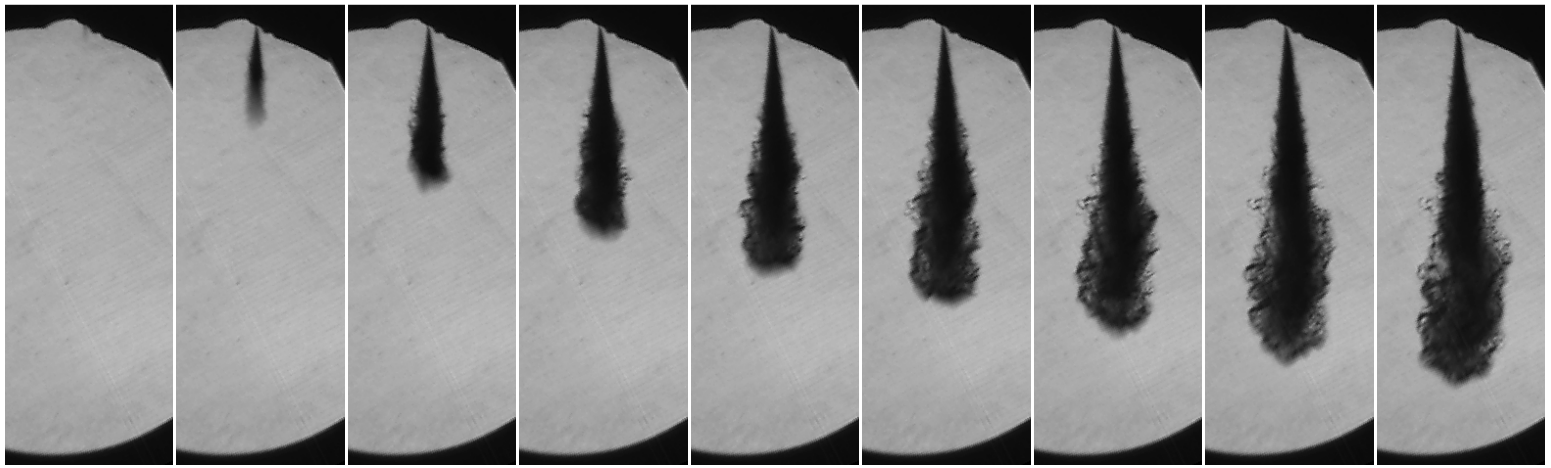

0.133ms 0.4ms 0.667ms 0.933ms 1.2ms 1.467ms 1.733ms 2.0ms 2.267ms

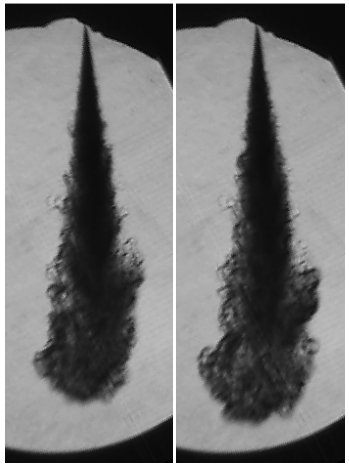

2.533ms 2.8ms

P_{inj} = 200b, P_{back} = atmospheric, Diesel

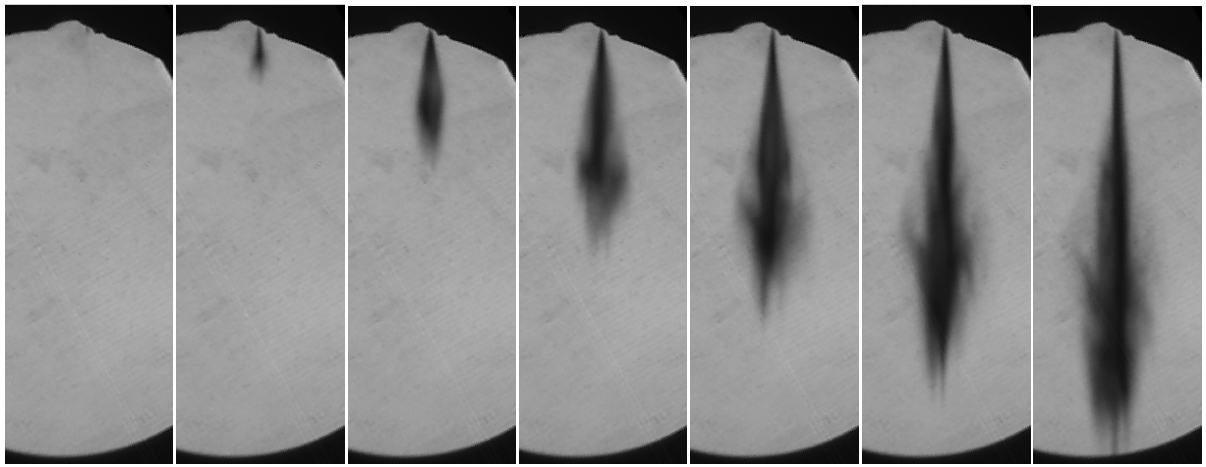

0.133ms 0.4ms 0.667ms 0.933ms 1.2ms 1.467ms 1.733ms

P_{inj} = 300b, P_{back} = atmospheric, Diesel

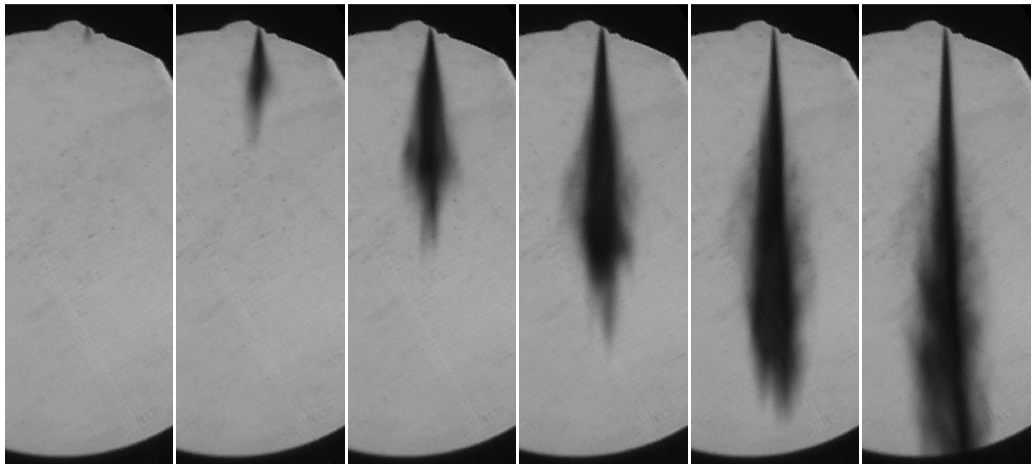

0.133ms 0.4ms 0.667ms 0.933ms 1.2ms 1.467ms

P_{inj} = 400b, P_{back} = atmospheric, Diesel

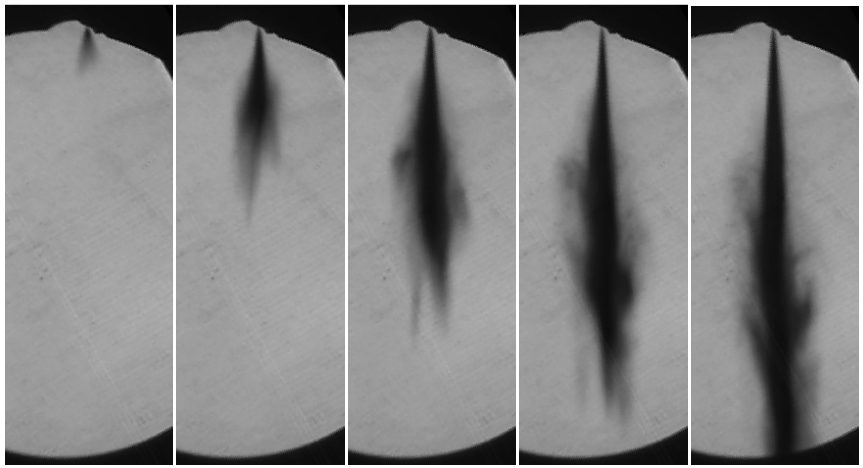

0.133ms 0.4ms 0.667ms 0.933ms 1.2ms

P_{inj} = 500b, P_{back} = atmospheric, Diesel

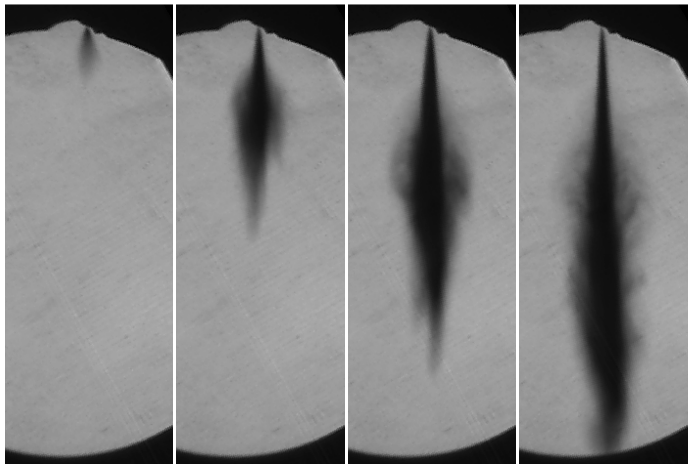

0.133ms 0.4ms 0.667ms 0.933ms

P_{inj} = 200b, P_{back} = 6b, Diesel

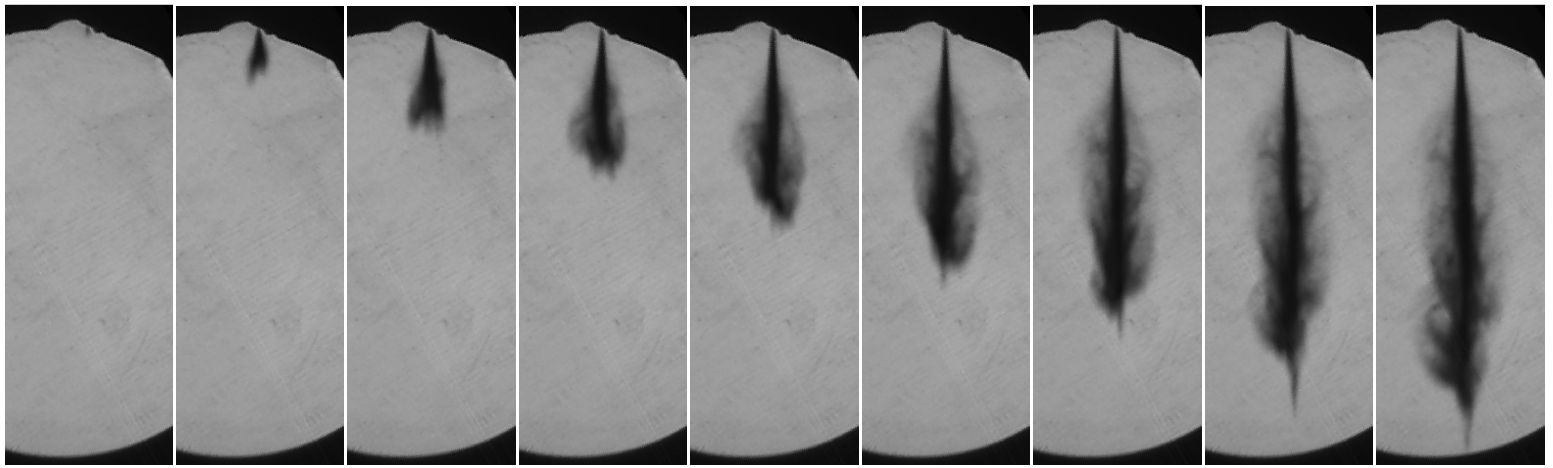

0.133ms 0.4ms 0.667ms 0.933ms 1.2ms 1.467ms 1.733ms 2.0ms 2.267ms

P_{inj} = 300b, P_{back} = 6b, Diesel

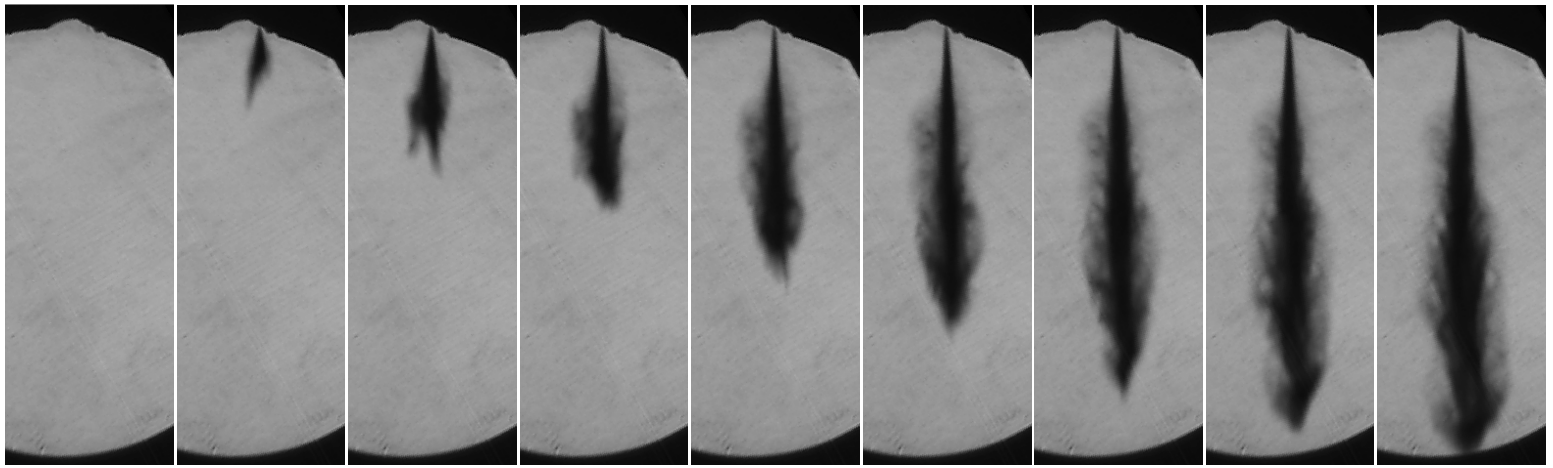

0.133ms 0.4ms 0.667ms 0.933ms 1.2ms 1.467ms 1.733ms 2.0ms 2.267ms

P_{inj} = 400b, P_{back} = 6b, Diesel

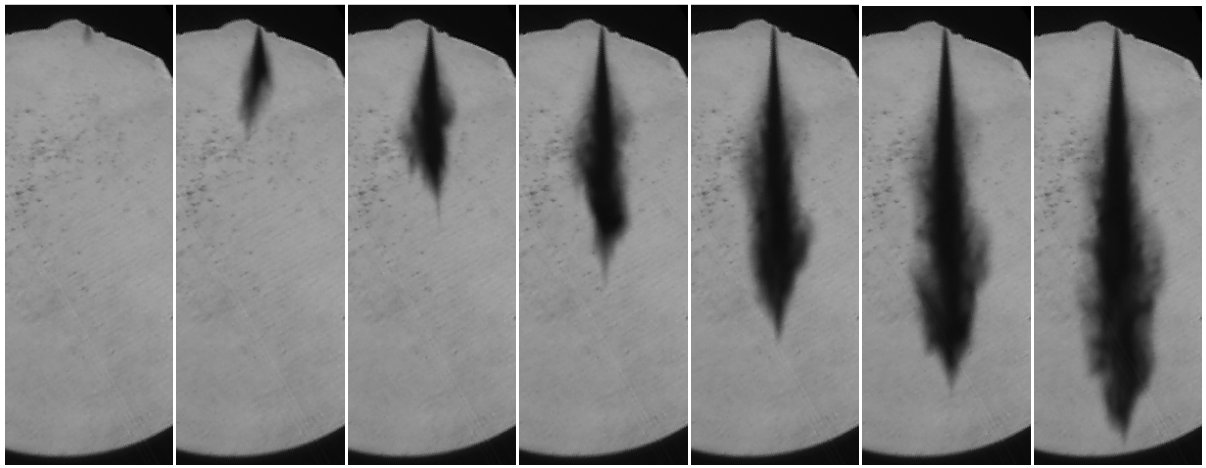

0.133ms 0.4ms 0.667ms 0.933ms 1.2ms 1.467ms 1.733ms

P_{inj} = 500b, P_{back} = 6b, Diesel

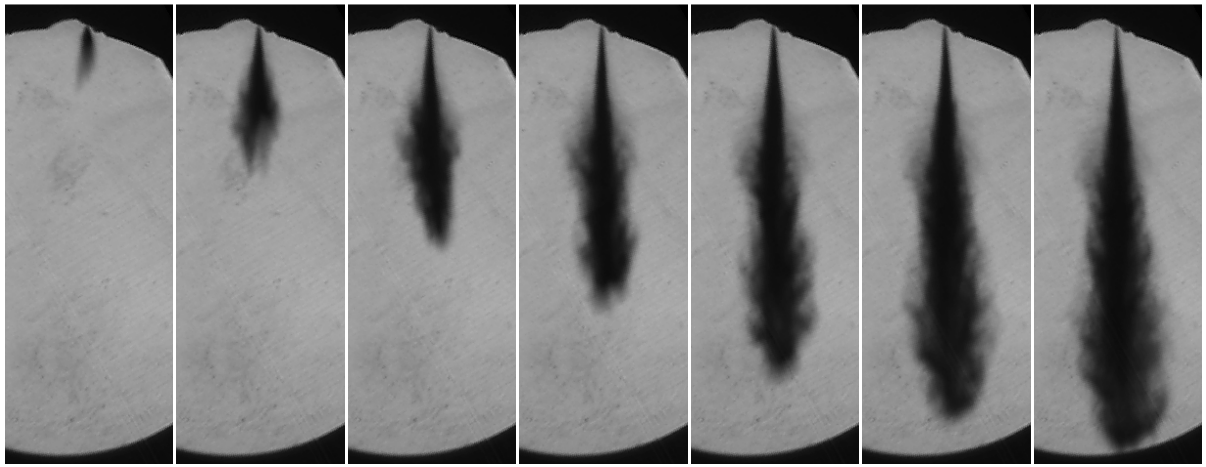

0.133ms 0.4ms 0.667ms 0.933ms 1.2ms 1.467ms 1.733ms

P_{inj} = 200b, P_{back} = 10b, Diesel

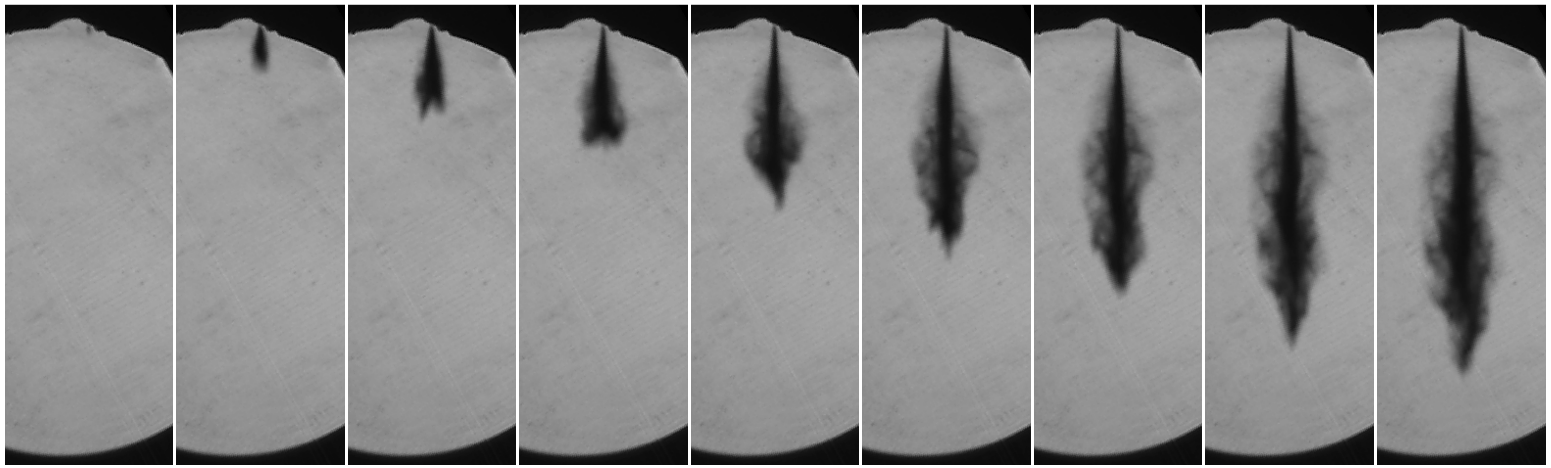

0.133ms 0.4ms 0.667ms 0.933ms 1.2ms 1.467ms 1.733ms 2.0ms 2.267ms

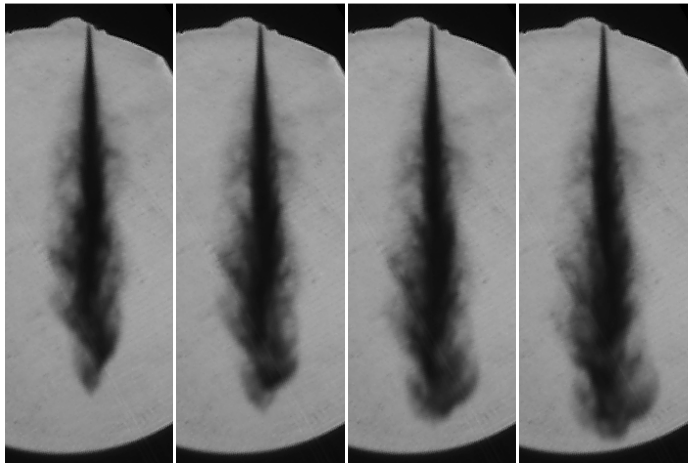

2.533ms 2.8ms 3.067ms 3.333ms

P_{inj} = 300b, P_{back} = 10b, Diesel

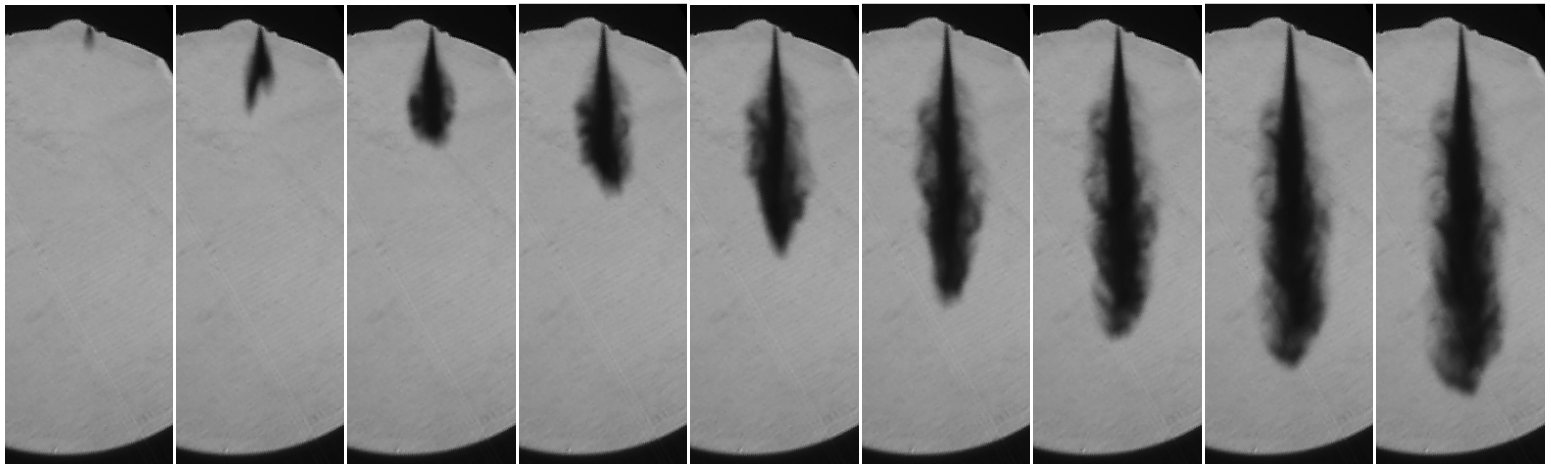

0.133ms 0.4ms 0.667ms 0.933ms 1.2ms 1.467ms 1.733ms 2.0ms 2.267ms

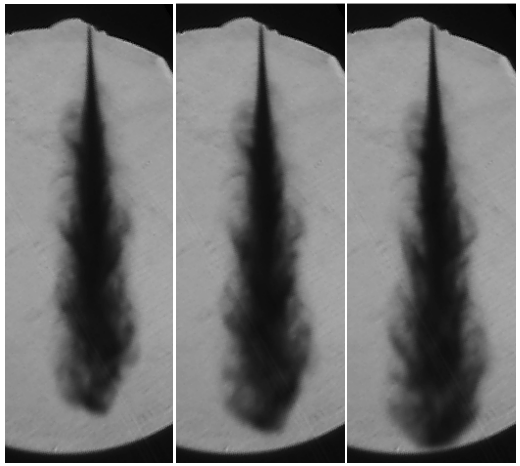

2.533ms 2.8ms 3.067ms

P_{inj} = 400b, P_{back} = 10b, Diesel

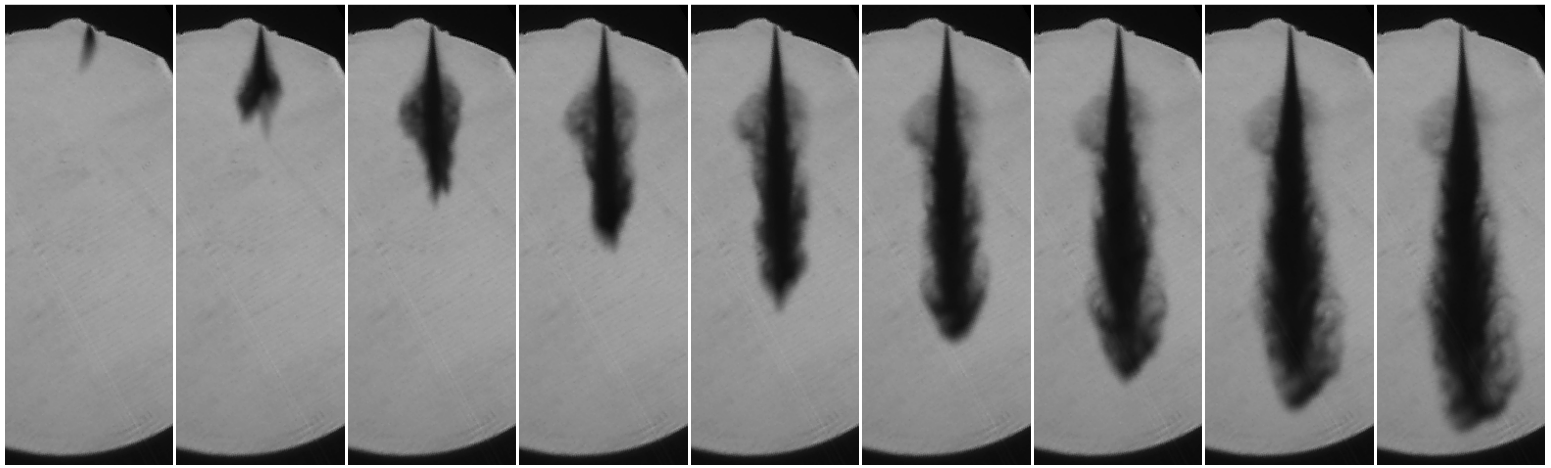

0.133ms 0.4ms 0.667ms 0.933ms 1.2ms 1.467ms 1.733ms 2.0ms 2.267ms

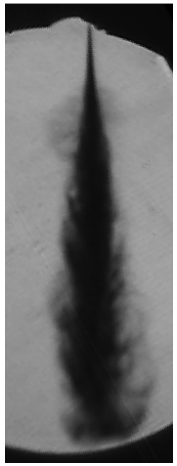

2.533ms

P_{inj} = 500b, P_{back} = 10b, Diesel

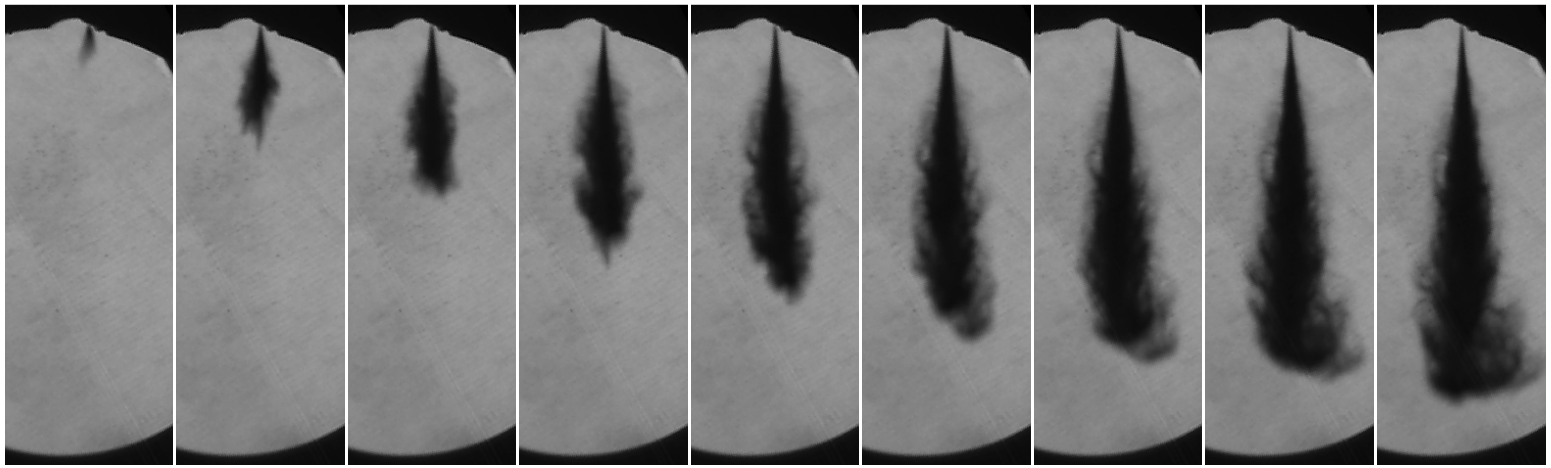

0.133ms 0.4ms 0.667ms 0.933ms 1.2ms 1.467ms 1.733ms 2.0ms 2.267ms

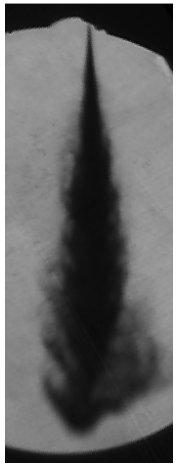

2.533ms

Appendix D: Spray Penetration, Mean Spray Velocity and Cone Angle

Spray Penetration

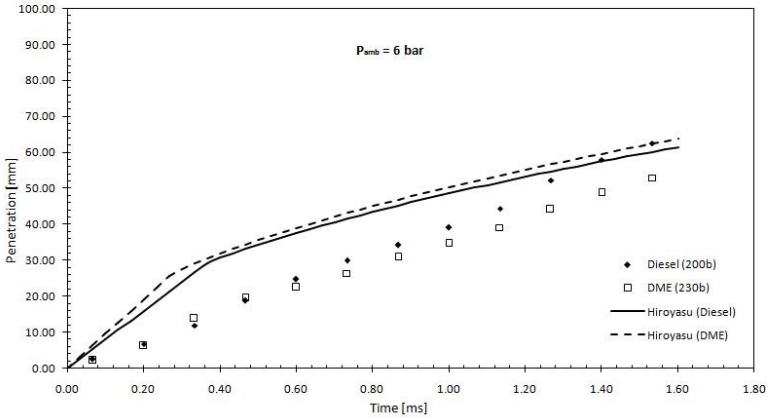

Figure C1: P_{inj} = 200b and P_b = 6b

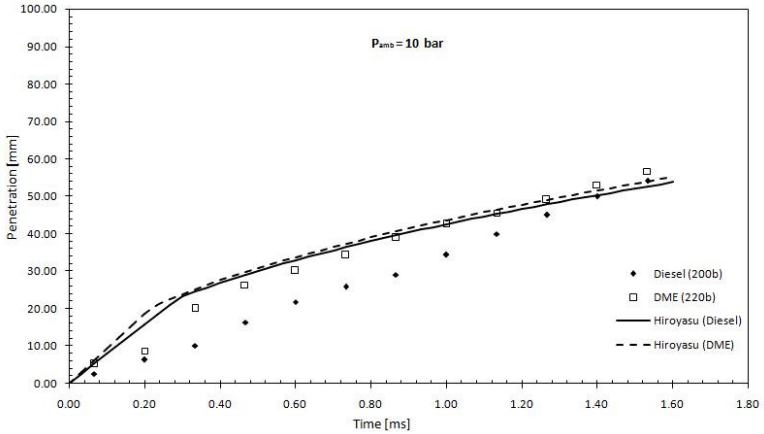

Figure C2: P_{inj} = 200b and P_b = 10b

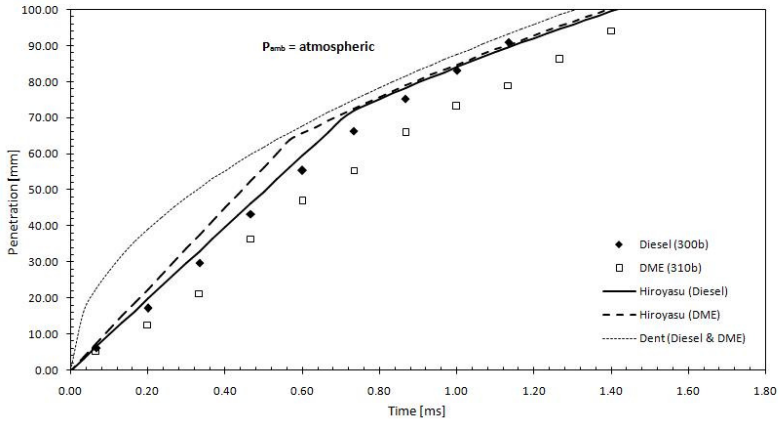

Figure C3: P_{inj} = 300b and P_b = atm

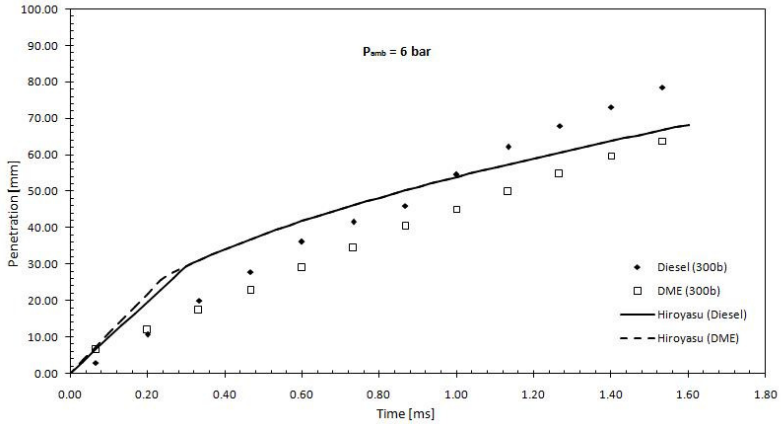

Figure C4: P_{inj} = 300b and P_b = 6b

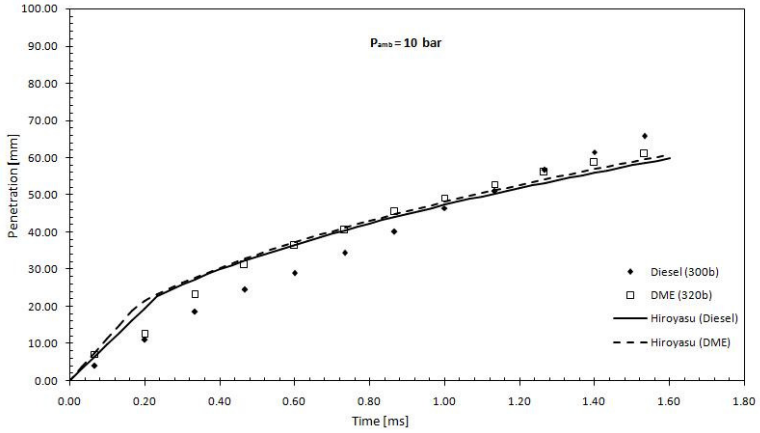

Figure C5: P_{inj} = 300b and P_b = 10b

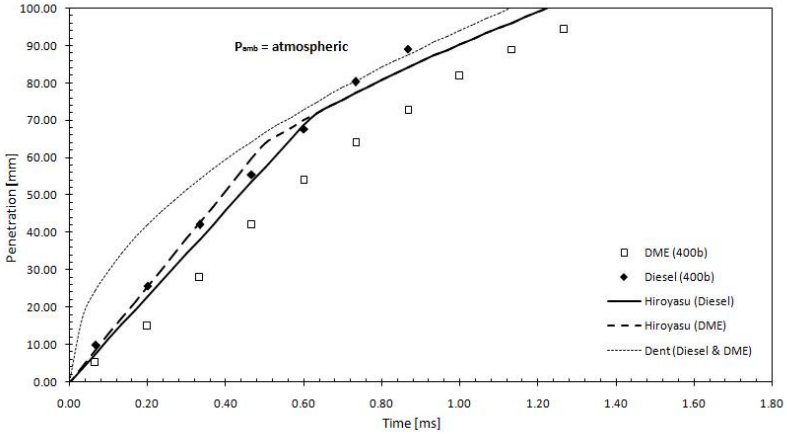

Figure C6: P_{inj} = 400b and P_b = atm

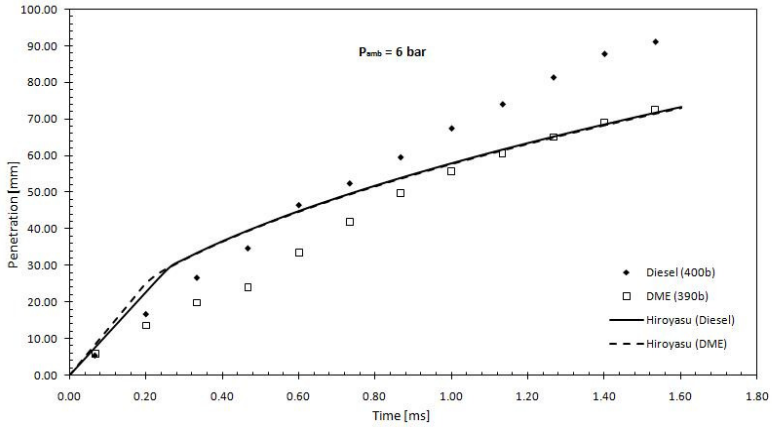

Figure C7: P_{inj} = 400b and P_b = 6b

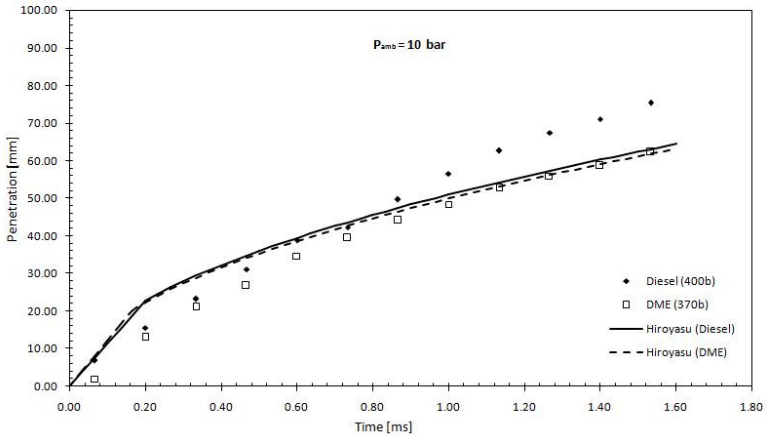

Figure C8: P_{inj} = 400b and P_b = 10b

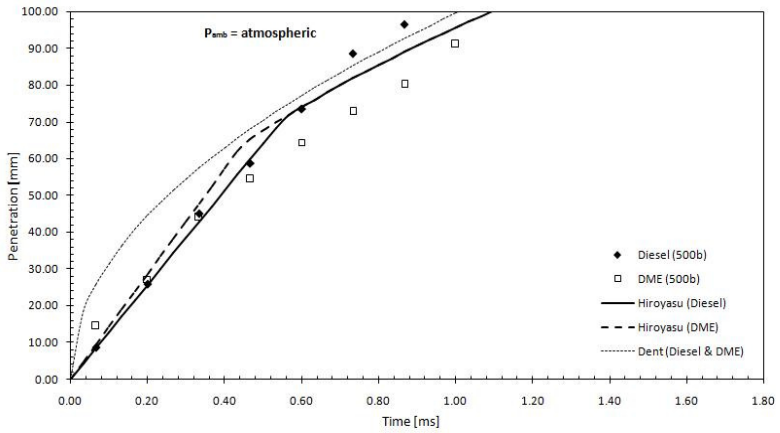

Figure C9: P_{inj} = 500b and P_b = atm

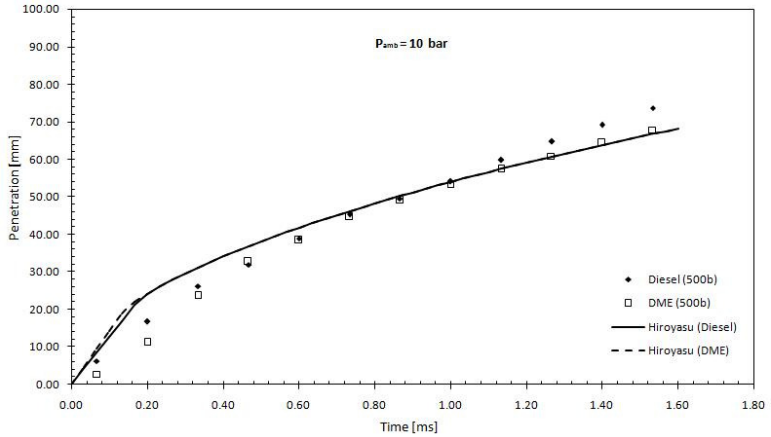

Figure C10: P_{inj} = 500b and P_b = 10b

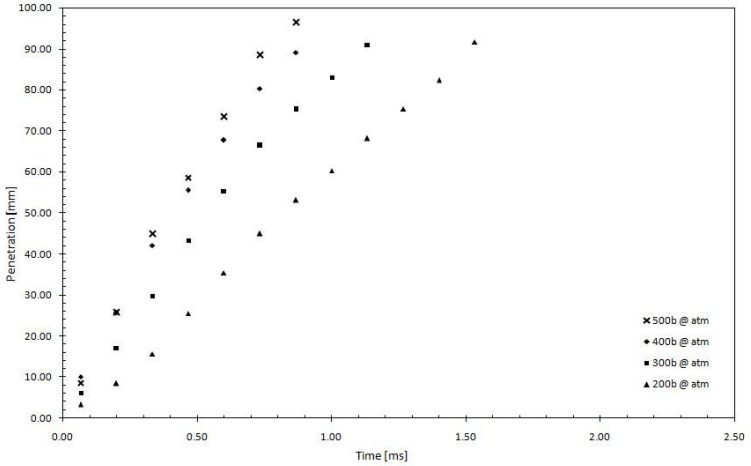

Figure C11: Diesel (P_{inj} = various and P_b = atm)

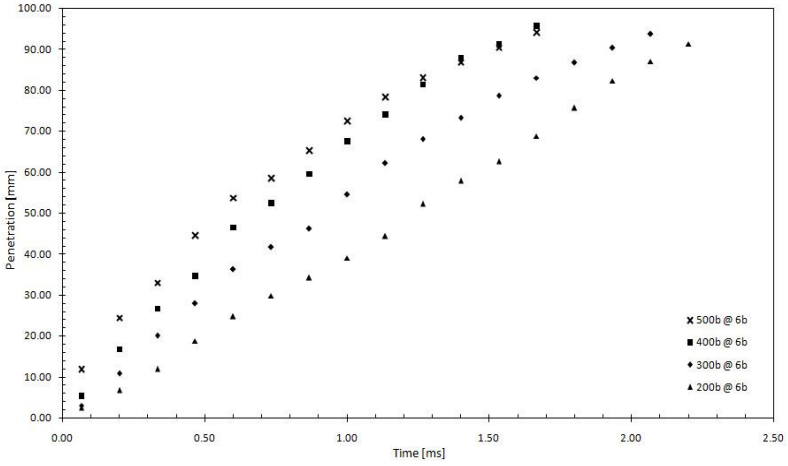

Figure C12: Diesel (P_{inj} = various and P_b = 6b)

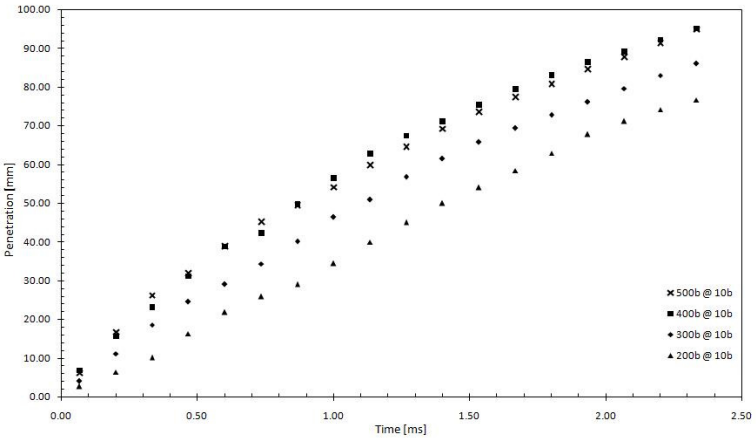

Figure C13: Diesel (P_{inj} = various and P_b = 10b)

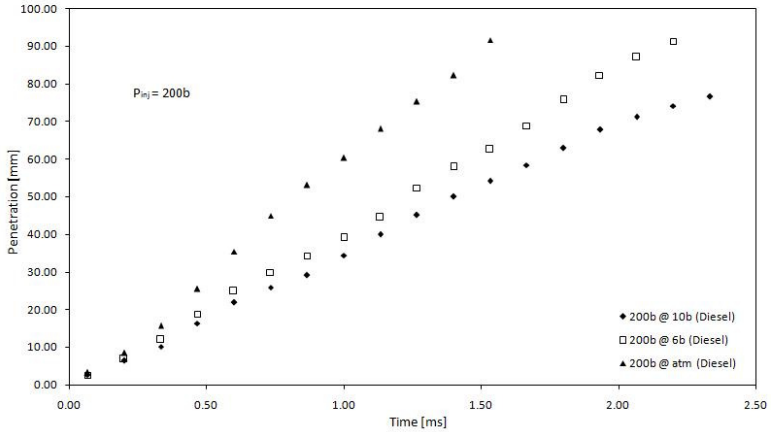

Figure C14: Diesel (P_{inj} = 200b and P_b = various)

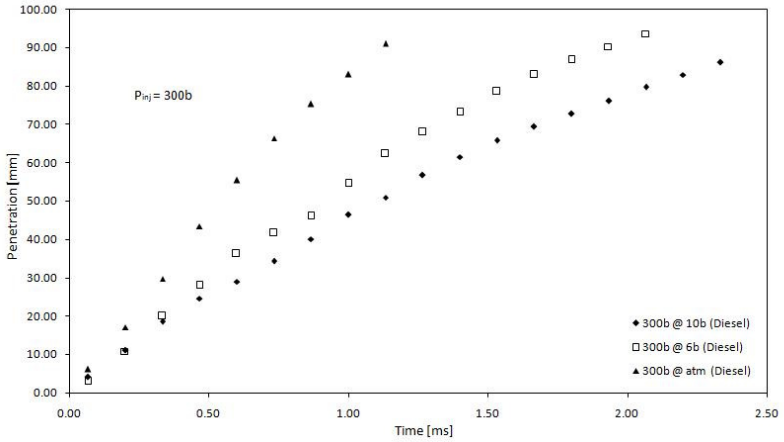

Figure C15: Diesel (Pinj = 300b and Pb = various)

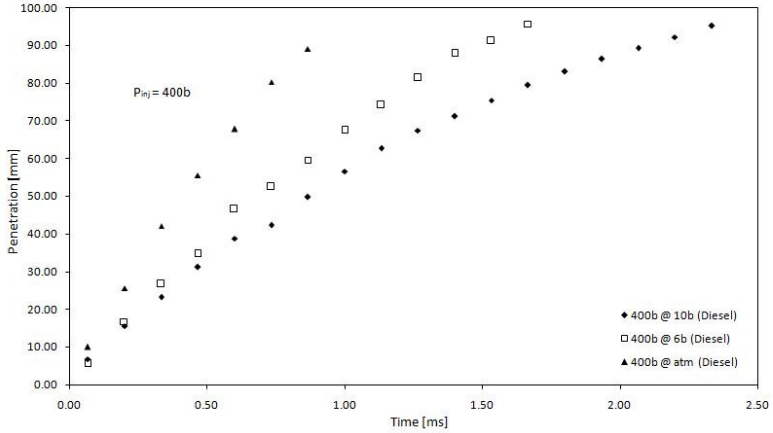

Figure C16: Diesel (Pinj = 400b and Pb = various)

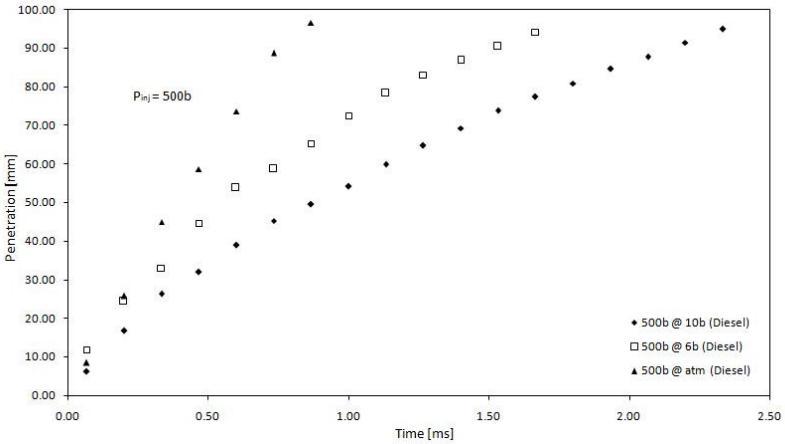

Figure C17: Diesel (Pinj = 500b and Pb = various)

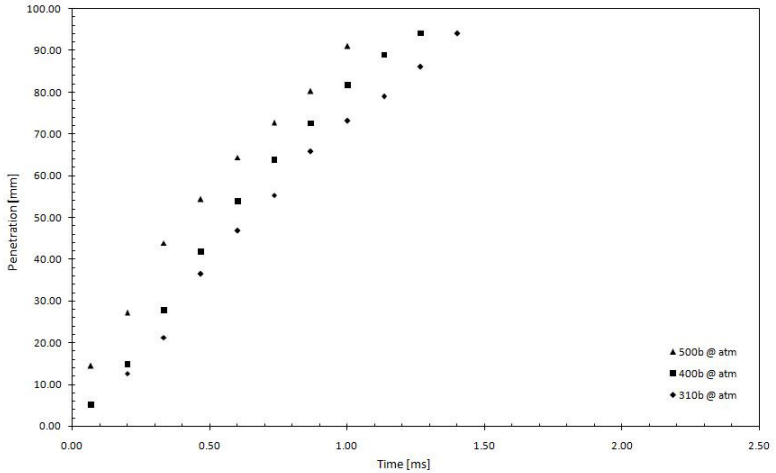

Figure C18: DME (P_{inj} = various and P_b = atm)

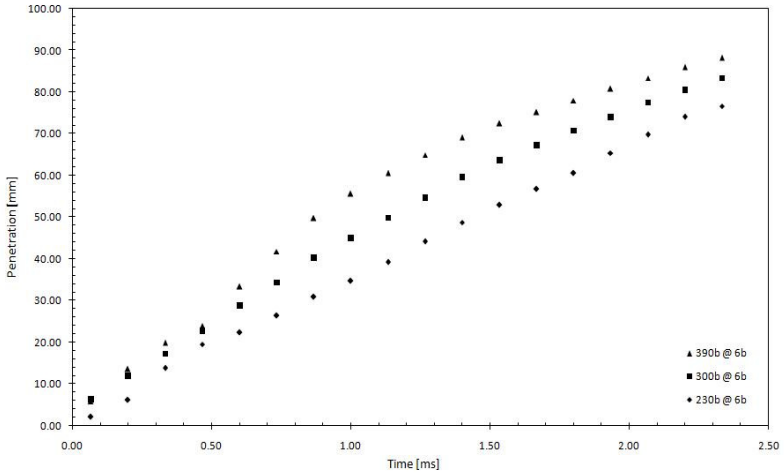

Figure C19: DME (P_{inj} = various and P_b = 6b)

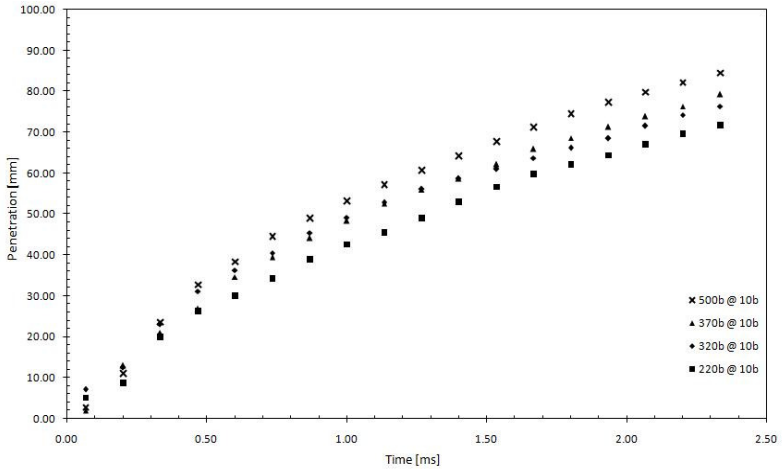

Figure C20: DME (P_{inj} = various and P_b = 10b)

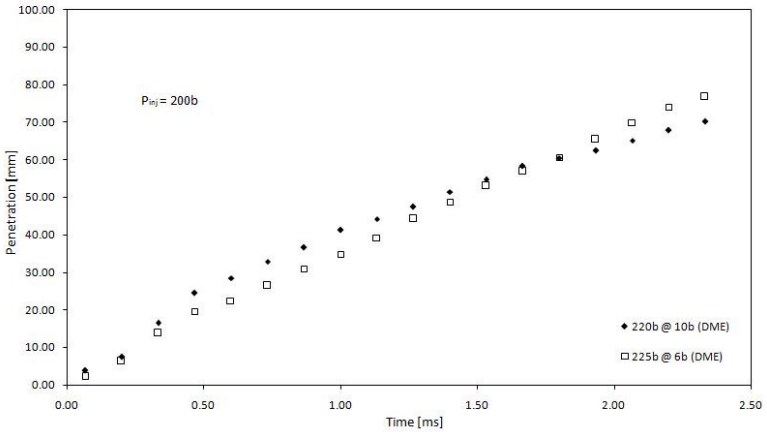

Figure C21: DME (P_{inj} = 200b and P_b = various)

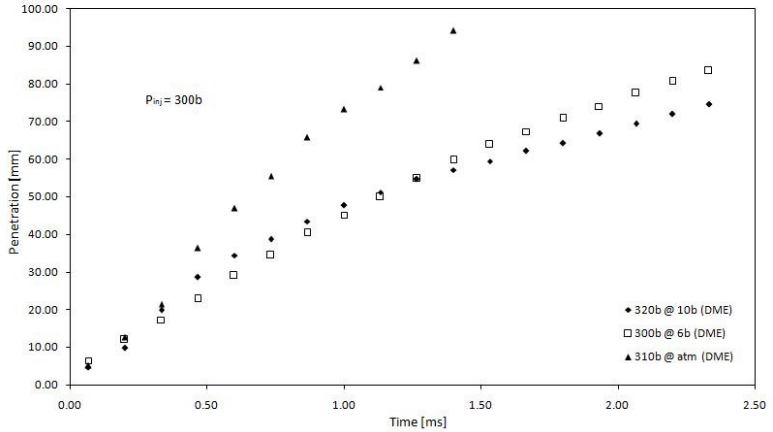

Figure C22: DME (P_{inj} = 300b and P_b = various)

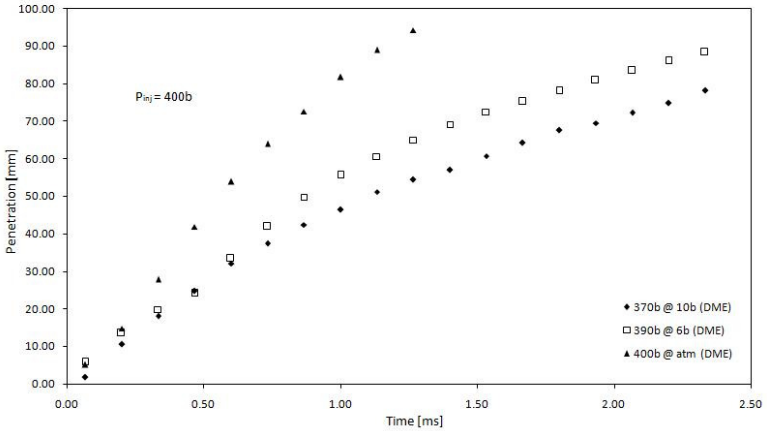

Figure C23: DME (P_{inj} = 400b and P_b = various)

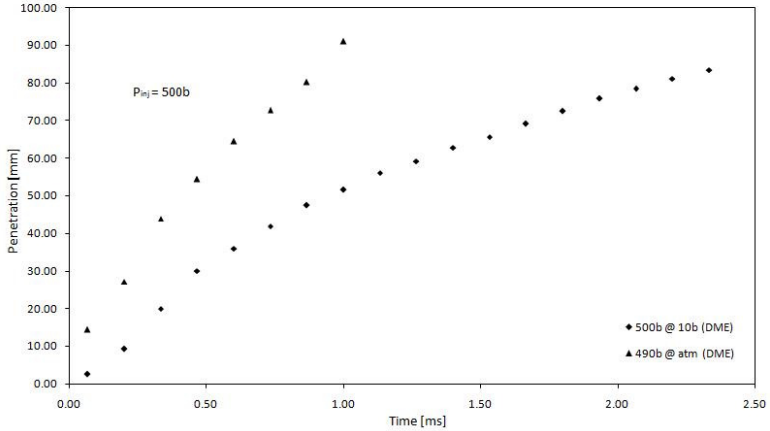

Figure C24: DME (P_{inj} = 500b and P_b = various)

Mean Spray Velocity

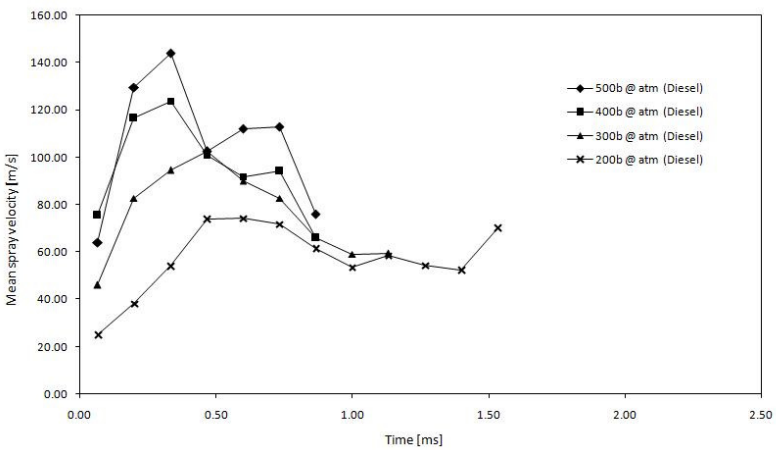

Figure C25: Diesel (P_{inj} = various and P_b = atm)

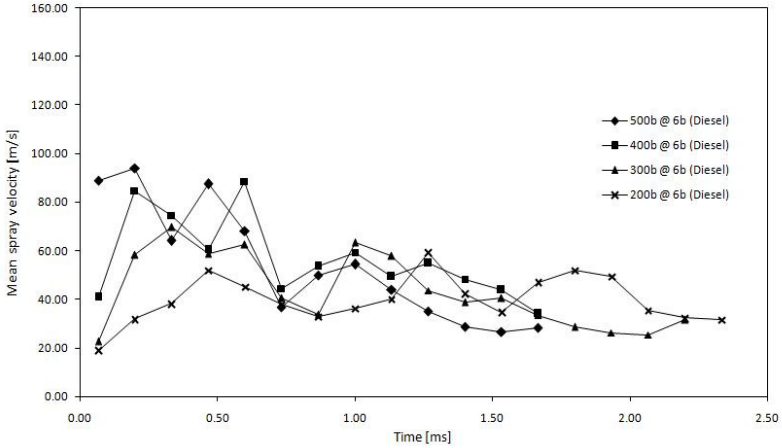

Figure C26: Diesel (P_{inj} = various and P_b = 6b)

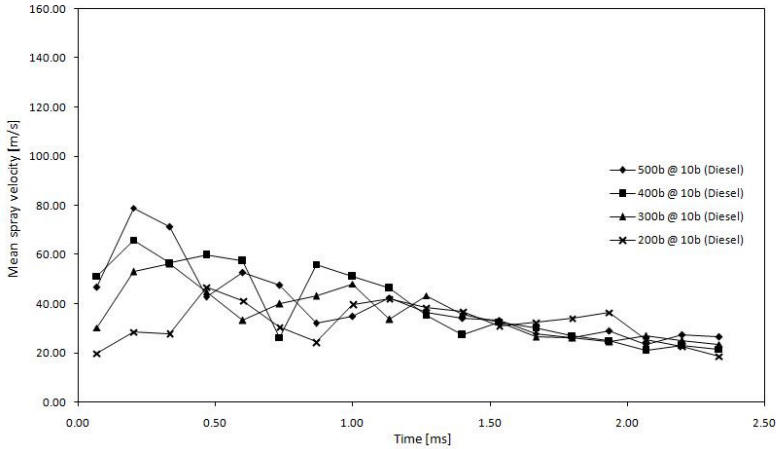

Figure C27: Diesel (P_{inj} = various and P_b = 10b)

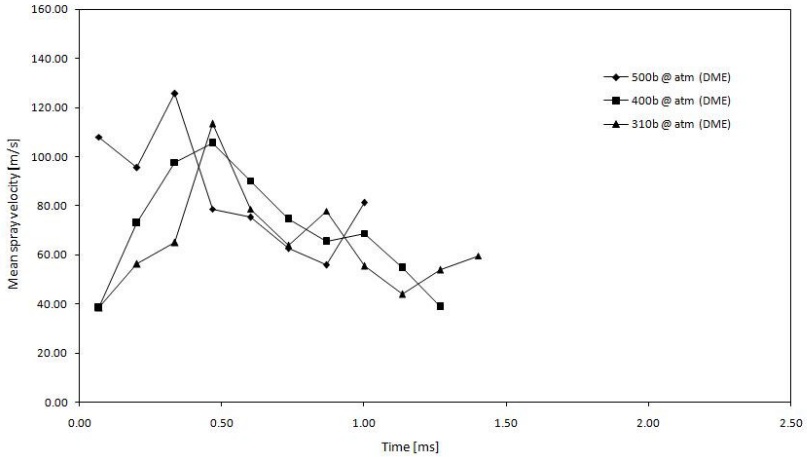

Figure C28: DME (P_{inj} = various and P_b = atm)

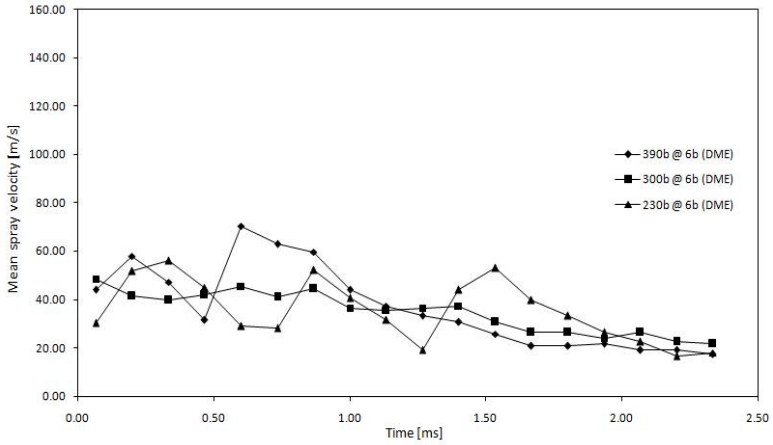

Figure C29: DME (Pinj = various and Pb = 6b)

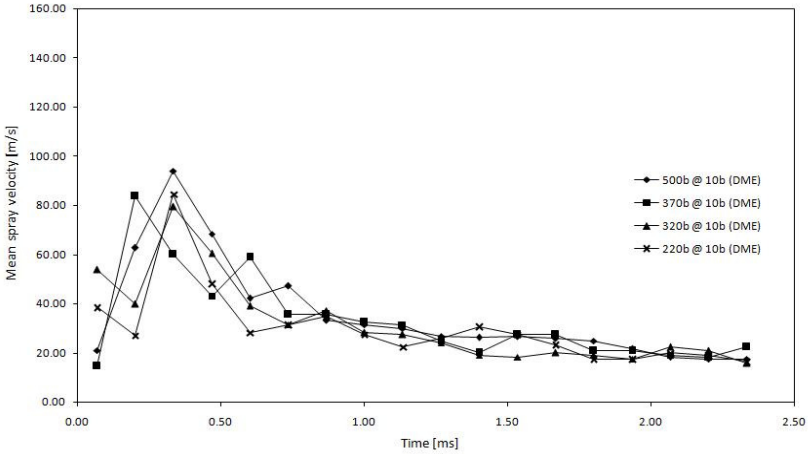

Figure C30: DME (Pinj = various and Pb = 10b)

Cone Angle

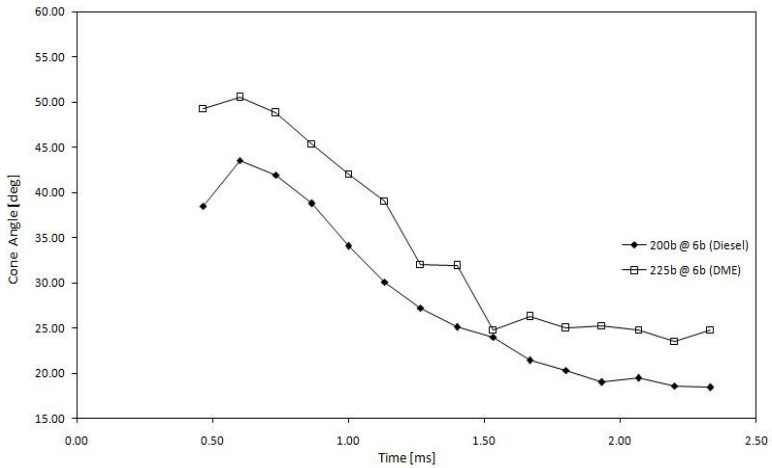

Figure C31: P_{inj} = 200b and P_b = 6b

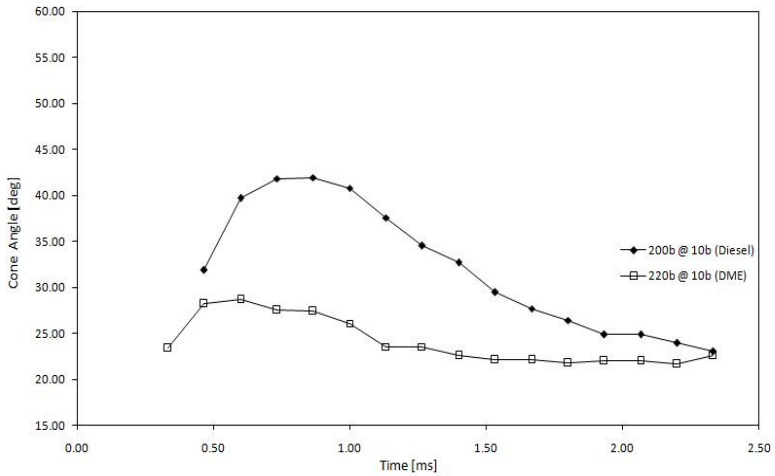

Figure C32: P_{inj} = 200b and P_b = 10b

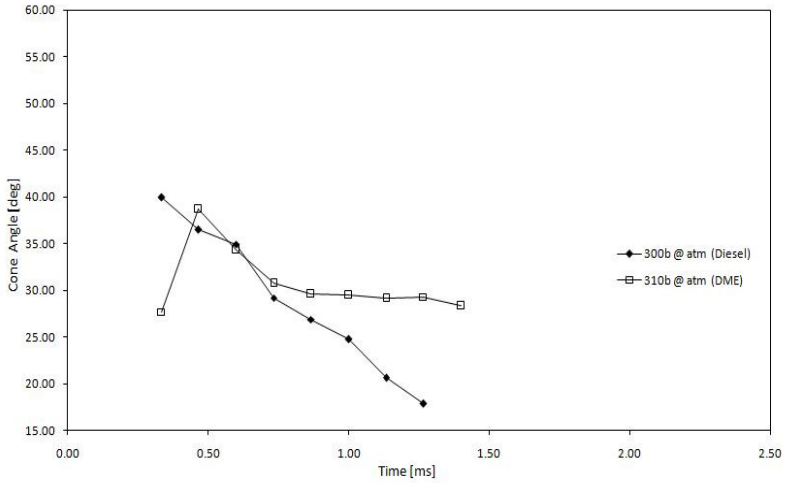

Figure C33: P_{inj} = 300b and P_b = atm

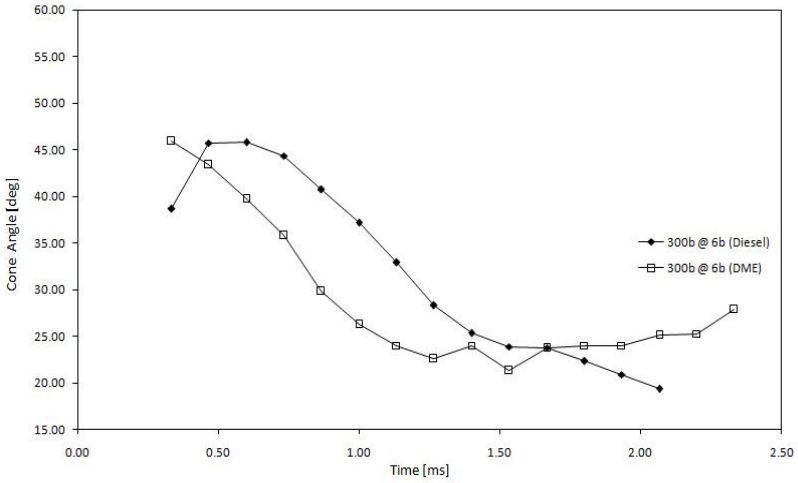

Figure C34: P_{inj} = 300b and P_b = 6b

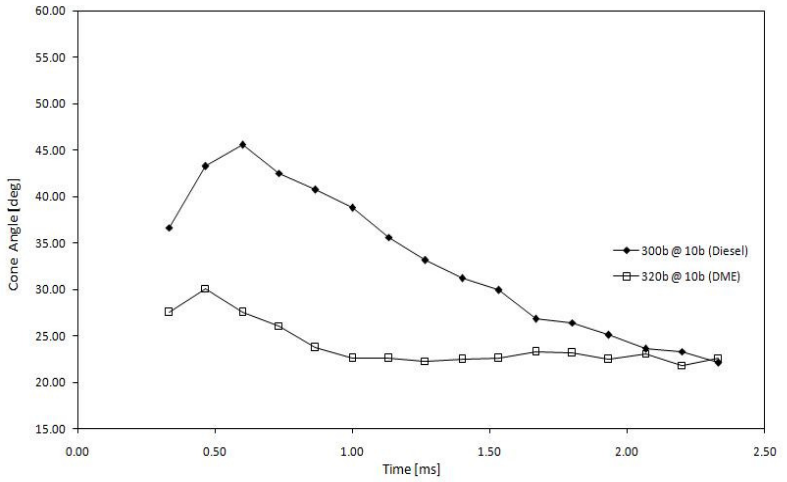

Figure C35: P_{inj} = 300b and P_b = 10b

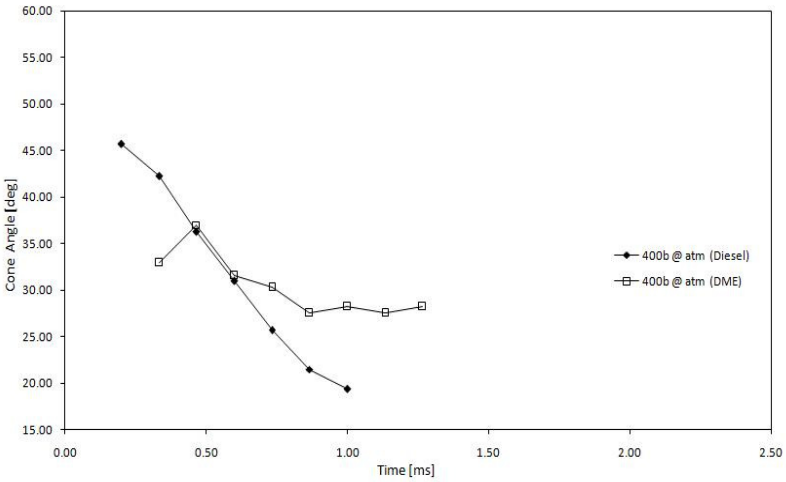

FigureC36: P_{inj} = 400b and P_b = atm

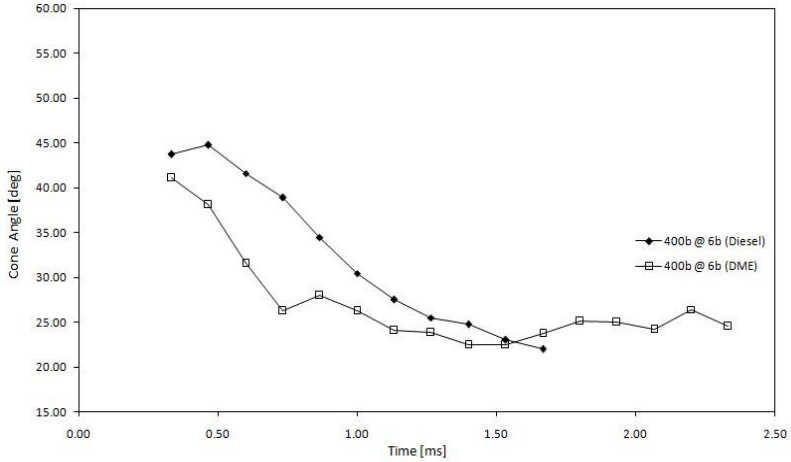

Figure C37: P_{inj} = 400b and P_b = 6b

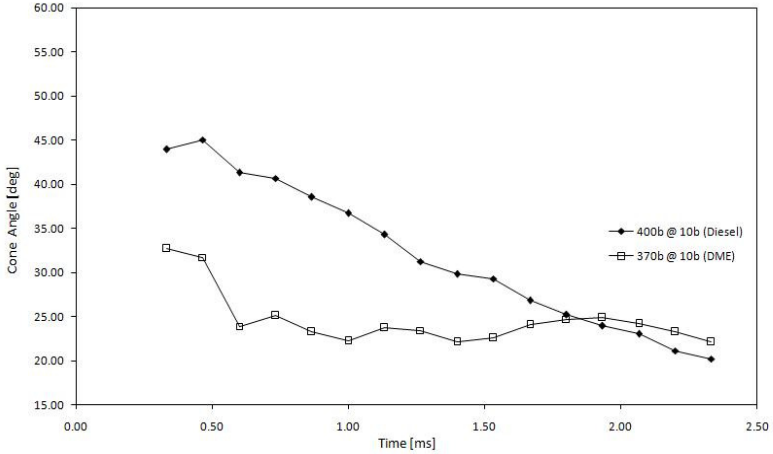

Figure C38: P_{inj} = 400b and P_b = 10b

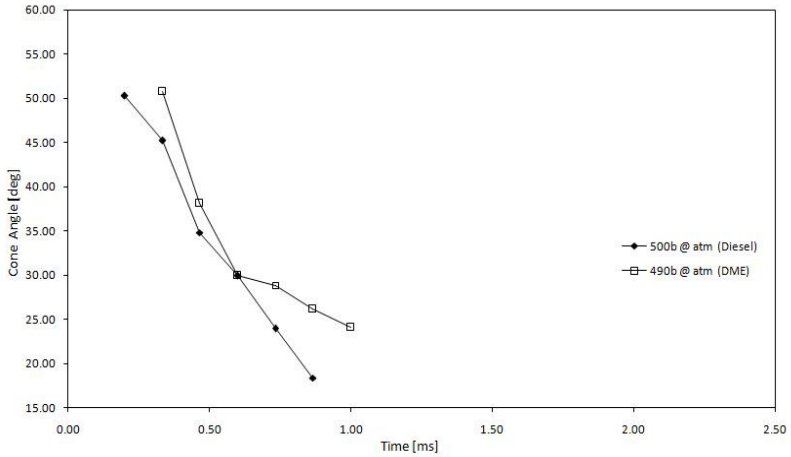

Figure C39: P_{inj} = 500b and P_b = atm

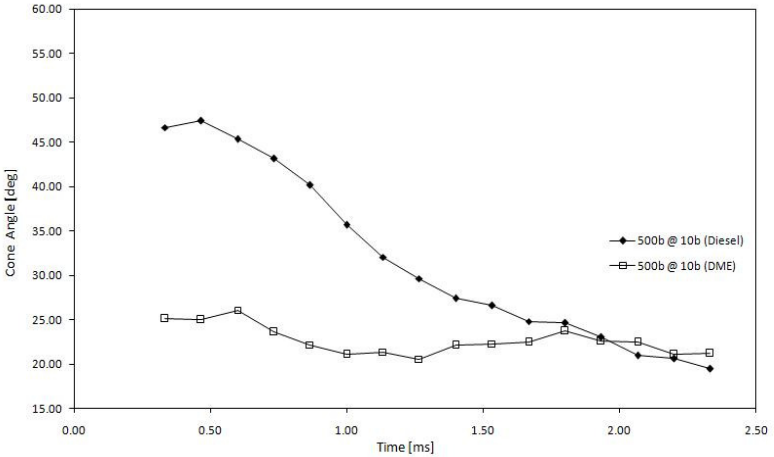

Figure C40: P_{inj} = 500b and P_b = 10b

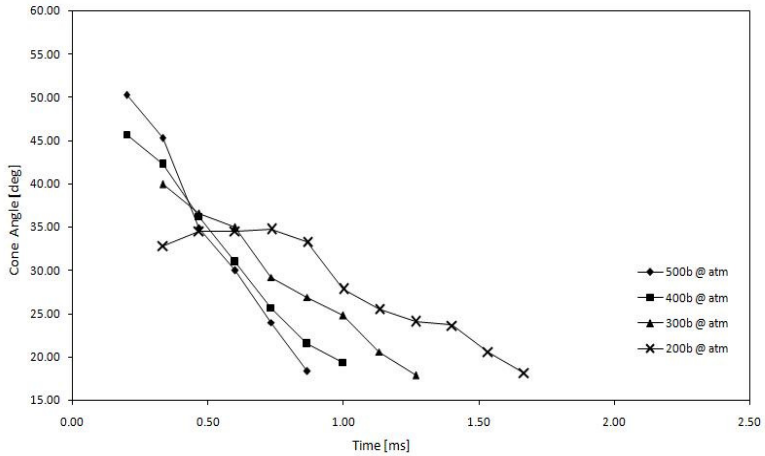

Figure C41: Diesel (P_{inj} = various and P_b = atm)

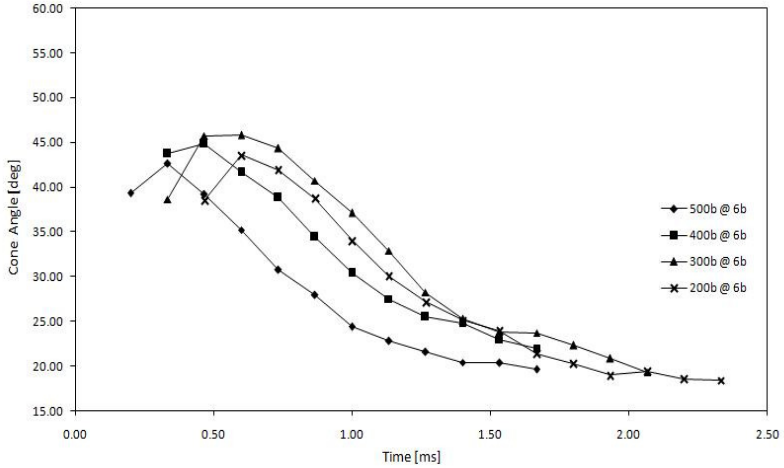

Figure C42: Diesel (P_{inj} = various and P_b = 6b)

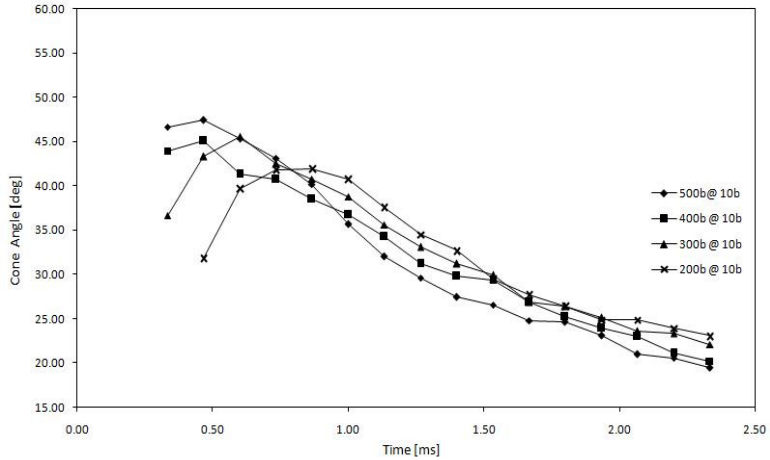

Figure C43: Diesel (P_{inj} = various and P_b = 10b)

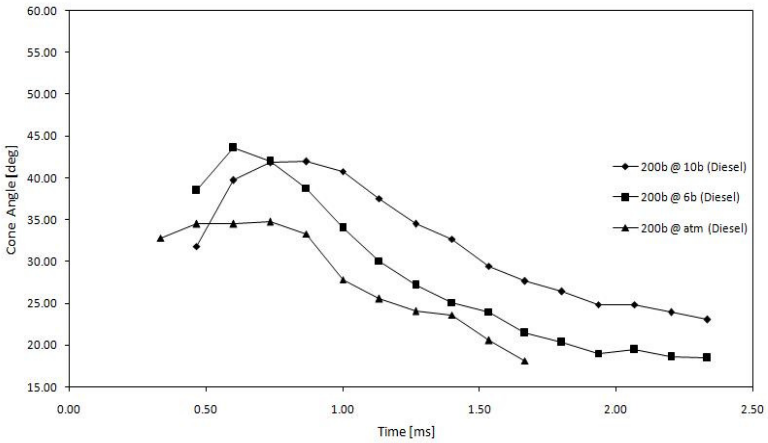

Figure C44: Diesel (P_{inj} = 200b and P_b = various)

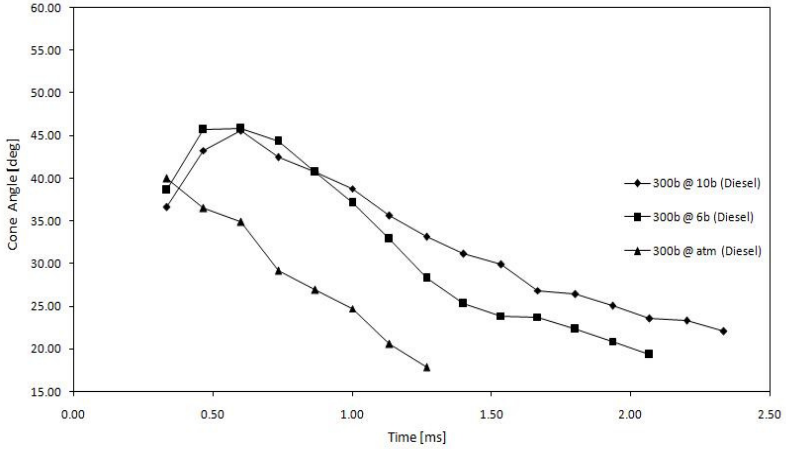

Figure C45: Diesel (P_{inj} = 300b and P_b = various)

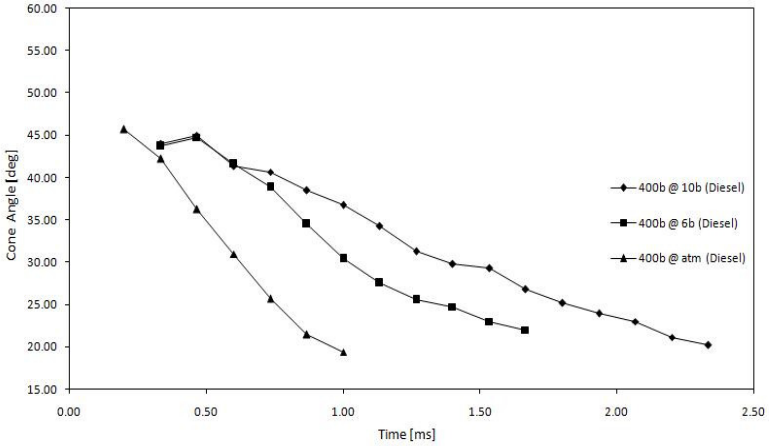

Figure C46: Diesel (P_{inj} = 400b and P_b = various)

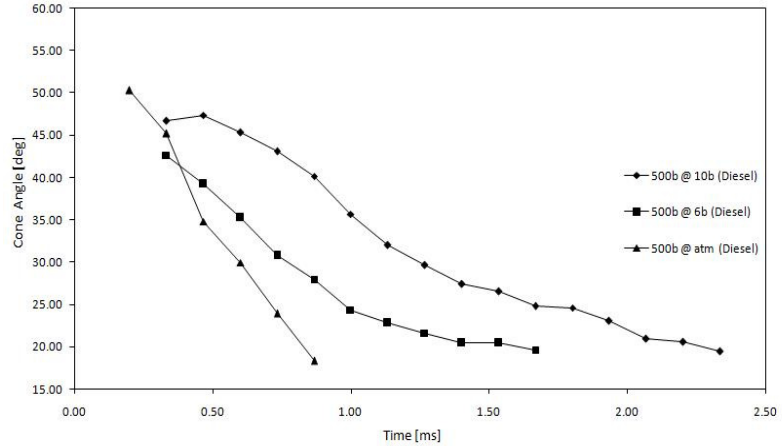

Figure C47: Diesel (P_{inj} = 500b and P_b = various)

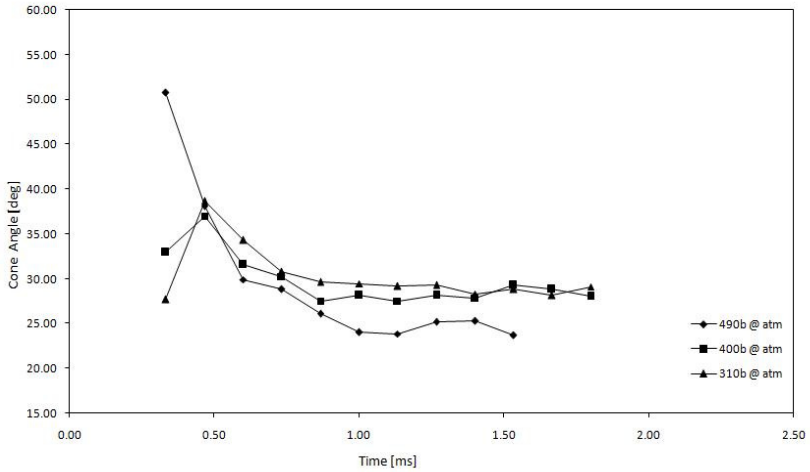

Figure C48: DME (P_{inj} = various and P_b = atm)

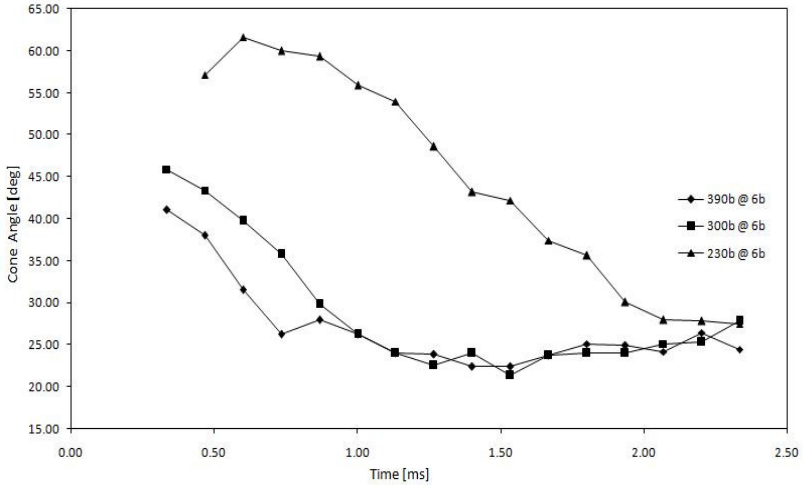

Figure C49: DME (P_{inj} = various and P_b = 6b)

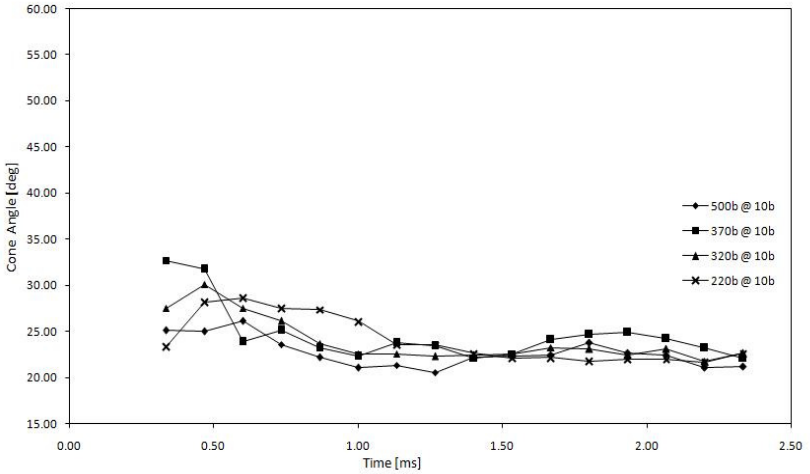

Figure C50: DME (P_{inj} = various and P_b = 6b)

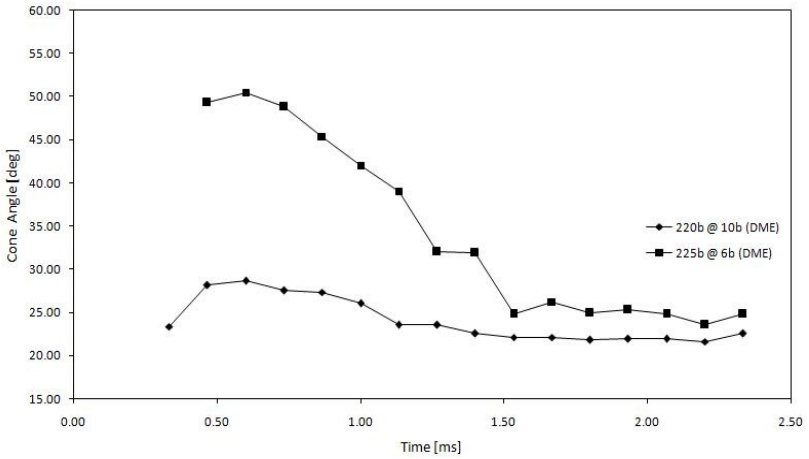

Figure C51: DME (P_{inj} = 200b and P_b = various)

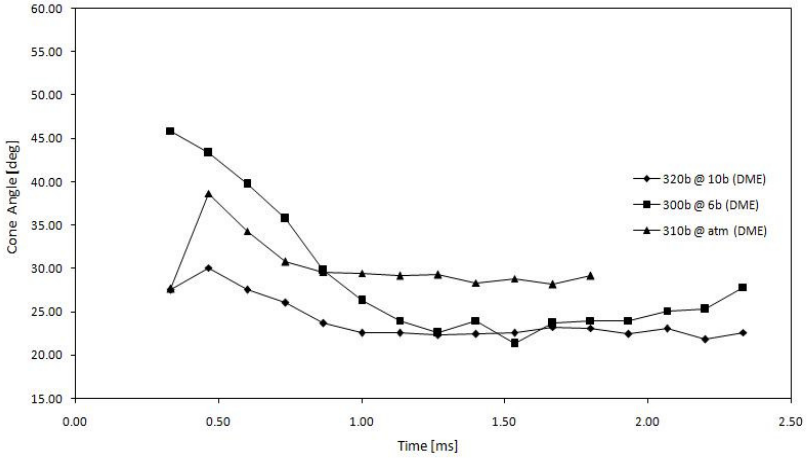

Figure C52: DME (P_{inj} = 300b and P_b = various)

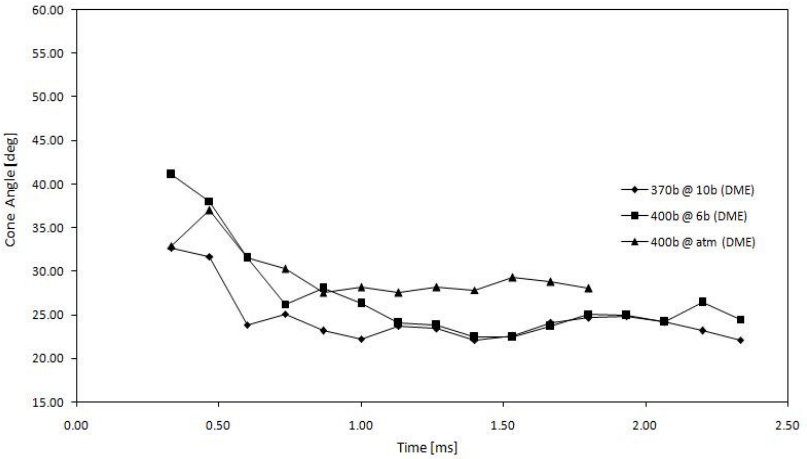

Figure C53: DME (P_{inj} = 400b and P_b = various)

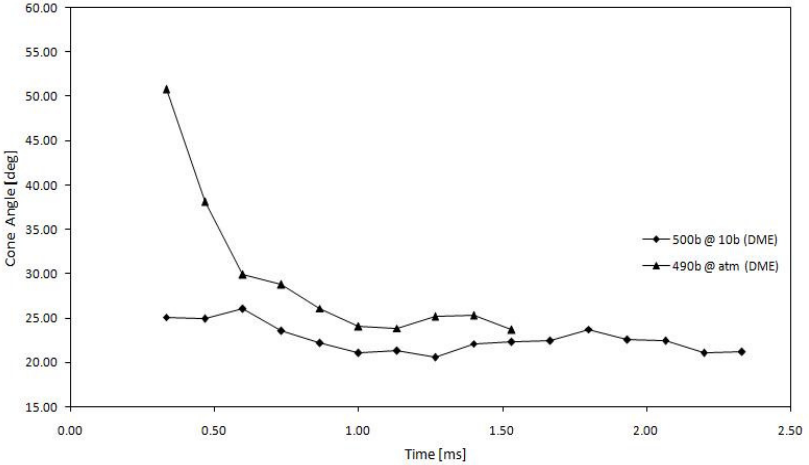

Figure C54: DME (P_{inj} = 500b and P_b = various)

Appendix E: Pressure Trace

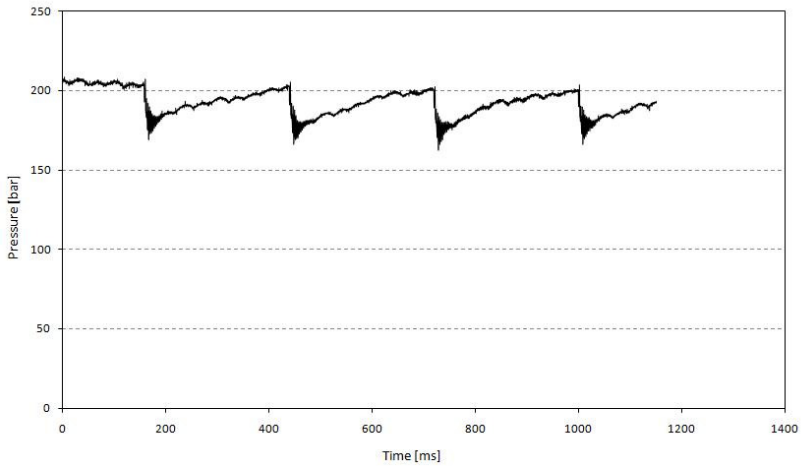

Figure D1: Diesel (P_{inj} = 200b, P_b = 6b)

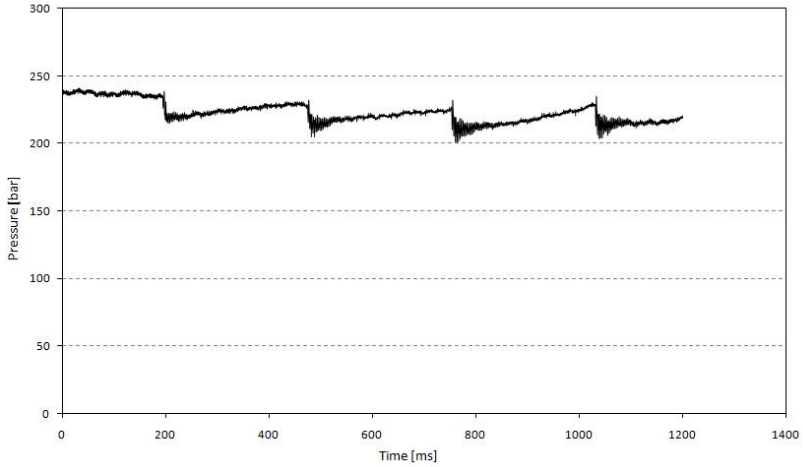

Figure D2: DME (P_{inj} = 200b, P_b = 6b)

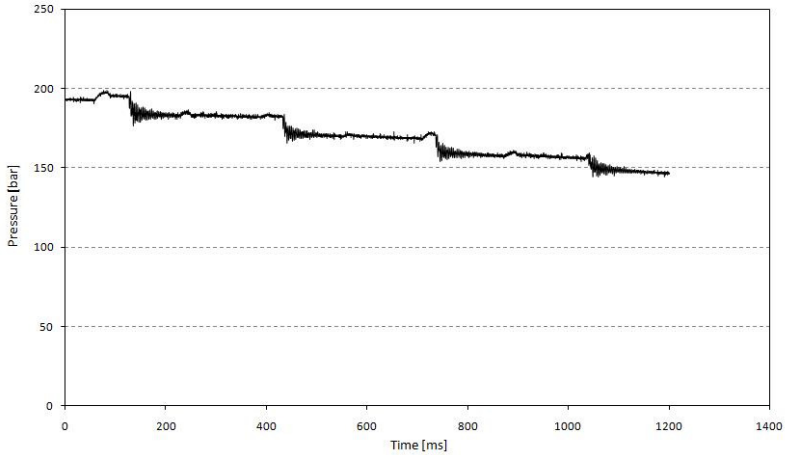

Figure D3: DME (P_{inj} = 200b, P_b = 8b)

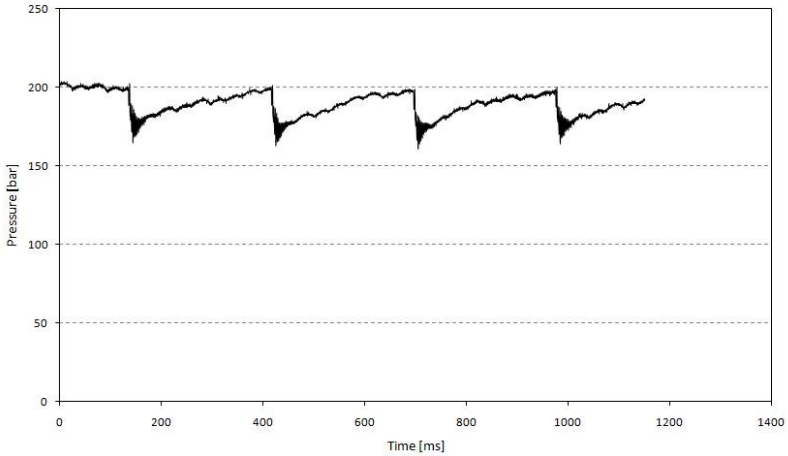

Figure D4: Diesel (Pinj = 200b, Pb = atm)

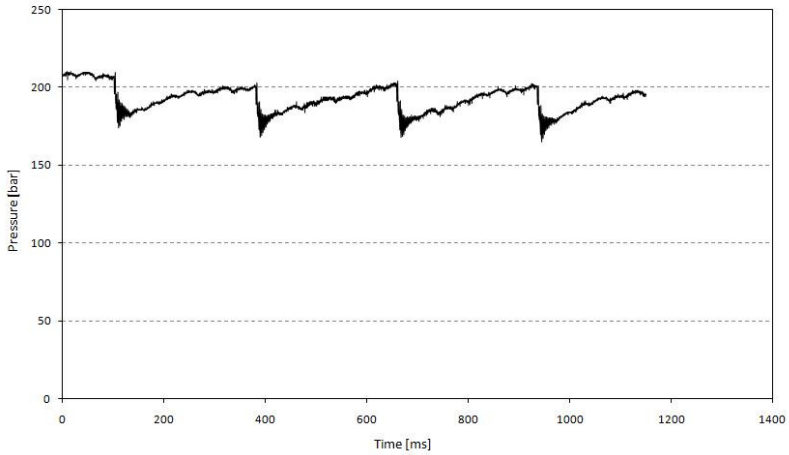

Figure D5: Diesel (Pinj = 200b, Pb = 10b)

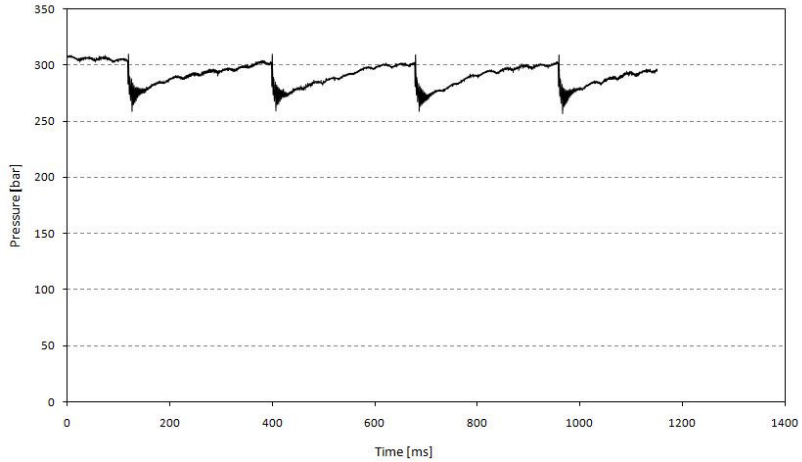

Figure D6: Diesel (Pinj = 300b, Pb = 6b)

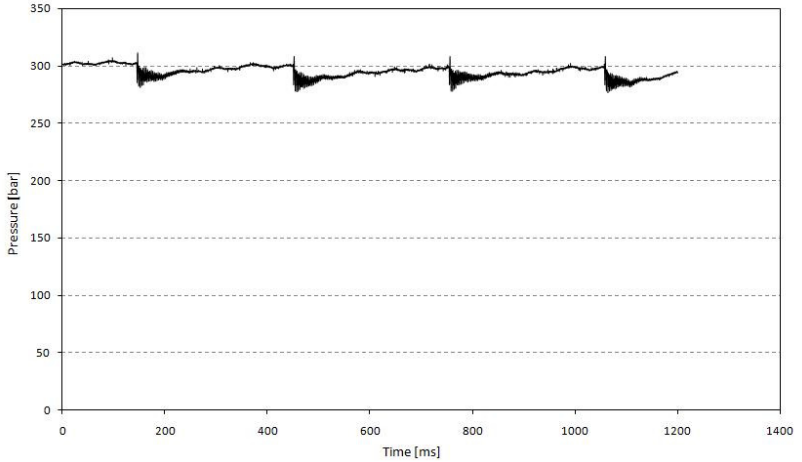

Figure D7: DME (Pinj = 300b, Pb = 8b)

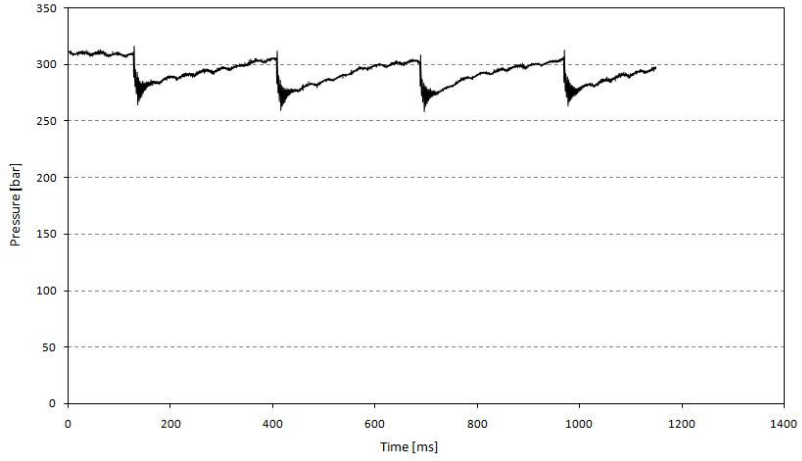

Figure D8: Diesel (Pinj = 300b, Pb = 10b)

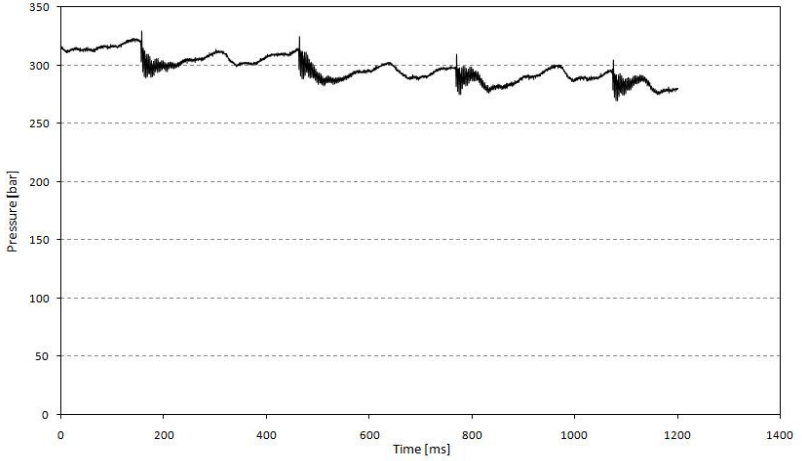

Figure D9: DME (Pinj = 300b, Pb = 10b)

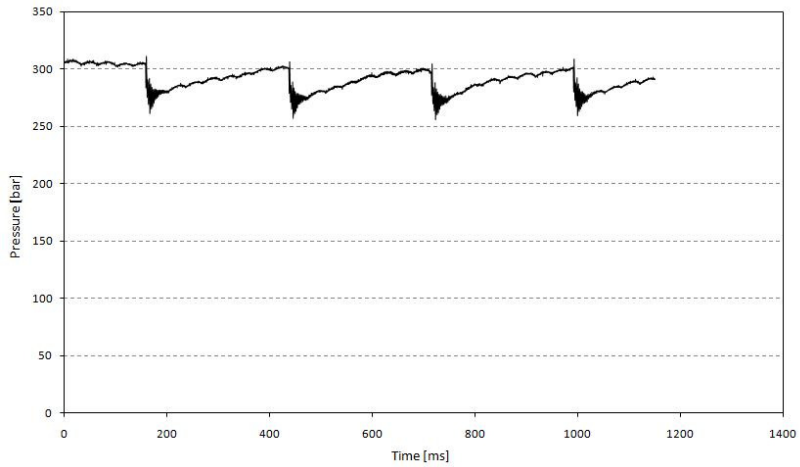

Figure D10: Diesel (Pinj = 300b, Pb = atm)

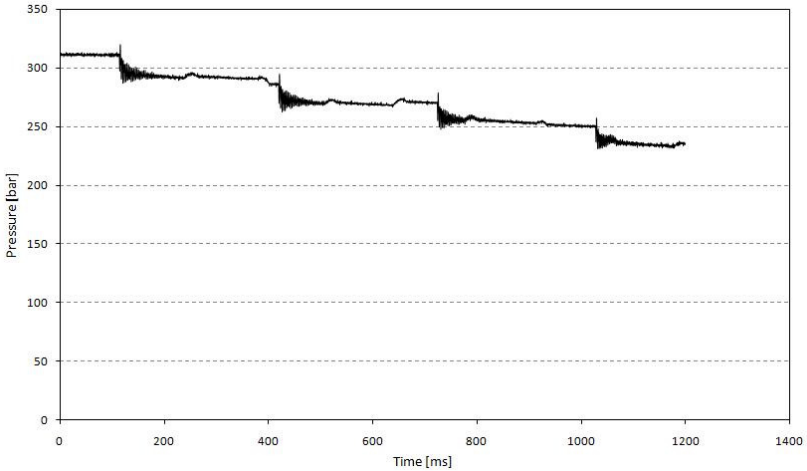

Figure D11: DME (Pinj = 300b, Pb = atm)

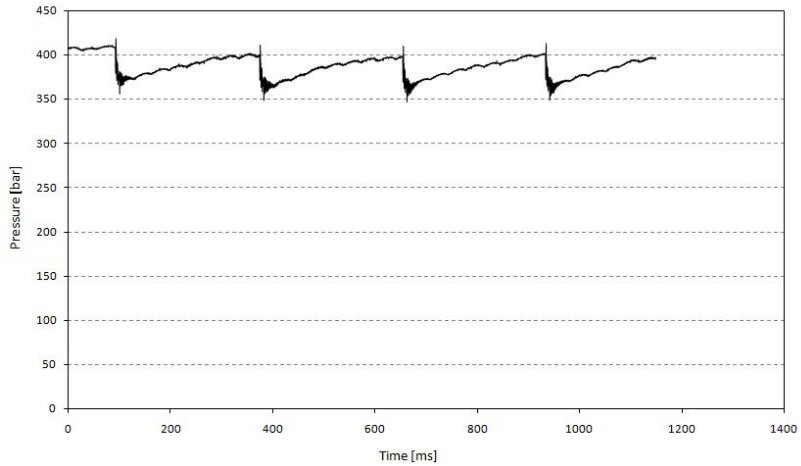

Figure D12: Diesel (Pinj = 400b, Pb = 6b)

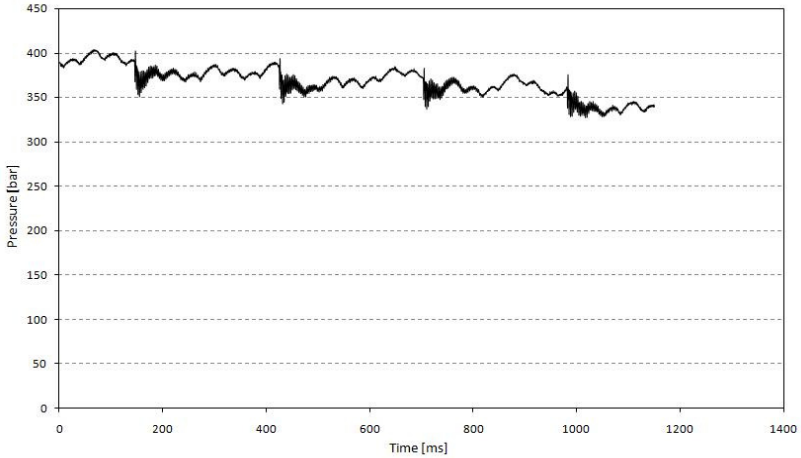

Figure D13: DME (Pinj = 400b, Pb = 6b)

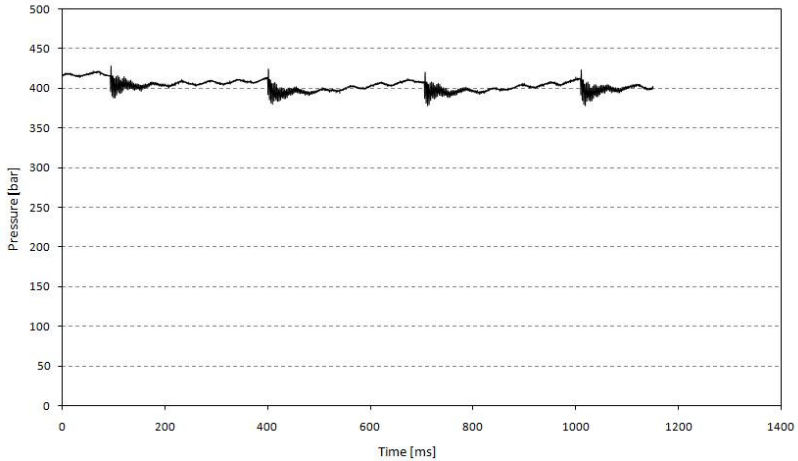

Figure D14: DME (Pinj = 400b, Pb = 8b)

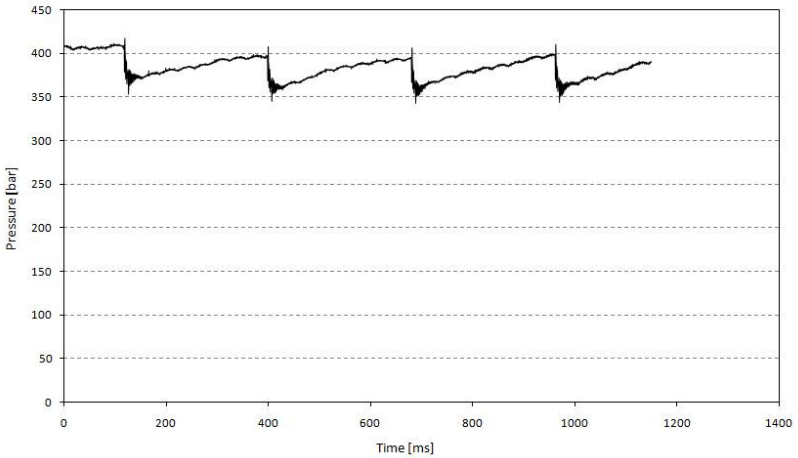

Figure D15: Diesel (Pinj = 400b, Pb = 10b)

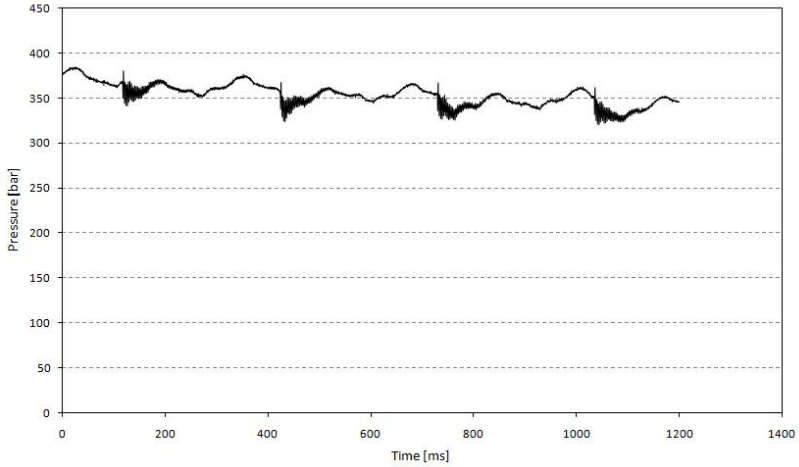

Figure D16: DME (Pinj = 400b, Pb = 10b)

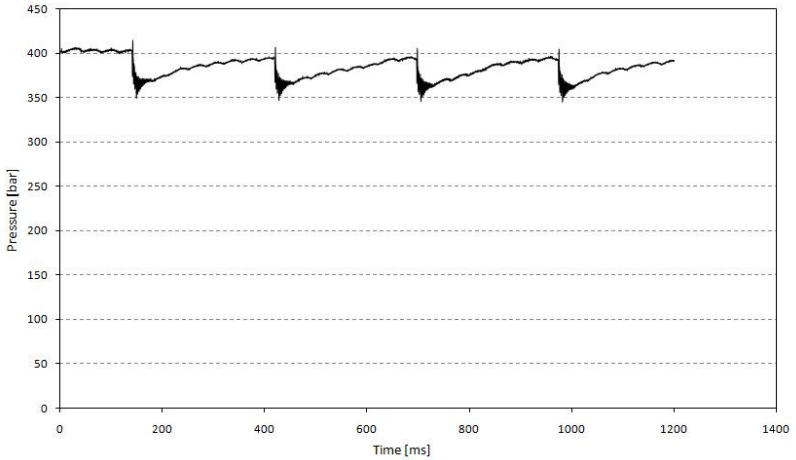

Figure D17: Diesel (Pinj = 400b, Pb = atm)

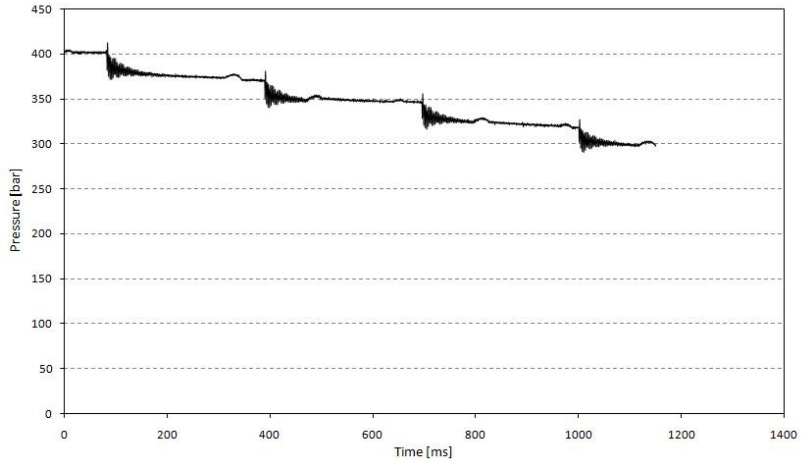

Figure D18: DME (Pinj = 400b, Pb = atm)

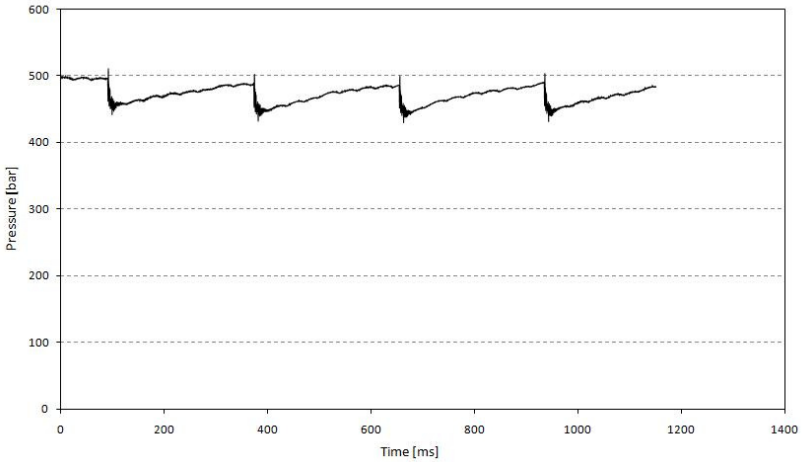

Figure D19: Diesel (Pinj = 500b, Pb = 6b)

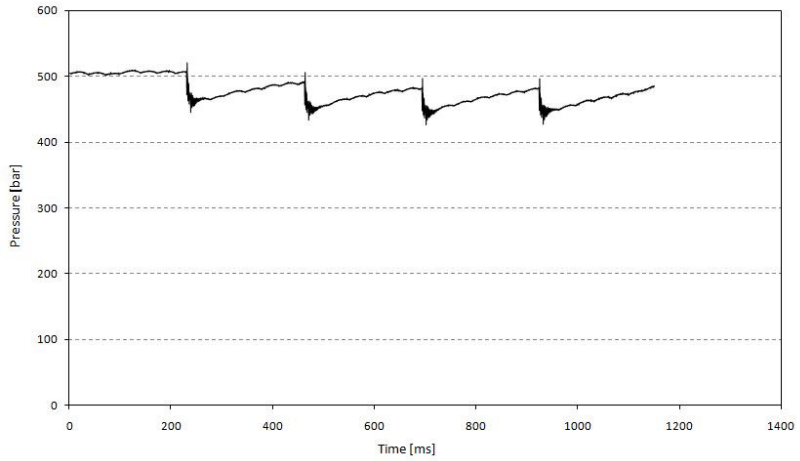

Figure D20: Diesel (Pinj = 500b, Pb = 10b)

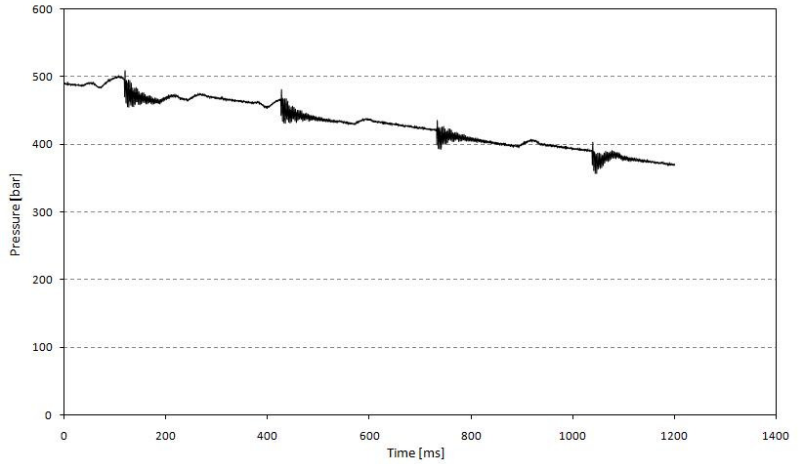

Figure D21: DME (Pinj = 500b, Pb = 10b)

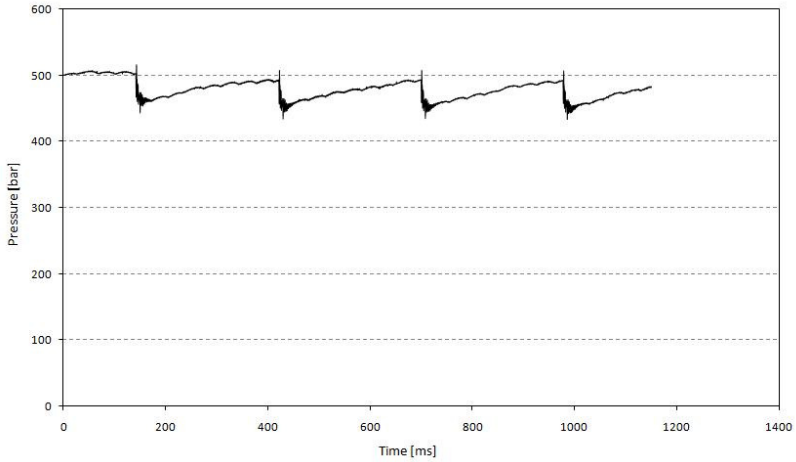

Figure D22: Diesel (Pinj = 500b, Pb = atm)

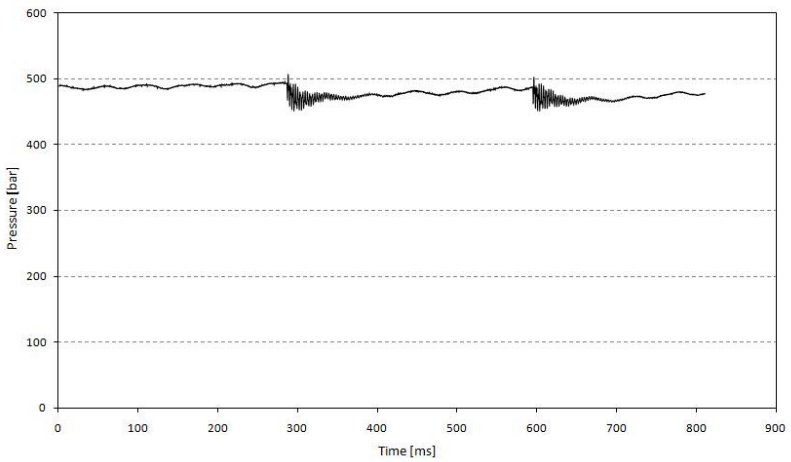

Figure D23: DME (Pinj = 500b, Pb = atm)

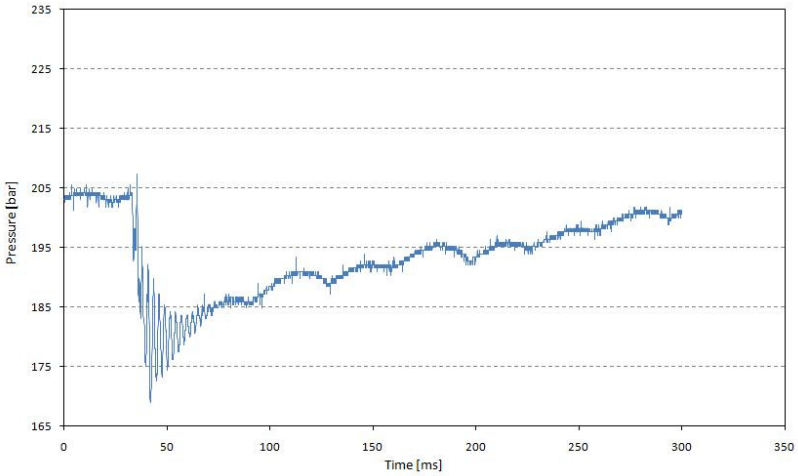

Figure D24: Diesel close-up (Pinj = 200b, Pb = 6b)

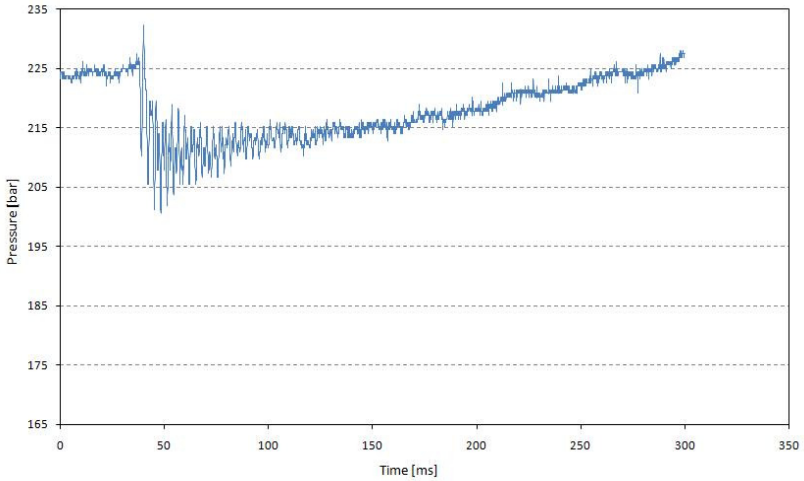

Figure D25: DME close-up (Pinj = 200b, Pb = 6b)

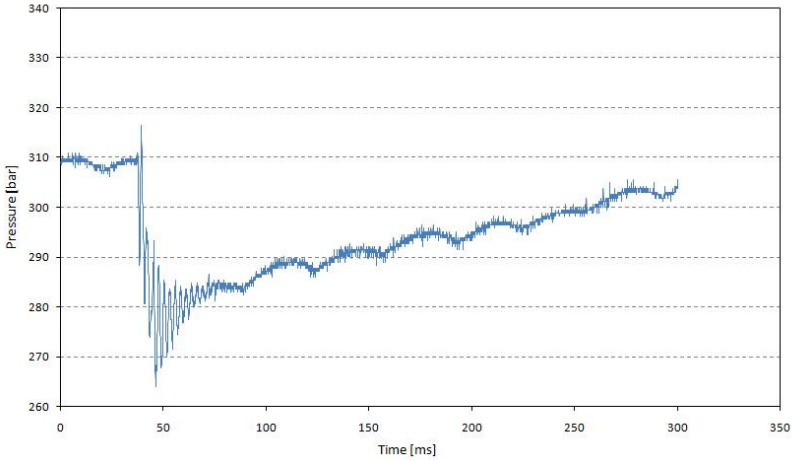

Figure D26: Diesel close-up (Pinj = 300b, Pb = 10b)

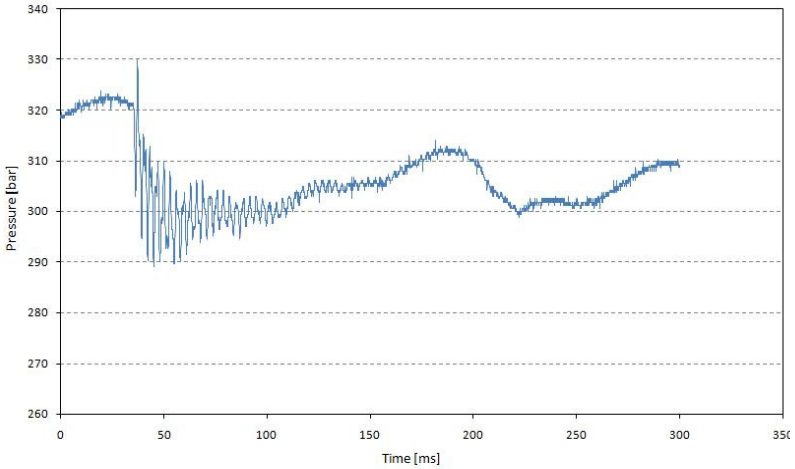

Figure D27: DME close-up (Pinj = 300b, Pb = 10b)

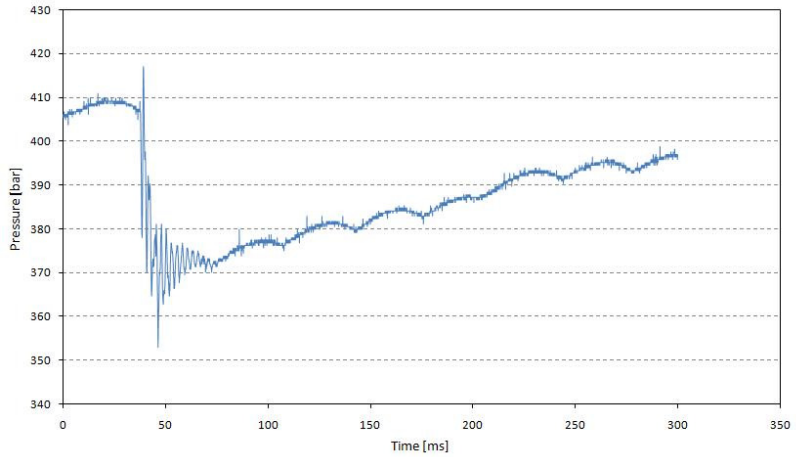

Figure D28: Diesel close-up (Pinj = 400b, Pb = 10b)

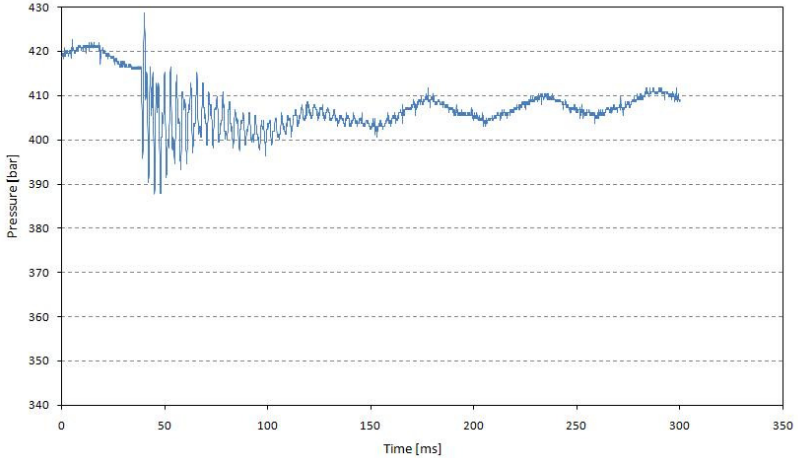

Figure D29: DME close-up (Pinj = 400b, Pb = 8b)

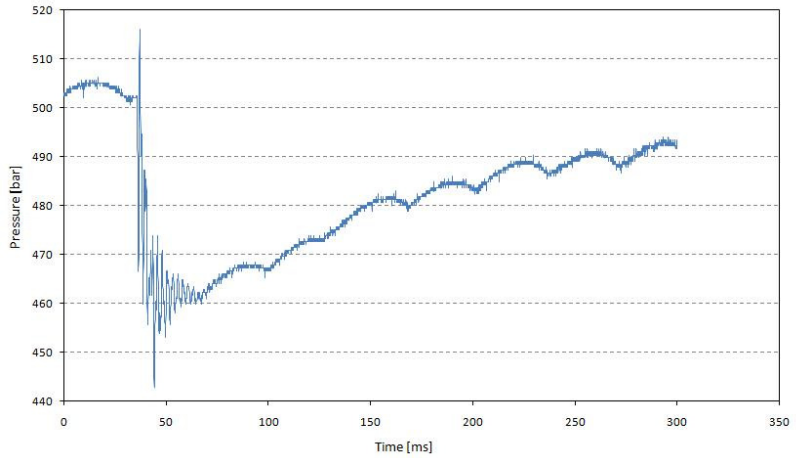

Figure D30: Diesel close-up (Pinj = 500b, Pb = atm)

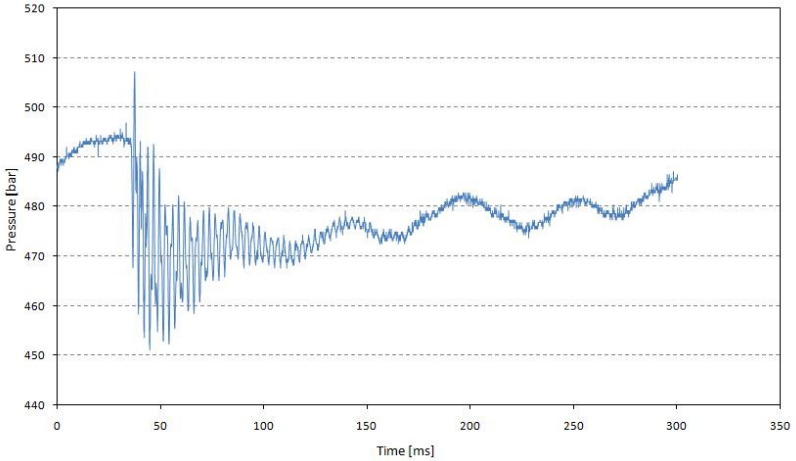

Figure D31: DME close-up (Pinj = 500b, Pb = atm)